GALLIUM OXIDE AND OXYNITRIDES: ACHIEVING THIN FILM CRYSTALLINITY AT LOW THERMAL BUDGETS

by

Elham Rafie Borujeny

A thesis submitted in partial fulfillment of the requirements for the degree of

Doctor of Philosophy

in

Chemical Engineering

Department of Chemical and Materials Engineering
University of Alberta

Abstract

Growing demand for electrical energy calls for more efficient electronic devices not only in terms of performance but also in terms of energy-efficient fabrication processes. With traditional semiconductors (such as silicon) reaching their limits in electrical power handling, alternative semiconducting materials have been considered to overcome fundamental material limitations and meet the stringent requirements of efficiency, reliability, and cost effectiveness. Gallium nitride (GaN) has been one of the frontrunners to replace silicon for power electronic and optoelectronic applications. However, gallium oxide (Ga_2O_3) has recently attracted considerable attention as a suitable candidate that can compete with and complement GaN electronics and lead to more efficient devices. Even though Ga_2O_3 is not a new material, its application as a wide bandgap semiconductor in electronic devices is new. For electronic applications, two crystalline Ga_2O_3 phases are of interest, α-Ga_2O_3 and β-Ga_2O_3. However, high quality crystalline Ga_2O_3 thin films can currently be obtained on very limited substrates in specific process conditions or at high temperatures. This work demonstrates a number of novel strategies for energy-efficient fabrication of high quality crystalline films of gallium oxide and oxynitrides as emerging wide bandgap semiconductors with applications in a broad range of electronic devices. Atomic layer deposition (ALD) is used to achieve dense and pinhole-free films of gallium oxide at low thermal budgets (with a special focus on temperatures < 300°C). After determining the onset temperature for crystallinity formation to be 190°C (the lowest reported value in the literature so far), the deposition process conditions are presented that result in either amorphous or mixed-phase crystalline films with superior properties. Furthermore, for the first time in the literature, by taking advantage of the unique crystallographic features of Ga_2O_3, a universal and robust approach is proposed to control the crystallinity of Ga_2O_3 thin films in situ and achieve single-phase α-Ga_2O_3 films on GaN-compatible non-native substrates at low thermal budgets. The step-by-step process is then revised so that the energetics of the process can lead to high quality epitaxial β-Ga_2O_3 films at low temperatures. Discovering

universal methods to obtain single-phase crystalline films of α-Ga_2O_3 and β-Ga_2O_3 are major novel contributions of this work. In addition, this work showcases a series of ALD depositions for controlled incorporation of oxygen in the crystal structure of GaN at low temperature to obtain gallium oxynitride films with tunable structure and properties.

Preface

Parts of the work presented in this thesis have been published in the following journal, patent applications, and conferences (listed in chronological order). In addition, two manuscript drafts based on parts of the work presented in this thesis will be submitted to two additional journals as shown at the end of the following list.

TEM sample preparations and data acquisitions, 2D XRD data acquisition for Figure 2.5, and part of the XRD data acquisition for Appendix B were carried out by other individuals upon author's request due to unavailability of the instruments to the author (this specifically refers to acquisition of the TEM data on α-Ga_2O_3 carried out by Dr. Huikai Cheng of Thermo Fisher Scientific, acquisition of the 2D XRD data for Figure 2.5 along with part of the XRD data for Appendix B carried out by Ms. Victoria M. Jarvis of the McMaster Analytical X-ray Diffraction Facility (MAX), and acquisition of part of the XRD data for Appendix B carried out by Dr. Oles Sendetskyi of the University of Alberta and the National Research Council-Nanotechnology Research Centre, Canada). Any other information in this thesis has been produced by the author.

[1] "**On Achieving Single-Phase Crystalline Gallium Oxide Thin Films at Low Thermal Budgets**", E. Rafie Borujeny, K. Cadien, Accepted for Oral Presentation at The American Vacuum Society 67th International Symposium (AVS 67), October 24-29, 2021, North Carolina, USA.

[2] "**Gallium Oxynitride Thin Films with Tunable Properties for Electronic and Photonic Applications**", E. Rafie Borujeny, K. Cadien, Accepted for Poster Presen-

tation at The American Vacuum Society 67th International Symposium (AVS 67), October 24-29, 2021, North Carolina, USA.

[3] "**Crystallinity Control via Atomic Level Scaffolding**", E. Rafie Borujeny, K. Cadien, Contributed Oral Presentation at The International Conference on Atomic Layer Deposition (ALD 2021), June 27-June 30, 2021, Florida, USA.

[4] "**Revisiting Process Optimization in Atomic Layer Deposition: Going Beyond Growth Rate**", E. Rafie Borujeny, K. Cadien, Poster Presentation at The International Conference on Atomic Layer Deposition (ALD 2021), June 27-June 30, 2021, Florida, USA.

[5] "**From Amorphous to β-Gallium Oxide: Practical Implementation of Energetics Considerations in Process Design and Optimization**", E. Rafie Borujeny, K. Cadien, Oral Presntation at 239th ECS Meeting, May 30-June 3, 2021, Digital Meeting.

[6] "**Deposition of Beta-Gallium Oxide Thin Films**", E. Rafie Borujeny, K. Cadien, United States Provisional Patent No. 63/173,260, Filed on April 09, 2021.

[7] "**Deposition of Alpha-Gallium Oxide Thin Films**", E. Rafie Borujeny, K. Cadien, United States Provisional Patent No. 63/137,874, Filed on January 15, 2021.

[8] "**Low Thermal Budget Heteroepitaxial Gallium Oxide Thin Films Enabled by Atomic Layer Deposition**", E. Rafie Borujeny, O. Sendetskyi, M. Fleischauer, K. Cadien, ACS Applied Materials & Interfaces, 12, 39, 44225-44237, August 2020.

[9] "**ALD-Grown Gallium Oxide Thin Films with Properties Close to Bulk Wafers**", E. Rafie Borujeny, K. Cadien, Poster Presentation at The International Conference on Atomic Layer Deposition (ALD 2020), June 29-July 1, 2020, Ghent, Belgium.

In Preparation:

- "**Heteroepitaxial Gallium Oxynitride Thin Films for Energy-Efficient High Performance Electronic Devices**", E. Rafie Borujeny, K. Cadien, Manuscript in Preparation.

- "**Bridging the Gap Between Gallium Oxide and Gallium Nitride: Heteroepitaxy via Atomic Level Scaffolding**", E. Rafie Borujeny, H. Cheng, K. Cadien, Manuscript in Preparation.

To all who helped me throughout this journey, especially my family.

Contents

List of Tables

List of Figures

Chapter 1

Introduction

1.1 Background

Research into new materials for power electronic devices (devices that convert DC power generated by solar cells and fuel cells to AC power, thereby making it usable by consumers, or devices that convert AC power supplied by a provider to DC power, thereby making it usable in charging the battery of an electric car or a portable electronic device) has emerged as an inseparable part of sustainable development and efficient handling of electrical energy during the past three decades. Currently, the most commonly used semiconducting materials in building electronic devices, namely silicon (Si) and gallium arsenide (GaAs), have reached their limits in speed, temperature and power handling. Therefore, building more efficient electronic devices from advanced materials and by means of an energy-efficient fabrication process will have a large impact on improving the energy accessibility in the world and advancing the social and economic security of humanity by building a cleaner and more abundant low-carbon energy future. Wide bandgap semiconductors such as SiC

and GaN have been considered as candidate materials for power devices to overcome the limitations of their traditional predecessors in meeting the growing needs and the stringent requirements of the high energy demand society today. During the past few years, gallium oxide (Ga_2O_3) has also been proposed as an alternative material for both optoelectronic and power semiconductor devices to compete with and complement the outstanding properties of GaN as the front-runner material in those applications. However, to date, high quality crystalline films of these semiconductors are only grown at high temperature processes (> 500°C), which consume a lot of energy to build thick layers of the material and substantially increase the carbon foot print. Development of low temperature technologies for crystalline growth of these materials and proof of the quality of the material (as has been attempted in this work) will lead to energy-efficient electronic devices, not only in performance but also an energy-efficient fabrication process.

1.2 Literature Review

Gallium oxide is an important inorganic solid-state material in several fields. Traditionally, gallium oxide has been used for its catalytic properties [11, 12] as well as its gas sensing abilities in both oxidizing and reducing environments [11–13]. It has also been used as a passive component (e.g., as gate oxide, i.e., an insulator) in electronic devices [11, 12, 14–20]. Meanwhile, during the past few years, gallium oxide has attracted attention as an emerging semiconducting material for the active layers of solid-state electronic devices [10–12, 21], offering superior properties to the traditional semiconducting materials (such as Si) and competitive and complementary properties to the more recent ones (such as SiC

and GaN) and thus finding applications in power electronics (for smaller, lighter, and more efficient power handling circuitries, including both DC/DC and DC/AC power converters in automotive applications, such as in hybrid cars, and more efficient converters that handle electricity produced by renewable energy resources), optoelectronics (including transparent conductive oxides (TCO's) and interlayers in solar cells and even in flexible electronics, flat-panel displays, and touch screens), communications infrastructure, and devices in harsh environments.

Compared to SiC and GaN, which are currently the front-runner materials in similar applications outperforming the traditional Si devices, gallium oxide has a wider bandgap (which, for example, expands the operating spectral range of transparent devices to deep UV), a larger breakdown field (which enables power devices to withstand higher voltages while being smaller in size and lighter in weight), lower on-resistance (which results in lower conduction loss in the active layer of the electronic device), and extremely low reverse leakage current (which results in more efficient electronic devices in off-state). References [10] and [21] compare properties of gallium oxide with common semiconductor materials in-use today showing the exceptionally high figures of merit (FOM) of gallium oxide in power handling.

Crystalline forms of gallium oxide are desirable in these applications to ensure stability and repeatability of the device performance. Gallium oxide has several crystalline polymorphs [11, 12, 22, 23]; α- and β-gallium oxide are the most studied polymorphs. Among those two, β-gallium oxide is the most stable polymorph of gallium oxide with a monoclinic crystal structure belonging to the space group C2/m. α-Gallium oxide is isostructural to α-aluminum oxide, belonging to the rhombohedral space group R$\bar{3}$c (which can be pro-

jected on a hexagonal coordinate system as well). Interestingly, α-gallium oxide, which can exist at ambient to high temperatures and pressures, has a larger bandgap, larger breakdown voltage, larger refractive index, and larger dielectric constant as well as an $\sim$20% smaller effective mass of electrons compared to β-gallium oxide [11, 23], which make it even more advantageous in emerging applications of gallium oxide in solid-state electronics. γ-Gallium oxide, isostructural to Al_2MgO_4 with cubic structure in space group $Fd\bar{3}m$, is also agreed to be a metastable polymorph of gallium oxide which is only obtained in specific process conditions. Information about other gallium oxide polymorphs, namely ε, κ, and δ, is limited and, in some cases, debated in the literature [24, 25] mainly due to the fact that these polymorphs are hard to obtain as isolated phases, which makes their structure determination challenging. For example, some researchers believe δ-gallium oxide to be a nanocrystalline form of ε or κ as opposed to being a new phase [24]. ε-Gallium oxide is considered orthorhombic in some studies [26, 27]; however, some studies believe ε-gallium oxide has a hexagonal structure, and κ-gallium oxide is the orthorhombic polymorph which only forms either as a transient phase impossible to isolate [24] or as nanoscale subdomains possessing 6-fold symmetry which might be reported as hexagonal ε-gallium oxide if their size falls below the resolution of the probing technique [25].

Thin films of gallium oxide are required for fabricating electronic devices. Even though processes for producing bulk β-gallium oxide wafers are developed and such wafers have become commercially available during the past few years to serve as templates for thin film growth, deposition of gallium oxide on foreign substrates (especially those that are available to the semiconductor industry at cheaper prices and larger dimensions) is required. Deposition of such crystalline thin films on foreign substrates is challenging and

is usually only possible for high-temperature processes which consume a lot of energy. References [11] and [28] provide an overview of the gallium oxide growth techniques. In this work, we present energy-efficient processes for the growth of crystalline gallium oxide and oxynitride thin films at low temperatures by means of plasma-enhanced atomic layer deposition (PEALD).

Atomic layer deposition (ALD) [29–33] is a promising nanofabrication technique for growing thin layers of a wide range of materials with atomic-level control over thickness, excellent conformality on patterned structures, and exceptional uniformity over large areas. ALD consists of self-limiting reactions that introduce precursors or reactants to the substrate surface one by one in a cycle and eventually form a monolayer of target material on the surface. Repeating the cycles results in formation of dense pinhole-free films that very often provide superior properties compared to films deposited by other methods. ALD processes use either molecular species (including water, oxygen, ozone, and ammonia) or species in plasma state as oxidizing or reducing reactant. The former process is commonly termed thermal ALD (TALD), since thermal energy is the only available source of energy for reactions to proceed, while the latter is termed plasma-enhanced ALD (PEALD). Using species in the plasma state makes the ALD process more complex while providing access to new reaction pathways and products that would not be achievable otherwise.

There are only a few literature reports of gallium oxide grown by ALD [13–20, 34–49]. They mostly result in amorphous films that require high-temperature annealing to crystallize. However, there are very few reports [35,42,43,46,47,49] of ALD growth of crystalline gallium oxide. In particular, Boschi et al. [49] reported ε-Ga_2O_3 deposited on c-plane sapphire at 550°C by an unoptimized thermal ALD process (i.e., using water as the oxidant)

and indicated that the process conditions need optimization. Hao et al. [35] obtained crystalline Ga_2O_3 films on GaN wafers at 250°C and observed an epitaxial interface between Ga_2O_3 and GaN. Roberts et al. [42] obtained crystalline gallium oxide films on sapphire at 250°C which consisted of α-Ga_2O_3 columns originating from the substrate interface. Another gallium oxide polymorph, believed to be ε-Ga_2O_3, was observed at the tip of the columns, and there was a significant amorphous component to the film located near the surface and between the α-phase columns. Roberts et al. [43] also obtained crystalline gallium oxide films on sapphire at deposition temperatures $\geq$ 250°C. The films were predominantly α-phase in the temperature range 250-350°C while they consisted of a mixture of α and ε phases above 350°C. In addition, the very recent publications of Boris et al. [46] and Wheeler et al. [47] have reported ALD growth of crystalline Ga_2O_3: Boris et al. [46] investigated the role of plasma conditions on the crystallinity of titanium oxide and gallium oxide films grown by PEALD and obtained crystalline films in the temperature range 300-600°C on c-plane sapphire, while Wheeler et al. [47] explored this further and obtained crystalline Ga_2O_3 films from 265 to 475°C on the c-plane sapphire substrate.

While during the past few years, Ga_2O_3 has been proposed as an alternative material for power semiconductor devices due to its larger bandgap, and therefore larger breakdown field, GaN is still the front-runner material in many device applications (particularly the higher frequency ones) owing to its larger electron mobility compared to Ga_2O_3. Table 1.1 and Figure 1.1 show this by comparing the key properties of w-GaN and β-Ga_2O_3 and depicting the upper-limits for power and frequency ranges that each of these materials can handle. Compared to traditional semiconductors (such as Si and GaAs), GaN exhibits superior properties including stability at high temperature, high thermal conductivity, high

	GaN	**Ga_2O_3**
Dielectric Constant, ε	9	10
Breakdown Field, E_{Br} [MV/cm]	3.3	8
Electron Mobility, μ [$cm^2/(V.s)$]	1250	300
Baliga Figure of Merit (BFOM) = $\varepsilon.\mu.E_{Br}^3$	**846.0**	**3214.1**

Table 1.1: Key properties of GaN and Ga_2O_3 taken from reference [10].

electron mobility, and high breakdown field. These outstanding properties strongly depend on GaN crystal structure, with perfectly single crystal GaN exhibiting the most superior properties. Thanks to nearly three decades of research on GaN electronics, strategies for GaN heteroepitaxy on common substrates (such as sapphire, Si, SiC, diamond, and even β-Ga_2O_3) as well as n- and p-type doping of GaN have been successfully developed and are being used in commercial power conversion devices today [50–52]. Wurtzite GaN (w-GaN) with a hexagonal crystal structure (belonging to the space group $P6_3mc$) is the widely used polymorph in GaN electronic devices. Even though studies exist on dry and wet oxidation of GaN to convert it to Ga_2O_3 (which will be either amorphous or β-Ga_2O_3) for use in passive electronic components [53, 54], it is well known that uncontrolled inclusion of oxygen in GaN can deteriorate the crystal structure and is considered contamination [55]. ALD can provide the means to incorporate oxygen into the crystal structure of w-GaN to increase its bandgap while obtaining uniform pinhole-free crystalline films. This is a subject that has not been investigated much in the literature by using ALD and will be

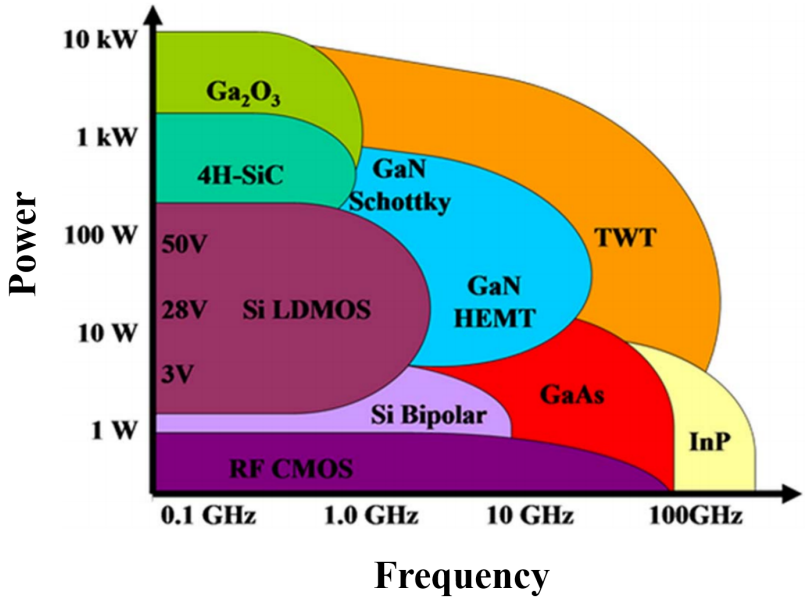

Figure 1.1: Power-frequency diagram of the application space for several semiconductor materials. While GaN is suitable for moderate-to-high power and/or high frequency applications, Ga_2O_3 will overtake the applications at ultrahigh power or moderate frequency. Image reproduced with permission from reference [10].

explored in this work by using plasma-enhanced ALD.

1.3 Objectives of This Work

The objective of this work is to find the most energy-efficient fabrication process for growing thick (> 10 nm) crystalline gallium oxide (Ga_2O_3) films. Furthermore, taking advantage of the ability to grow high quality Ga_2O_3 films at low temperatures and considering the strong technological relevance between Ga_2O_3 and GaN, this work also presents thin film deposition strategies that bridge the gap between Ga_2O_3 and GaN and enable the growth of high quality single-phase gallium oxide (i.e., either α-Ga_2O_3 or β-Ga_2O_3) and gallium oxynitride films at low temperatures.

1.4 Outline of This Thesis

The current chapter provides an introduction to highlight the importance of the subject of Ga_2O_3 crystalline thin film growth.

In Chapter 2, we use an optimized PEALD process to deposit gallium oxide thin films on a variety of common substrates aiming to obtain crystalline gallium oxide at very low temperatures. We determine the onset of crystallinity formation to be as low as 190°C on c-plane sapphire, above which crystalline films consisting of highly oriented α-Ga_2O_3 (006) and β-$Ga_2O_3(\bar{2}01)$ planes are obtained. Starting from the films deposited at the onset of crystallinity (i.e., 190°C), we report that crystalline films consisting of purely β-$Ga_2O_3(\bar{2}01)$ set of planes parallel to the surface form by annealing at the relatively low temperature of 550°C. Both of the temperatures at which we obtained the crystalline as-deposited (onset at 190°C) and the highly crystalline annealed (550°C) films are, to the best of our knowledge, the lowest temperatures reported in the literature so far at which ALD-grown crystalline gallium oxide film is obtained as-deposited and annealed, respectively. In terms of long-term phase stability, our films were all stable, with no change in their crystallinity, for 25 months after their fabrication (this time limit is reported merely because analysis beyond that time was not conducted). This work provides insights into the development of a low-temperature crystalline gallium oxide technology that will lead to energy-efficient electronic devices, not only in performance but also in an energy-efficient fabrication process.

In Chapter 3, we introduce a self-regulated process for controlling Ga_2O_3 crystallinity, enabled by atomic layer deposition (ALD), to achieve α-Ga_2O_3 through stepwise in-situ

plasma-enhanced oxidation of wurtzite GaN (w-GaN). More specifically, α-Ga_2O_3 is deposited in consecutive cycles each consisting of an optimized sequence of triethylgallium (TEG, as the gallium precursor) dose, argon purge, forming gas (i.e., 95% nitrogen / 5% hydrogen) plasma dose, argon purge, oxygen plasma dose, and argon purge. The first four steps of this sequence result in a coherent monolayer of w-GaN through which Ga atoms form a stable and highly symmetric scaffold (i.e., possessing 6-fold symmetry) that steers the oxygen atoms into forming the crystal structure of α-Ga_2O_3 upon oxygen plasma exposure in the remaining two steps of the sequence. The cycles are repeated until the desired thickness of material is deposited. The entire deposition is optimized to achieve crystallinity at the low temperature of 277°C, thereby establishing an energy-efficient fabrication process for growing crystalline Ga_2O_3 films on non-native substrates on which a monolayer of heteroepitaxial w-GaN can be initially grown to serve as the template. Once such template is available, the deposition process would proceed in cycles described above to achieve α-Ga_2O_3 through stepwise construction of an atomic scale hexagonal scaffold of Ga atoms while taking advantage of plasma species to transform nitride to oxide at a low thermal budget. Additionally, this GaN-mediated deposition strategy provides a new platform for direct deployment of GaN dopant candidates to Ga_2O_3 during growth and moving toward realization of bipolar Ga_2O_3 electronic devices. Fabrication of Ga_2O_3 devices on GaN-compatible non-native substrates using this deposition strategy also allows for the transfer of pertinent thermal management technologies that are already established for GaN electronics [56] which will mitigate the low thermal conductivity of Ga_2O_3 and make devices available that are able to concurrently handle higher power, higher voltage, and higher operating temperatures.

In Chapter 4, we present a deposition strategy that achieves high quality β-Ga_2O_3 films by using metastable Ga_2O_3 as an intermediate layer (also referred to as buffer layer and/or seed layer in the following pages) prior to β-Ga_2O_3 deposition. This process enables deposition of high quality β-Ga_2O_3 on substrates (e.g., wafers, membranes, multilayers, or laminated structures) that are compatible with different Ga_2O_3 polymorphs (i.e., not just with β-Ga_2O_3 but also with metastable polymorphs) and paves the way for accelerated development of β-Ga_2O_3 devices on non-native substrates.

In Chapter 5, we investigate the possibility of low temperature growth of gallium oxynitride films by atomic layer deposition (ALD) in an attempt to preserve the crystal structure of w-GaN as the background matrix material while inserting oxygen anions in the GaN lattice to increase the bandgap (and thus the breakdown voltage). We show that we can obtain uniform pinhole-free films for use in electronic device applications or for use as buffer layers in epitaxial growth techniques.

Chapter 6 concludes this thesis and provides directions for future research.

Chapter 2

Low Thermal Budget Heteroepitaxial Gallium Oxide Thin Films Enabled by Atomic Layer Deposition

2.1 Chapter Overview

This work explores the applicability of atomic layer deposition (ALD) in producing highly oriented crystalline gallium oxide films on foreign substrates at low thermal budgets. The effects of substrate, deposition temperature, and annealing process on formation of crystalline gallium oxide are discussed. The Ga_2O_3 films of this work exhibited a strong preferred orientation on the c-plane sapphire substrate. The onset of formation of crystalline gallium oxide is determined, at which only two sets of planes, i.e., α-Ga_2O_3(006) and β-$Ga_2O_3(\bar{4}02)$, are present parallel to the surface. More specifically, this work reports, for the first time, that epitaxial gallium oxide films on sapphire start to form at deposition

temperatures $\geq$ 190°C by using an optimized plasma-enhanced ALD process such that α-$Ga_2O_3(006)\|\alpha$-$Al_2O_3(006)$ and β-$Ga_2O_3(\bar{2}01)\|\alpha$-$Al_2O_3(006)$. Both α-$Ga_2O_3(006)$ and β-$Ga_2O_3(\bar{2}01)$ planes are polar planes (i.e., consisting of only one type of atom, either Ga or O) and, therefore, favorable to form by ALD at such low deposition temperatures. Ellipsometry and van der Pauw measurements confirmed that the crystalline films have optical and electrical properties close to bulk gallium oxide. The film grown at 277°C was determined to have superior properties among as-deposited films. Using Transmission Electron Microscopy (TEM) to locate α-Ga_2O_3 and β-Ga_2O_3 domains in the as-deposited crystalline films, we proposed a short annealing scheme to limit the development of α-Ga_2O_3 domains in the film and produce pure β-Ga_2O_3 films via an energy-efficient process. A pure β-Ga_2O_3 phase on sapphire with β-$Ga_2O_3(\bar{2}01)\|\alpha$-$Al_2O_3(006)$ was successfully achieved by using the proposed process at the low annealing temperature of 550°C preceded by the low deposition temperature of 190°C. The results of this work enable epitaxial growth of gallium oxide thin films, with superior material properties offered by ALD, not only with potential applications as a high-performance material in reducing global energy consumption but also with an energy-efficient fabrication process.

2.2 Experimental Details

Gallium oxide films were deposited on c-plane sapphire, p-Si(100), n-Si(111), and p-Si(110) wafers as well as glass slides by using a Kurt J. Lesker ALD 150-LX system equipped with a remote inductively coupled plasma (ICP) source and a load lock. All wafers were prime quality and polished on one side. Sapphire wafers, in particular, were

epi-polished to $R_a < 0.3$ nm. Detailed specification of the substrates can be found in Appendix A. Substrates were exposed to 60 s oxygen plasma to remove contamination and pretreat the surface right before the depositions. Depositions were done by using an optimized recipe consisting of 0.1 s triethylgallium, TEG (Strem Chemicals, Inc., electronic grade (99.9999% Ga) in stainless steel Swagelok cylinder assembly which was not heated during the depositions), 20 s Ar purge, 10 s oxygen plasma, and 12 s Ar purge (see references [4] and [5] for details of the optimization procedures that were used in this work). The pressure of the reactor was ∼1.1 Torr with ∼1000 sccm continuous flow of Ar. In addition, 60 sccm oxygen was introduced to the reactor during plasma exposure with ∼600 W forward power. This setup is also explained in detail elsewhere [57]. Ar and oxygen gases were of ultrahigh purity (99.999%, Praxair Canada, Inc.). Depositions were done in the ALD window at selected nominal substrate temperatures ($T_{nominal}$) of 130, 200, 250, 300, 350, and 400°C. As per vendor's standard measurements, these nominal temperatures correspond to actual T_{sub}'s of 125, 190, 233, 277, 315, and 352°C, respectively; that is, there is a deviation between the heater set temperature and the actual substrate temperature at larger temperatures since the reactor walls are always kept at colder temperatures than the substrate (chamber walls are kept at 130°C while the top plate of the cylindrical reactor is kept at 120°C). The error in all actual temperatures is ±3°C. A total of 700 cycles of deposition were done at each temperature to get ∼40 nm gallium oxide. At the end of the depositions, the samples were left in the reactor to cool to ∼95°C (under a vacuum of ∼1.1 Torr and with Ar flowing) before transferring out of the reactor.

A J.A. Woollam M-2000DI spectroscopic ellipsometer, permanently mounted on the reactor at an incident angle of 70°, was used for in-situ monitoring of the depositions. In-situ

ellipsometry is a particularly useful technique in this case since the effect of measurement temperature on optical properties of gallium oxide is limited to the third decimal place of the measured values [58]. Ellipsometry measurements using this setup were done in the spectral range of 0.73-6.40 eV (equivalent to 190-1700 nm) at intervals less than 0.05 eV. Data analysis was done by using CompleteEASE software.

Out-of-plane coupled 1D XRD scans were performed by using a Rigaku Ultima-IV diffractometer equipped with a cobalt source, a D/Tex ultrahigh-speed position sensitive detector, and a K-β filter at a scan rate of 2°/min and 0.02° steps (which is equivalent to 0.6 s/step exposure). Out-of-plane coupled 2D XRD (XRD^2) scans were performed by using a Bruker D8 Discover diffractometer equipped with a cobalt source, a Göble mirror, a rotary absorber, a UBC collimator, and a Vantec 500 detector as well as a sample-to-detector distance of 20 cm at an exposure of 450 s/step with 5° increments; 180° φ-rotation at a rate of 60°/min was done for all XRD^2 out-of-plane coupled scans. Experimental details pertinent to off-specular φ-scans to study in-plane orientation can be found in Appendix B.2.

The surface morphology of the films was examined by using a Bruker Dimension Edge atomic force microscope (AFM) with Si cantilevers (Olympus, OMCL-AC160TS-W2) in tapping mode with drive voltages between 2.2 and 2.4 V at a scan rate of 1 Hz. Areas as large as 3 μm by 3 μm were scanned, and the results did not change by analyzing smaller surface areas. NanoScope Analysis software was used to remove tilt by applying a first-order-flattening filter and to analyze the data.

Resistivity was measured by using the van der Pauw method by a Keithley 4200-SCS instrument using 1 pA source current. On the lowest current source ranges (i.e., 1 and 10

pA) of the Keithley 4200- SCS instrument, the input resistance of the voltmeter is > 10^{16} Ω to make measurements on highly resistive samples possible. Prior to measurements, circular contacts consisting of ∼20 nm Ti followed by ∼80 nm Au were sputtered on the top surface of the films.

Cross-section TEM samples were prepared by low-energy ion polishing at 2 kV (to minimize damage) using a ThermoFisher Helios G4 PFIB UXe DualBeam system. TEM images were obtained with high angle annular dark field (HAADF) STEM microscopy at 200 kV by using a Thermo Scientific Themis Z S/TEM instrument.

2.3 Results and Discussion

2.3.1 Bandgap, Thickness, and Optical Properties at Different Deposition Temperatures

The bandgap (E_g), thickness, and optical properties of the films obtained from ellipsometry at the end of 700 deposition cycles at different substrate temperatures on sapphire are shown in Table 2.1 as well as Figures 2.1 and 2.2. Because sapphire is a dielectric with a very wide bandgap (∼9 eV), the Cauchy model was used to determine optical constants of the sapphire substrate over the entire measured spectral range. A delta offset was also added to the model to correct for strained windows. Because the general structure of the gallium oxide film optical constants (n, k) versus wavelength was not known before the measurements, a B-spline model was first used to fit for n, k, and film thickness, and then the model was parametrized to a Tauc–Lorentz model to provide a good starting point for

heater set temp ($T_{nominal}$, °C)	actual deposition temp (T_{sub} ± 3 °C)	thickness (Å)	E_g (eV)	MSE
130	125	391.47 ± 1.55	4.157 ± 0.020	3.402
200	190	369.72 ± 0.86	4.094 ± 0.014	2.837
250	233	391.20 ± 0.72	4.215 ± 0.016	3.139
300	277	397.31 ± 0.55	4.878 ± 0.022	4.715
350	315	383.52 ± 0.58	4.229 ± 0.029	3.731
400	352	371.48 ± 0.53	4.002 ± 0.030	3.060

Table 2.1: Results of modeling the ellipsometry data for Ga_2O_3 films grown on sapphire substrate at different temperatures after 700 cycles of deposition.

fitting a final Tauc–Lorentz model to the experimental data. This procedure was extremely beneficial in obtaining very low mean-squared error (MSE) values for the final fits and obtaining repeatable fit results (including n, k, E_g, and thickness).

As shown in Table 2.1, after 700 deposition cycles, the thickness of all the films is ∼38 nm on average, resulting in an overall growth per cycle (GPC) of 0.55 ± 0.02 Å/cycle in the temperature range 125-352°C. The values of GPC on sapphire were in close agreement with GPC values obtained on p-Si(100).

The bandgap of gallium oxide depends on its crystal structure. For instance, α-Ga_2O_3, which is a metastable phase of gallium oxide, has the largest bandgap of ∼5.2 eV among all gallium oxide polymorphs; meanwhile, the bandgap of β-Ga_2O_3, which is the most stable phase of gallium oxide, is relatively smaller and varies between 4.6 and 4.9 eV in the literature reports [11]. Furthermore, the presence of localized electronic states (such as defect states) is known to cause the value of optical bandgap to appear smaller than single-crystal values. Optical constants of gallium oxide also depend on its crystal structure with α-Ga_2O_3 having a larger refractive index (n) than β-Ga_2O_3, which is consistent with the higher packing density of atoms in α-Ga_2O_3 compared to β-Ga_2O_3 (i.e., α-Ga_2O_3 has a smaller molar volume than β-Ga_2O_3) [22, 23]. Furthermore, presence of amorphous

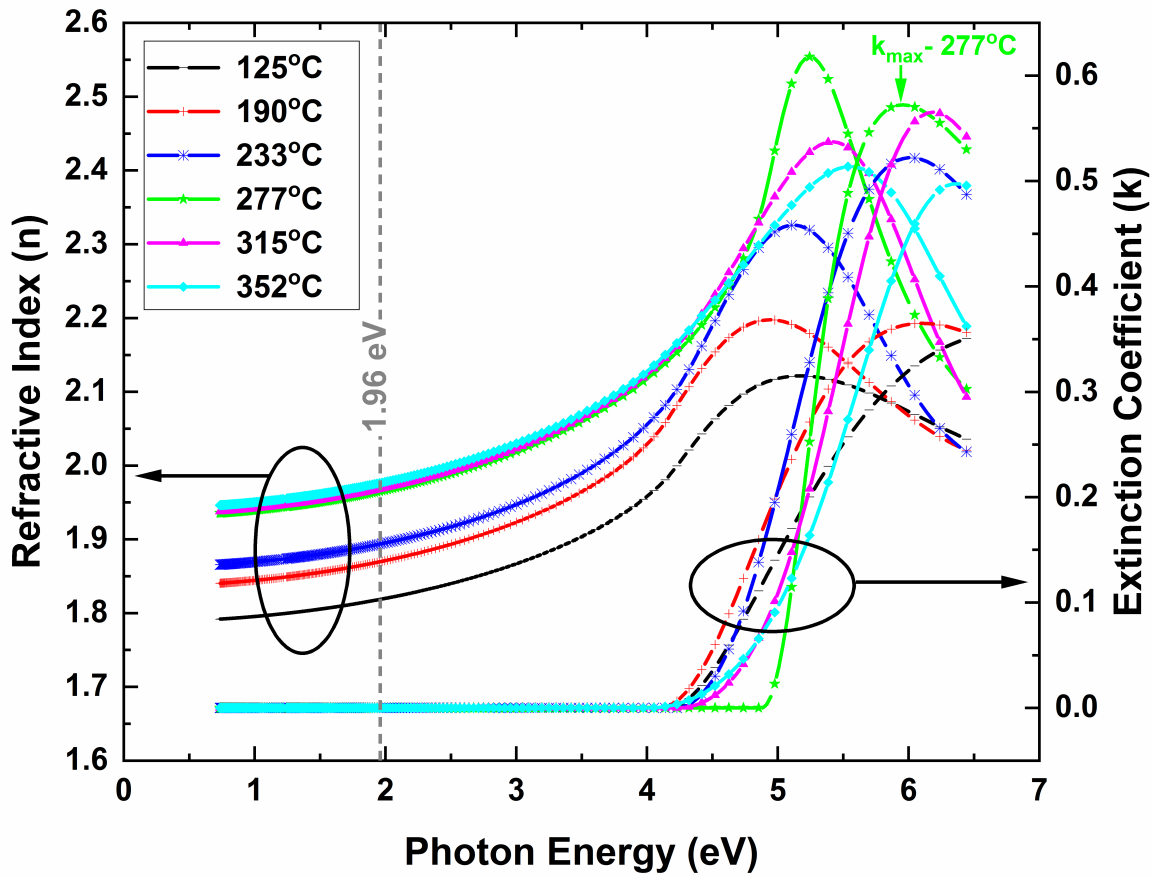

Figure 2.1: Optical constants of Ga_2O_3 films grown on sapphire at the end of the deposition (i.e., after 700 cycles) as a function of photon energy. The photon energy corresponding to 632.8 nm (i.e., 1.96 eV) has been identified by a dashed line for reference, and the maximum value of the extinction coefficient for the film deposited at 277°C has been identified and labeled to provide an example of identifying k_{max}.

phase results in a decrease in the value of refractive index compared to extended crystalline phases.

Figure 2.1 shows the dispersion of refractive index (n) and extinction coefficient (k) for gallium oxide films deposited at different temperatures on sapphire in this study over the entire measured spectral range based on the final Tauc–Lorentz models. In addition, Figure 2.2 compares the optical bandgap for the same gallium oxide films as well as their refractive index (n) at the selected photon energy of 632.8 nm (equivalent to 1.96 eV) at which light absorption does not occur in gallium oxide (i.e., k = 0 at 632.8 nm). As evident from both

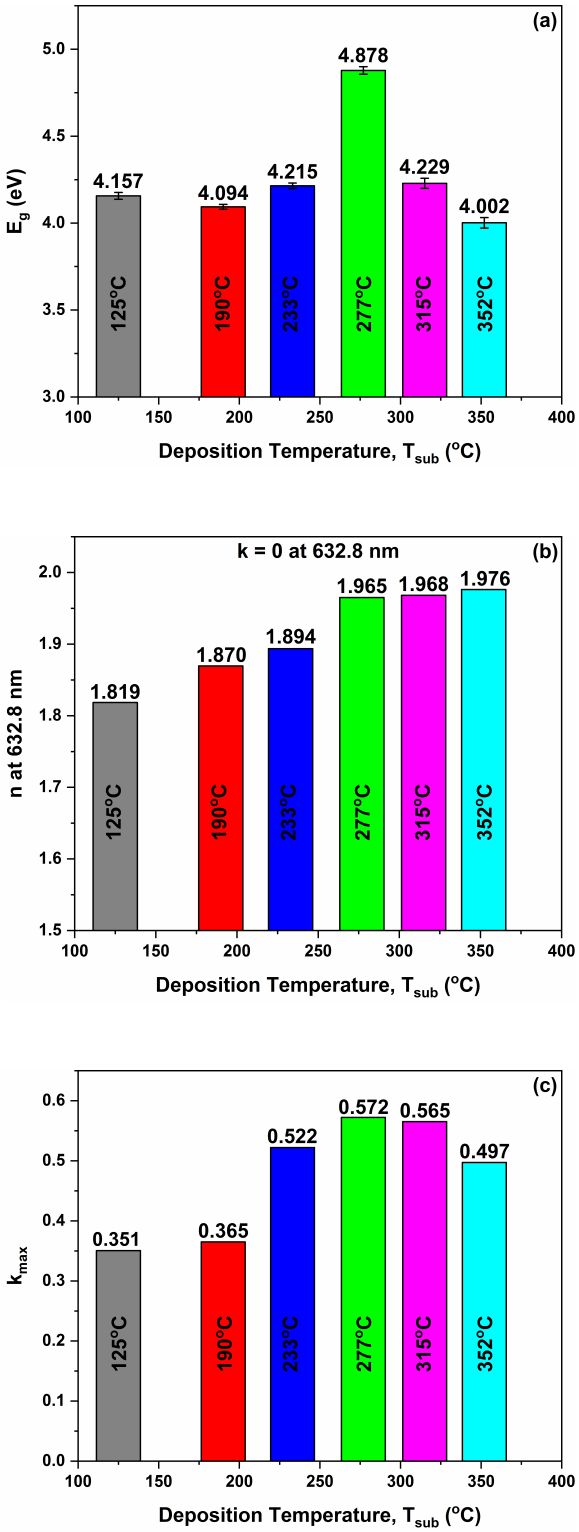

Figure 2.2: (a) Bandgap, (b) refractive index at 632.8 nm, and (c) maximum value of extinction coefficient for Ga_2O_3 films grown on sapphire at different temperatures after 700 cycles of deposition. The error in refractive index and extinction coefficient values is limited to ±0.001 in all cases.

Figures 2.1 and 2.2b, films deposited at lower temperatures of 125 and 190°C have a lower refractive index in the entire spectral range (including at 632.8 nm) compared to higher temperature films. Based on Figure 2.2a, the low-temperature films also have lower optical bandgaps compared to that of bulk gallium oxide. Therefore, these low-temperature films are expected to have a relatively large defect density and high amorphous content. On the other hand, the film grown at T_{sub} = 277°C has the largest bandgap and comparatively large refractive indices in the measured spectral range; therefore, this film is anticipated to have a higher crystalline quality with possible presence of the α-phase (i.e., the metastable phase with the largest bandgap). As the deposition temperature increases beyond 277°C, the films show refractive index values close to the 277°C film; therefore, they are also expected to be dense and crystalline but with lower amount of α-phase or more defects based on their lower bandgap values compared to the 277°C film (see Figure 2.2a). XRD and cross-section TEM measurements were performed to assess these hypotheses (see sections 2.3.3 and 2.3.4). Based on the Tauc–Lorentz model [59], as the photon energy (or the frequency) of the incident light increases, light absorption starts to occur near the bandgap energy (below which k = 0, indicating no light absorption) and goes up further until it reaches a maximum value (i.e., k_{max}) when the oscillation frequency of the incident electromagnetic wave of light just passes the resonant frequency of the Lorentz oscillator for electric polarization. As the photon energy increases further, the frequency of the incident light becomes too large for the electrons to follow, and therefore k decreases. This is consistent with the dispersion curves of k presented in Figure 2.1. As shown in Figure 2.1, no light absorption occurs at photon energies less than E_g (i.e., k = 0), and the maximum value of extinction coefficient (k_{max}) occurs at photon energies greater than E_g for each film. The k_{max} values

for gallium oxide films grown at different temperatures are extracted from Figure 2.1 and depicted in Figure 2.2c. Comparing k_{max} values, we observe that the films grown at higher temperatures show a larger value of maximum k than the films grown at lower temperatures. A larger value of k_{max} represents a larger concentration of free carriers in the conduction band after the free carriers have been excited to the conduction band by photons having high-enough energy. If the electron mobility in the films is similar or follows the same trend as k_{max}, one would expect that the films grown at higher temperatures be more conductive than the films grown at lower temperatures. The resistivity of the films was measured by using the van der Pauw method to evaluate this hypothesis (see section 2.3.2).

2.3.2 Resistivity as a Function of Deposition Temperature

Commercially available β-Ga_2O_3 wafers [60, 61] are reported to have resistivities > 10^6 MΩ·cm, with Fe-doped insulating β-Ga_2O_3 having resistivity > 10^{10} MΩ·cm. The resistivity of the wafers can be decreased by different doping strategies. On the other hand, it is well-known that very thin films (< 200 nm) have higher resistivity values compared to those of bulk wafers due to size constraints, surface effects, and so on. The results of van der Pauw resistivity measurements on films grown on sapphire are summarized in Figure 2.3.

All the films have resistivity values close to bulk wafers (i.e., $\sim 10^6$ MΩ·cm) despite their very thin nature (only ∼38 nm; see Table 2.1 for exact thickness values). In particular, the film grown at T_{sub} = 277°C has the lowest resistivity, which is consistent with the fact that k_{max} for this film was the highest among all the films (see Figure 2.2). It is worth

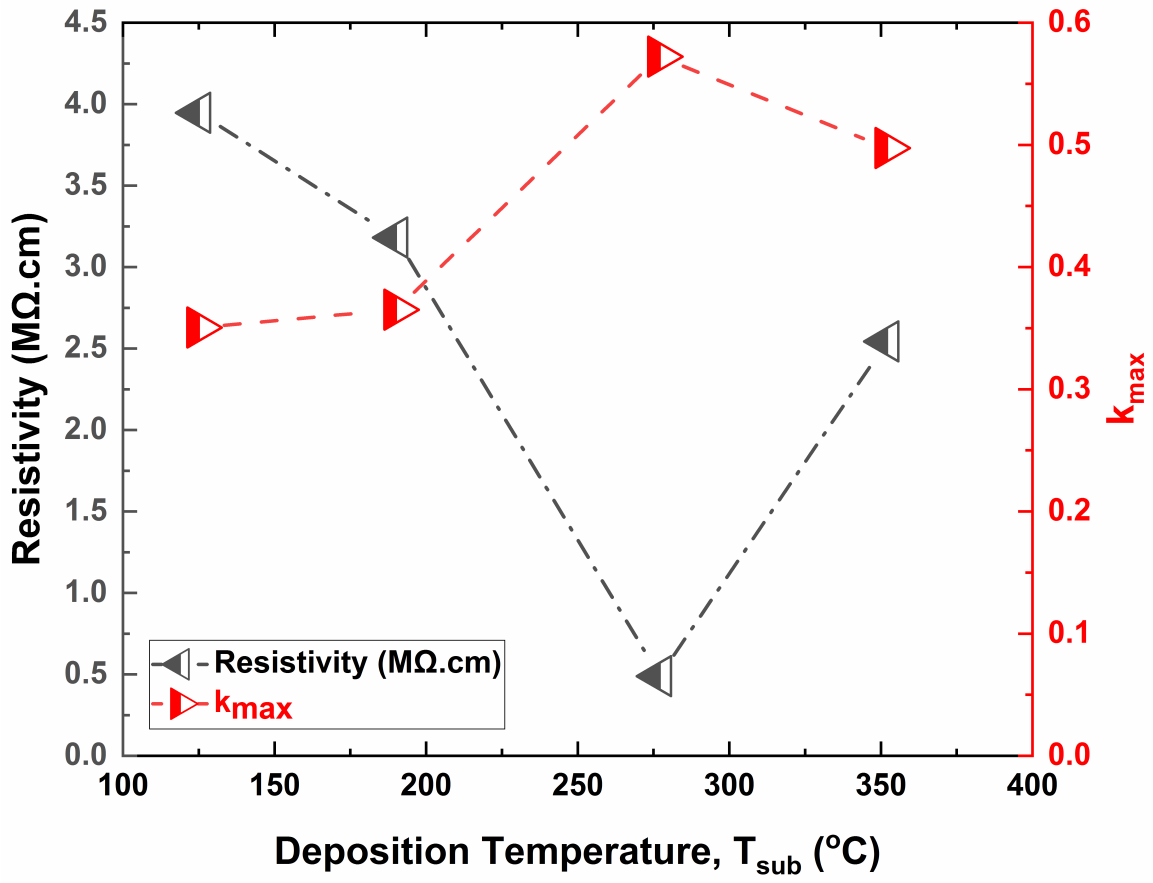

Figure 2.3: Resistivity of ∼38 nm Ga_2O_3 films grown on sapphire as a function of deposition temperature. For comparison, the maximum value of the extinction coefficient (k_{max}) obtained from in-situ ellipsometry measurements at the end of the depositions is also plotted. In all cases, the error in resistivity and extinction coefficient values is limited to ±0.078 MΩ·cm and ±0.001, respectively.

noting that the film grown at T_{sub} = 277°C also had the largest bandgap and high refractive indices compared to the other as-deposited films studied in this work (see section 2.3.1). Specifically at 632.8 nm, as shown in Figure 2.2b, the 277°C film has a high refractive index of 1.965, which is exceptionally close to the reported value of 1.97 for bulk β-Ga_2O_3 wafers [60]. These observations indicate that T_{sub} = 277°C achieves the highest quality among as-deposited films while maintaining a low thermal budget deposition process.

2.3.3 Crystal Structure as a Function of Deposition Temperature

XRD patterns were obtained for gallium oxide samples grown at different deposition temperatures on sapphire, Si(100), Si(111), Si(110), and glass. In each case, the XRD pattern of the corresponding substrate was used as a reference to better distinguish thin film peaks in the patterns. No crystallinity was observed on Si(100), Si(111), Si(110), and glass at any deposition temperatures studied in this work. Meanwhile, gallium oxide films on sapphire showed peaks in their XRD patterns at $T_{sub} \geq 190°C$.

Figure 2.4 shows the results of out-of-plane 1D coupled XRD scans of the films deposited on sapphire as well as the corresponding scan of the bare sapphire substrate as reference. The patterns have been converted to Cu wavelength for easier comparison with literature patterns. The single crystal c-plane sapphire substrate is expected to show a peak at $2\theta = 41.80°$ corresponding to α-Al_2O_3(006) planes (considering the average of K-α1 and K-α2 peak locations) [62]. The α-Al_2O_3(006) peak is evident in Figure 2.4 as the strongest peak. It is worth noting that in the diffraction pattern of powdered α-Al_2O_3 with completely random grains this peak is expected to show very weak intensity (having $\sim 1\%$ of the intensity of the strongest peak in α-Al_2O_3 powder diffraction pattern). However, since the c-plane sapphire substrate is a highly oriented single-crystal form of α-Al_2O_3 with (006) planes parallel to the substrate surface, the intensity of this peak will become extremely strong in out-of-plane coupled XRD measurements, and all the other peaks from the α-Al_2O_3 powder diffraction pattern will become relatively weak or absent.

Comparing the reference sapphire pattern with patterns of the thin film coated samples in Figure 2.4, four major peaks can be distinguished as thin film peaks corresponding to

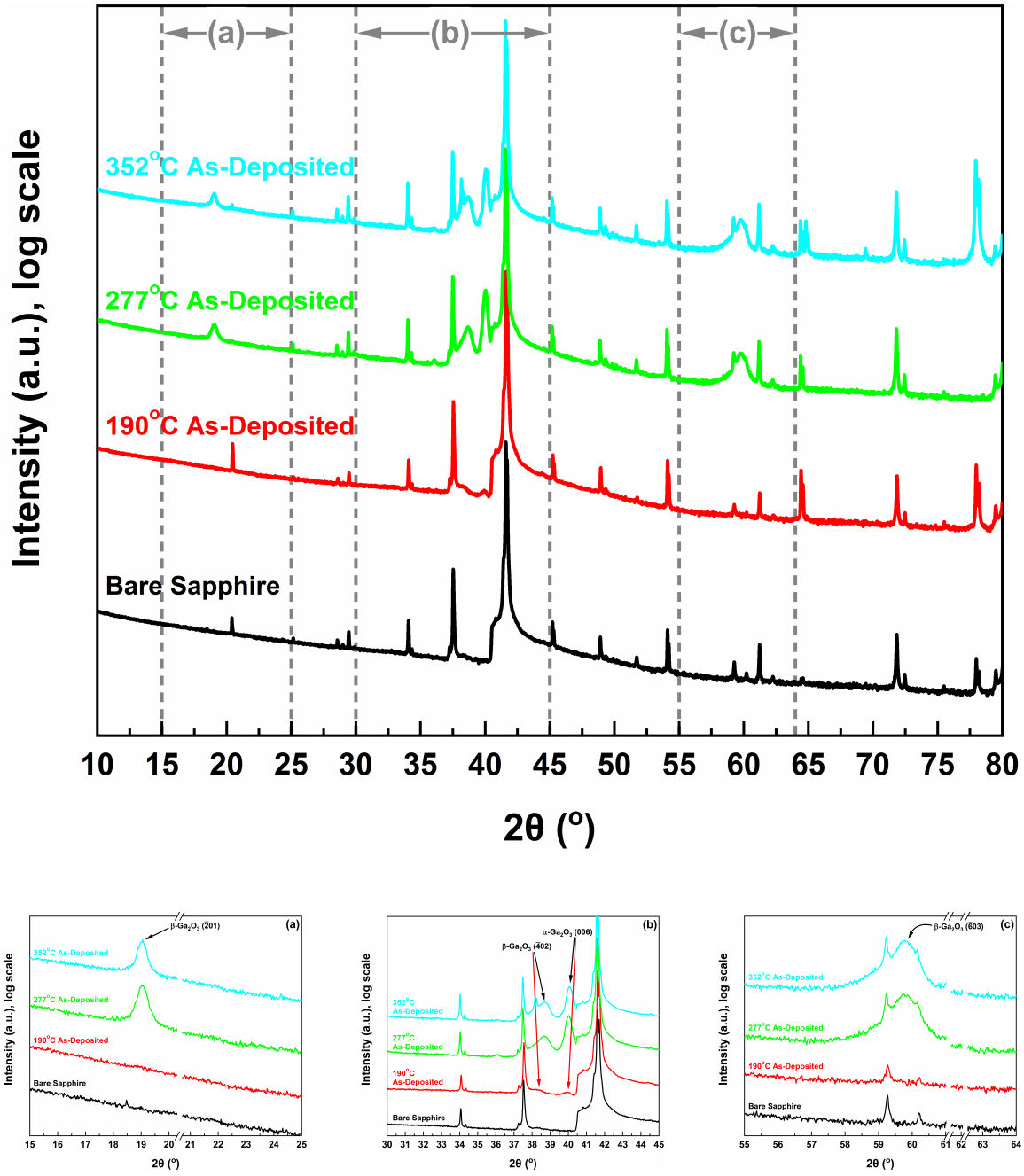

Figure 2.4: 1D XRD patterns for Ga_2O_3 samples grown on sapphire at T_{sub} = 190, 277, and 352°C. 1D XRD pattern of the bare c-plane sapphire substrate is included as reference to help distinguish thin film peaks in the patterns. Regions of the patterns that include thin film peaks are shown in more detail in the bottom panels (a), (b), and (c). The data have been collected using cobalt X-ray source. However, the patterns have been converted to Cu wavelength for easier comparison with literature patterns.

	observed intensity ratio ±0.01% (assuming 100% for the strongest thin film peak of each corresponding phase)			simulated powder intensity ratio (assuming 100% for the strongest powder peak of each corresponding phase)
peak location in Cu wavelength	T_{sub} = 190 °C	T_{sub} = 277 °C	T_{sub} = 352 °C	
β-Ga_2O_3 $(\bar{2}01)$ at 18.97°		65.59	55.34	8.04
β-Ga_2O_3 $(\bar{4}02)$ at 38.50°	100.00	100.00	100.00	2.85
β-Ga_2O_3 $(\bar{6}03)$ at 59.27°		42.48	47.35	6.59
α-Ga_2O_3 (006) at 40.30°	100.00	100.00	100.00	3.00

Table 2.2: List of thin film peaks observed in both 1D XRD and 2D XRD out-of-plane coupled scans of as-deposited samples in this study along with their observed intensity ratio as well as their expected intensity ratio based on gallium oxide powder diffraction patterns.

regularly arranged planes of gallium oxide parallel to the surface. Table 2.2 lists these peaks, their observed intensity ratio relative to the strongest peak present for each gallium oxide phase in the thin films, and their intensity ratio expected based on gallium oxide powder diffraction patterns (gallium oxide powder diffraction patterns were simulated by using VESTA software [63] based on lattice and structure parameters retrieved from .cif files of refs [64] and [65] as well as refs [24] and [25]).

As can be seen in Figure 2.4 and Table 2.2, planes from two phases of gallium oxide, i.e., α-Ga_2O_3 and β-Ga_2O_3, are present in the diffraction pattern of the thin films.

β-$Ga_2O_3(\bar{2}01)$, $(\bar{4}02)$, and $(\bar{6}03)$ planes are present at 2θ = 18.97°, 38.50°, and 59.27°, respectively. No other peaks from β-Ga_2O_3 are present in the out-of-plane coupled 1D XRD patterns, which indicates strong preferential orientation of β-Ga_2O_3 phase in the films such that the b-axis of β-Ga_2O_3 is parallel to the substrate surface (or equivalently, perpendicular to the c-axis of sapphire) and β-$Ga_2O_3(\bar{2}01) \| \alpha$-$Al_2O_3(006)$.

Meanwhile, the metastable α-$Ga_2O_3(006)$ peak is also present at 2θ = 40.30°. α-Ga_2O_3 is isostructural to sapphire, both belonging to the space group $R\bar{3}c$, with only $\sim$4.77% lattice mismatch in a-axis and $\sim$3.50% in c-axis (lattice mismatch calculated based on the assumption that thickness of both crystals are similar, and therefore they can be treated by the same footing [66]). As listed in Table 2.2, the α-$Ga_2O_3(006)$ peak is also very strong in the thin film patterns compared to its simulated powder pattern intensity. This indicates strong preferential orientation of the α-Ga_2O_3 phase in the films such that the c-axis of α-Ga_2O_3 is parallel to the c-axis of sapphire (or equivalently, c-axis of both materials perpendicular to the substrate surface). In other words, α-$Ga_2O_3(006) \| \alpha$-$Al_2O_3(006)$.

Because 1D XRD scans have a higher resolution than XRD^2 scans, they were also used to determine the onset deposition temperature for crystallinity. As shown in Figure 2.4, the results confirm presence of both α-$Ga_2O_3(006)$ peak and β-$Ga_2O_3(\bar{4}02)$ peak at T_{sub} = 190°C, both with relatively similar and very low intensity, indicating the small population of these planes in the sample. T_{sub} = 190°C was the lowest temperature at which any thin film peaks were observed, indicating that 190°C is the onset of formation of crystalline phases in the film.

To examine the preferred orientation of the phases observed in Figure 2.4 further, out-of-plane XRD^2 coupled scans of the films deposited on sapphire along with the corre-

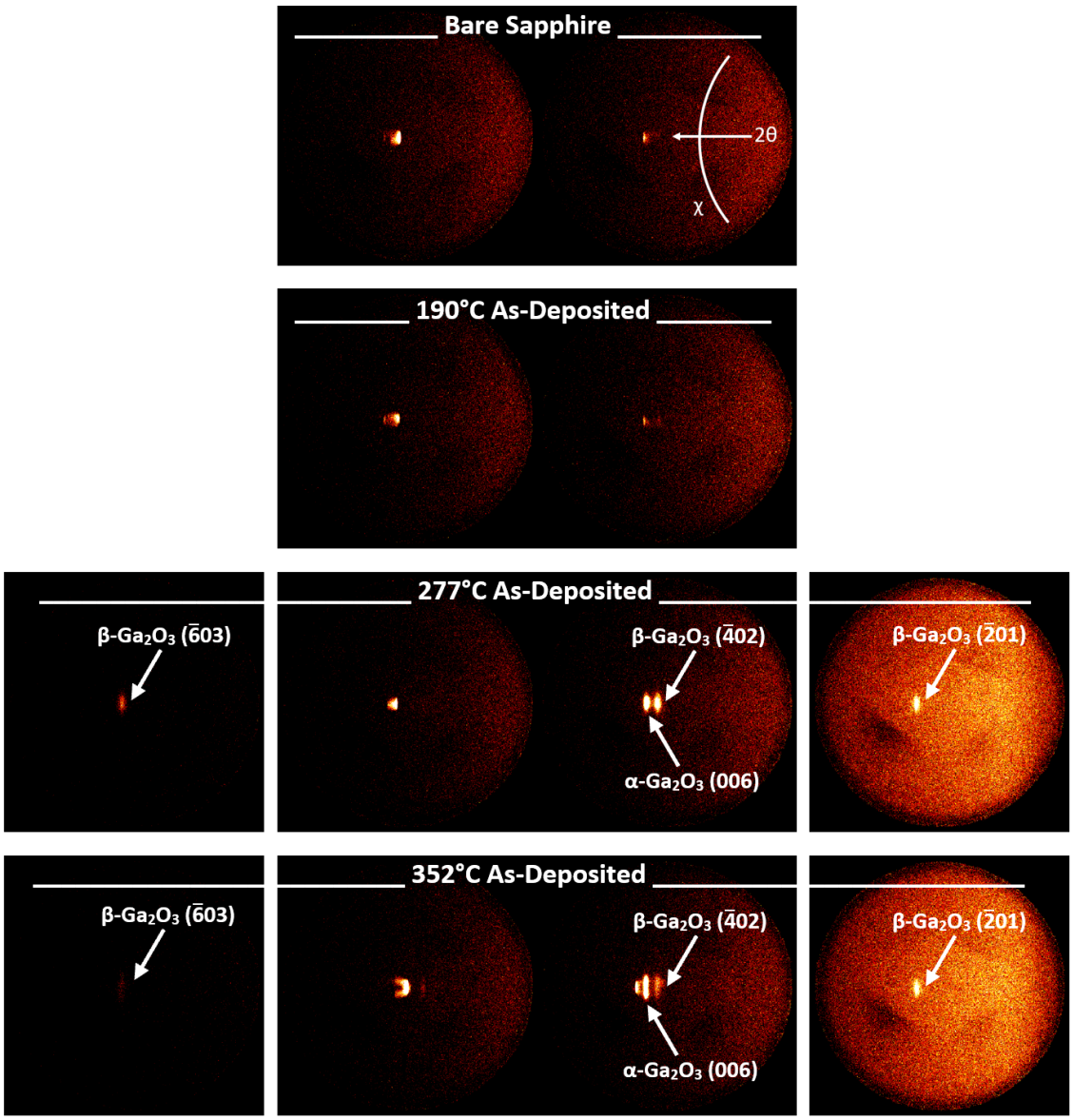

Figure 2.5: Coupled 2D XRD (XRD^2) patterns for Ga_2O_3 samples grown on sapphire at T_{sub} = 190, 277, and 352°C. The first panel shows an example of how 2θ and χ change in the XRD^2 patterns. All unlabeled peaks in the XRD^2 patterns correspond to the bare c-plane sapphire substrate peaks. φ-rotation has been done while collecting each individual scan frame to increase the chance of capturing misorientations.

sponding scan of the bare sapphire substrate as reference were also collected. To increase the chance of capturing any randomness or misorientation of existing crystal planes, φ-rotation (i.e., rotation about the normal to the substrate surface) has been performed while collecting each individual scan frame shown in Figure 2.5 (see section 2.2 for details).

The first panel in Figure 2.5 shows an example of how 2θ and χ change in the XRD^2 patterns: while χ changes along the circumference of each given arc, 2θ changes when moving horizontally from one arc to another (i.e., all points on the circumference of a given arc have the same 2θ). Any peaks observed at different 2θ values (i.e., at different horizontal locations) are indicative of the existence of a new set of crystal planes. Meanwhile, any peak broadening observed along χ (i.e., on the circumference of a given 2θ arc) is indicative of the degree of randomness of that specific set of crystal planes. As an example, sapphire peaks show minimum broadening in χ because the sapphire substrate is single crystal and extremely oriented. On the contrary, powders and polycrystalline films would show continuous or elongated intensity distributions along χ, respectively.

Comparing XRD^2 patterns of the thin film coated samples with the sapphire reference in Figure 2.5 reveals that the gallium oxide films are crystalline at T_{sub} = 277 and 352°C as is apparent from the presence of additional bright spots in their XRD^2 patterns. Furthermore, the narrow point-like distribution of intensities in the XRD^2 patterns in Figure 2.5 indicates that the films are not polycrystalline but have a strong preferential orientation (film intensity distributions along χ are as narrow as the single-crystal substrate intensity distributions). It is worth noting that at the lower temperature of 190°C, where 1D XRD had shown two weak peaks (corresponding to α-Ga_2O_3(006) and β-$Ga_2O_3(\bar{4}02)$) both with relatively the same but low intensity (see Figure 2.4 for reference), the peaks are not readily detected

in XRD^2 scans due to the very low intensity of the peaks as well as the limited resolution of the instrument. Nevertheless, XRD^2 scans still provide an efficient means to examine the overall crystallinity of each sample (including degree of preferred orientation of thin film lattice planes) over a wide range of χ, 2θ, and φ. In Figure 2.5, they are aimed at complementing 1D XRD scans of Figure 2.4 by examining randomness in crystalline films specifically by examining peak broadening along χ. Meanwhile, 1D XRD scans, which have higher resolution, were used to determine exact peak positions and to establish the onset of crystallinity.

As seen in Figure 2.5, at T_{sub} = 277°C, the α-Ga_2O_3(006) peak and the β-$Ga_2O_3(\bar{4}02)$ peak are strongly evident in the XRD^2 scans, both located at the low angle side of the sapphire(006) peak and both showing minimum broadening in χ similar to the single-crystal substrate. At T_{sub} = 352°C, the same peaks appear at the low angle side of the sapphire(006) peak. However, they are slightly more elongated along the χ direction, which indicates slightly less preferred orientation at T_{sub} = 352°C. We also observed that the crystalline film grown at T_{sub} = 352°C has a lower bandgap and slightly lower surface roughness compared to the crystalline film grown at T_{sub} = 277°C (see sections 2.3.1 and 2.3.5). Even though it is expected that films grown at higher temperatures show an improved crystalline quality, a slight loss of preferential orientation at this temperature has also been observed in our group's previous work on plasma-enhanced ALD growth of GaN using the same gallium precursor (i.e., triethylgallium (TEG)) [67]. It is reported that decomposition of TEG in H_2 and N_2 atmospheres takes place in the temperature ranges 220-330 and 270-380°C, respectively, in both cases through β-elimination [68]. However, the reactor walls in our deposition system are held at temperatures $\leq$ 130°C where TEG decomposition does not

occur (see section 2.2 for details). It is only at the vicinity of the substrate surface that the temperature is high enough for TEG decomposition to occur. We believe that at T_{sub} = 352°C in the Ar atmosphere of the reactor TEG decomposition may initiate near or at the surface, causing a partial change in the chemical reaction pathway (including slight poisoning of the surface with precursor ligands) and therefore a subtle loss of the expected crystallinity. However, the changes must be slight since crystallinity is not lost and the GPC is not significantly affected. This also indicates that the oxygen plasma is effective in removing any precursor ligands that may remain on the surface.

Rocking scans that capture the three closely located α-Al_2O_3(006), α-Ga_2O_3(006), and β-$Ga_2O_3(\bar{4}02)$ peaks were performed as well to examine the broadness of these peaks. The corresponding results, showing relatively narrow peaks (thereby confirming the high crystalline quality of the films), are presented in the Appendix. Strain in the films is also briefly discussed based on the rocking scan results in the Appendix. In addition to the highly oriented out-of-plane texture of the Ga_2O_3 films presented so far, we also performed off-specular φ-scans to examine in-plane orientation of the films (specifically the β-Ga_2O_3 phase) by studying planes that are nonparallel to the surface of the films on sapphire substrate. The results are presented in the Appendix and show three in-plane orientations of β-Ga_2O_3 matching the symmetry of the underlying sapphire substrate with approximately same population and all with the same normal orientation of β-$Ga_2O_3(\bar{2}01)\|\alpha$-$Al_2O_3$(006), which is consistent with previous observations in the literature [69–72].

Even though XRD provides proof of the presence of crystalline phases in the thin films and their degree of preferred orientation, it cannot provide information about the location of the crystalline phases within the film. To provide a more comprehensive picture of the

epitaxial relationship between the films and the substrate, cross-section TEM images were obtained. Section 2.3.4 provides a more complete picture of the nature of crystallinity in gallium oxide ALD films by studying cross-section TEM images that show the location of different crystalline phases in the film.

2.3.4 Cross-Section TEM Analysis of Gallium Oxide on Sapphire Grown at 277°C

High angle annular dark field (HAADF) STEM images of the gallium oxide film grown at T_{sub} = 277°C along with the sapphire substrate and their interface are shown in Figure 2.6. Individual atomic columns can be seen in this figure as a result of using a subangstrom STEM probe with high current. It is evident from Figure 2.6 that the first few monolayers of gallium oxide near the substrate interface are α-gallium oxide and completely coherent with the substrate (i.e., pseudomorphism). This is consistent with the results of the XRD scans and confirms the epitaxial relationship of α-$Ga_2O_3(006)\|\alpha$-$Al_2O_3(006)$. The formation of such pseudomorphic α-Ga_2O_3 monolayers along the sapphire interface could be a result of the 60 s oxygen plasma pretreatment which was performed in situ right before the ALD depositions and provided a starting surface consisting of an extended array of oxygen atoms completely coherent with the underlying sapphire substrate. Beyond the first few α-Ga_2O_3 pseudomorphic monolayers at the interface, either more α-$Ga_2O_3(006)$ planes or highly oriented β-$Ga_2O_3(\bar{2}01)$ planes start to appear in the bulk of the film, both oriented parallel to the substrate surface. XRD results also indicated the presence of highly oriented β-$Ga_2O_3(\bar{2}01)$, $(\bar{4}02)$, and $(\bar{6}03)$ planes oriented parallel to α-$Al_2O_3(006)$ planes. Both α-

$Ga_2O_3(006)$ and β-$Ga_2O_3(\bar{2}01)$ family of planes are polar planes (i.e., they contain only one type of atom, either gallium or oxygen), and therefore formation of these planes is favorable in ALD due to the stepwise nature of the ALD process that consists of self-limiting reactions which introduce each precursor or reactant to the surface one by one.

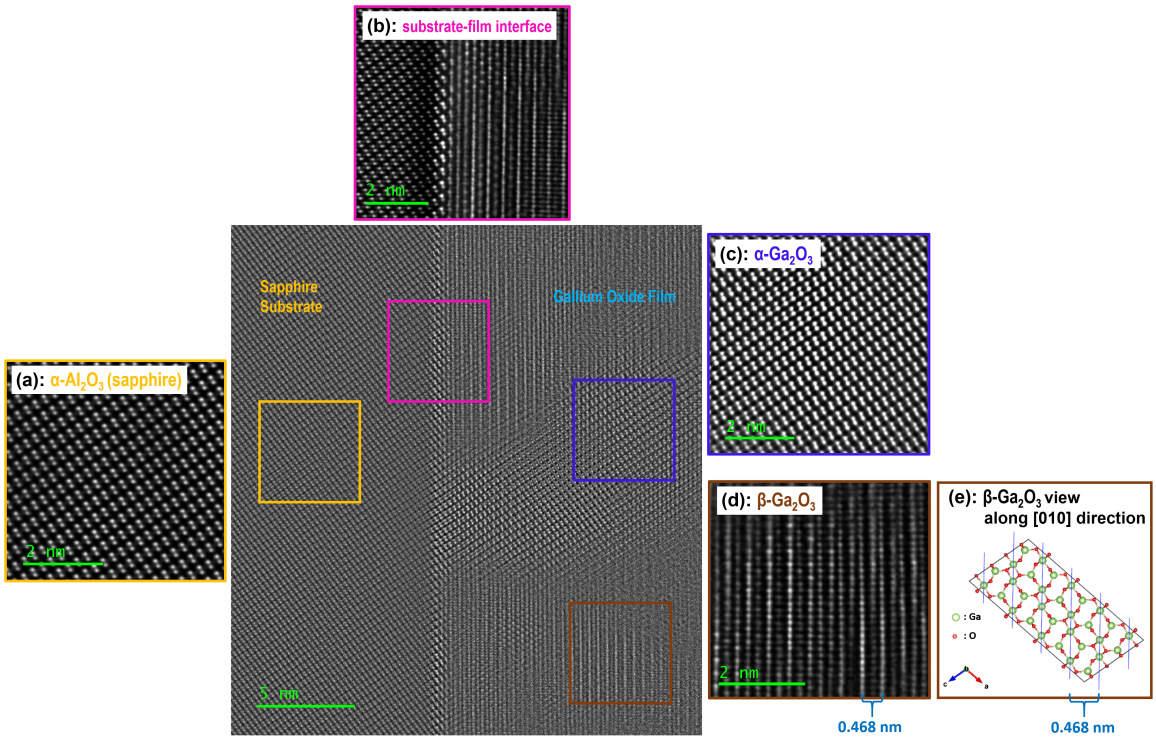

Figure 2.6: Atomic resolution HAADF STEM images of the Ga_2O_3 film grown on sapphire at T_{sub} = 277°C showing individual atomic columns of the film and the substrate. Bright dots correspond to individual gallium and aluminum atoms of the film and the substrate, respectively. Frame (e) depicts a VESTA schematic of β-Ga_2O_3 crystal [Ga atoms are larger green spheres, oxygen atoms are smaller red spheres] showing $(\bar{2}01)$ planes in blue alongside frame (d) which focuses on the actual β-Ga_2O_3 domains in the as-deposited film.

To provide a more clear picture of the highly oriented β-$Ga_2O_3(\bar{2}01)$ planes in the 277°C as-deposited sample, Figure 2.6 also shows a schematic of the corresponding β-gallium oxide planes in a perfect β-gallium oxide crystal simulated in VESTA [63, 64]. In addition to the matching distance of ∼0.468 nm for β-$Ga_2O_3(\bar{2}01)$ planes in the simulated crystal and the TEM images, the resemblance of the simulated and the actual β-Ga_2O_3

images in showing the location of high electron density gallium atoms in β-Ga_2O_3 is interesting and provides visual guidance of the quality of the β-Ga_2O_3 phase in the ALD films presented in this work. As can be visually seen in the VESTA-simulated β-gallium oxide crystal in Figure 2.6e as well, β-$Ga_2O_3(\bar{2}01)$, $(\bar{4}02)$, and $(\bar{6}03)$ planes are polar planes containing only one type of atom, either Ga or O. We believe this facilitates formation of epitaxial β-$Ga_2O_3(\bar{2}01)\|\alpha$-$Ga_2O_3(006)\|\alpha$-$Al_2O_3(006)$ during ALD cycles, which introduce separated Ga and O sources to the reactor in a stepwise manner, and will help in obtaining such epitaxial films at much lower temperatures by ALD compared to other deposition techniques.

It is worth noting that lower magnification (i.e., larger view area) STEM images (images not presented here) showed that the 277°C film was crystalline for almost the entire thickness and not just at the vicinity of the substrate. The large view in Figure 2.6 also confirms that presence of α-Ga_2O_3 is extended well beyond the substrate interface at some locations. Based on the TEM observations of the location of α-Ga_2O_3 and β-Ga_2O_3 in the film, an annealing strategy is employed in section 2.3.6 to hinder development of α-Ga_2O_3 beyond the few monolayers at the interfacial region and therefore obtain pure β-Ga_2O_3 phase in the bulk of the film.

2.3.5 Surface Roughness as a Function of Deposition Temperature

Surface roughness is an important indicator of the morphology of thin films [73]. AFM measurements were performed on gallium oxide films deposited on sapphire at several locations on each sample, and the representative statistics are shown in Table 2.3. If one

	bare sapphire	125 °C	190 °C	277 °C	352 °C
R_a (nm)	0.058	0.346	0.234	0.444	0.330
R_q (nm)	0.073	0.444	0.306	0.557	0.425
R_{max} (nm) (= max Z range)	0.84	4.23	3.27	5.22	3.50
skewness [compared to zero]	+0.096	+0.825	+1.070	−0.256	+0.700
kurtosis [compared to 3]	3.45 [almost normal]	4.31 [slightly spiked]	5.15 [spiked]	3.13 [normal]	3.81 [almost normal]

Table 2.3: AFM statistics for ∼38 nm Ga_2O_3 films grown on sapphire as a function of deposition temperature. While the nominal average roughness of the c-plane sapphire substrate is R_a < 0.3 nm, an example of actual statistics for a piece of bare sapphire is also included for reference.

uses the nominal average roughness of the bare sapphire substrate as a reference (R_a < 0.3 nm), it is evident that all of the films listed in Table 2.3 are very smooth based on their corresponding values of R_a. In all cases, root-mean-square roughness (R_q) is slightly larger than the average roughness (R_a), which is expected since R_a is known to represent the mean absolute profile, making no distinction between peaks and valleys, while R_q is more sensitive to peaks and valleys due to squaring of the amplitude in its calculation [74]. As shown in Table 2.3, the film grown at T_{sub} = 277°C is the roughest among all films with the largest R_a, R_q, and R_{max} (even though these values are still small by themselves). This could be attributed to the fact that the film grown at T_{sub} = 277°C is a crystalline film consisting of a mixture of highly oriented α- and β-gallium oxide phases even near the top surface (as confirmed by XRD and TEM results in sections 2.3.3 and 2.3.4) which makes this film appear relatively rougher than the other films.

Table 2.3 also lists the skewness parameter as a measure of the degree of bias of the roughness shape. Skewness is not large compared to zero for any of the films, indicating that the height distribution on the surface is almost symmetrical around the mean plane. Another parameter that was extracted from the AFM measurements and is shown in Table 2.3 is the kurtosis value as a measure of the population of sharp features in the surface

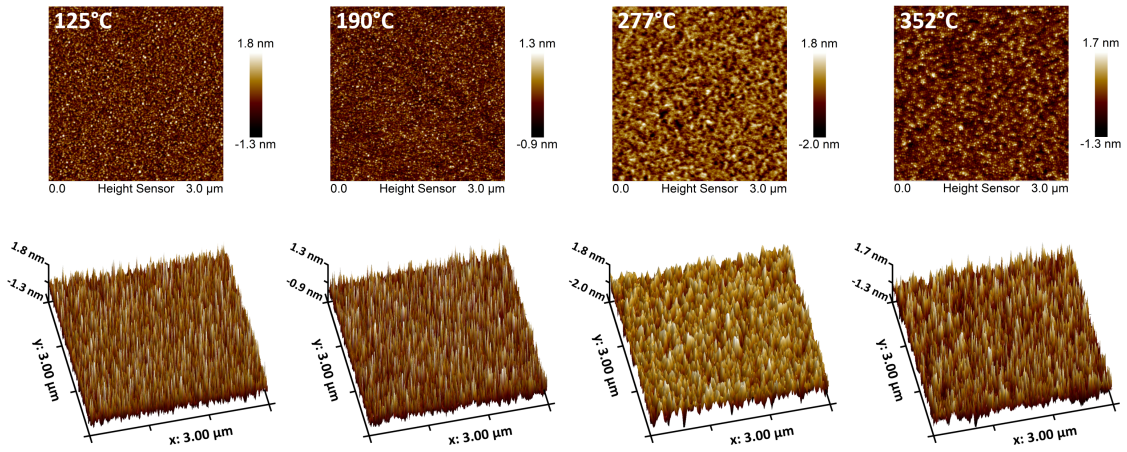

Figure 2.7: 2D and 3D AFM profiles for ∼38 nm Ga_2O_3 films grown on sapphire as a function of deposition temperature.

profile. A value of 3 for the kurtosis parameter indicates that sharp and indented features occur equally frequently in the height distribution, similar to a normal distribution, and that the population of outliers is negligible. As listed in Table 2.3, the film grown at T_{sub} = 190°C has a spiked height distribution indicated by its large kurtosis value. This could be attributed to the fact that this temperature is the onset of crystallinity for gallium oxide films on sapphire. Therefore, formation of crystalline domains within the mainly amorphous background material can cause the appearance of comparatively sharp features in the surface profile of the film. Accordingly, the completely amorphous film grown at T_{sub} = 125°C has a smaller kurtosis value. Interestingly, in spite of their crystalline nature, the films grown at higher temperatures (i.e., T_{sub} = 277 and 352°C, especially the former) also have a small kurtosis value, very close to the reference value of 3, which is indicative of a normal height distribution. This, combined with the small roughness value for these high-temperature crystalline films, could be an indication that gallium oxide has a high crystalline quality within the entire thickness of these films and not just near the film-

substrate interface. This is investigated in more detail in section 2.3.4 where cross-section TEM lamellas of the 277°C film were prepared and analyzed to examine their structure both at the film-substrate interface and in the bulk of the film.

Figure 2.7 provides visual representation of surface profile of the gallium oxide films on sapphire deposited at four different temperatures. For each sample, the scales of the 2D and 3D profiles are the same and were set in a way that low population tails in the height distribution are excluded. Figure 2.7 confirms the overall smooth surface of the films, consistent with the low roughness values reported in Table 2.3.

2.3.6 Annealing of Gallium Oxide on Sapphire Grown at 190°C

Analysis of the as-deposited ALD films in this work proves that it is possible to grow highly oriented crystalline gallium oxide films on c-plane sapphire at deposition temperatures that are hundreds of degrees lower compared to other common deposition techniques such as CVD. As mentioned earlier, the polar nature of β-$Ga_2O_3(\bar{2}01)$ planes makes them favorable to form by ALD; however, in as-deposited films, their formation must compete with the formation of α-$Ga_2O_3(006)$ planes which are also polar. Considering that α-Ga_2O_3 is isostructural to the sapphire substrate with very small lattice mismatches, its formation would be considerably favorable for sufficiently thin films especially if the thin film is formed one atomic layer at a time, thereby continuously preserving a substrate-like template at the growth surface as the deposition proceeds. This leads to the coexistence of β-$Ga_2O_3(\bar{2}01)$ planes and α-$Ga_2O_3(006)$ planes in the bulk of as-deposited films (i.e., away from the film-substrate interface). Therefore, if the formation of α-Ga_2O_3 during the ALD deposition can

be minimized in the bulk of the film or be specifically limited to a few monolayers at the film-substrate interfacial region, it could be possible to achieve pure β-Ga_2O_3 phase in the bulk of the film, after the deposition, by providing sufficient energy for short-range diffusion of atoms and subsequent formation of the most stable phase of Ga_2O_3 in the absence of a sustained underlying template that favors the formation of the metastable phases. To that end, instead of depositing the films at high temperatures (such as 277°C or more) to achieve crystallinity, we deposited the gallium oxide films at 190°C (i.e., at the onset temperature of formation of crystallinity in as-deposited films) and carried an annealing study to see whether annealing could improve the achievable crystallinity of gallium oxide ALD films grown at T_{sub} = 190°C and lead to pure β-Ga_2O_3 films in the bulk. The samples were isochronally annealed in air for 1 h at different temperatures between 235 and 550°C, and corresponding outof-plane coupled 1D XRD scans at selected temperatures are presented in Figure 2.8.

As shown in Figure 2.8, crystallinity appeared only at T > 470°C in the form of pure β-gallium oxide with highly oriented $(\bar{2}01)$ planes parallel to sapphire(006) planes (i.e., no α-gallium oxide peaks exist). Observing highly oriented single-phase ALD-grown gallium oxide films at such low annealing temperature has not been reported in the literature before and, we believe, is due to the fact that our starting film was at the onset of crystallinity instead of being completely amorphous which facilitated formation of epitaxial β-$Ga_2O_3(\bar{2}01)\|\alpha$-$Al_2O_3(006)$ at low annealing temperatures. In other words, we believe that by performing the ALD process at T_{sub} = 190°C development of α-Ga_2O_3 domains as a result of a preserved underlying crystalline template (similar to the case of layer-by-layer ALD growth at higher temperatures) has become limited in the bulk of the film while

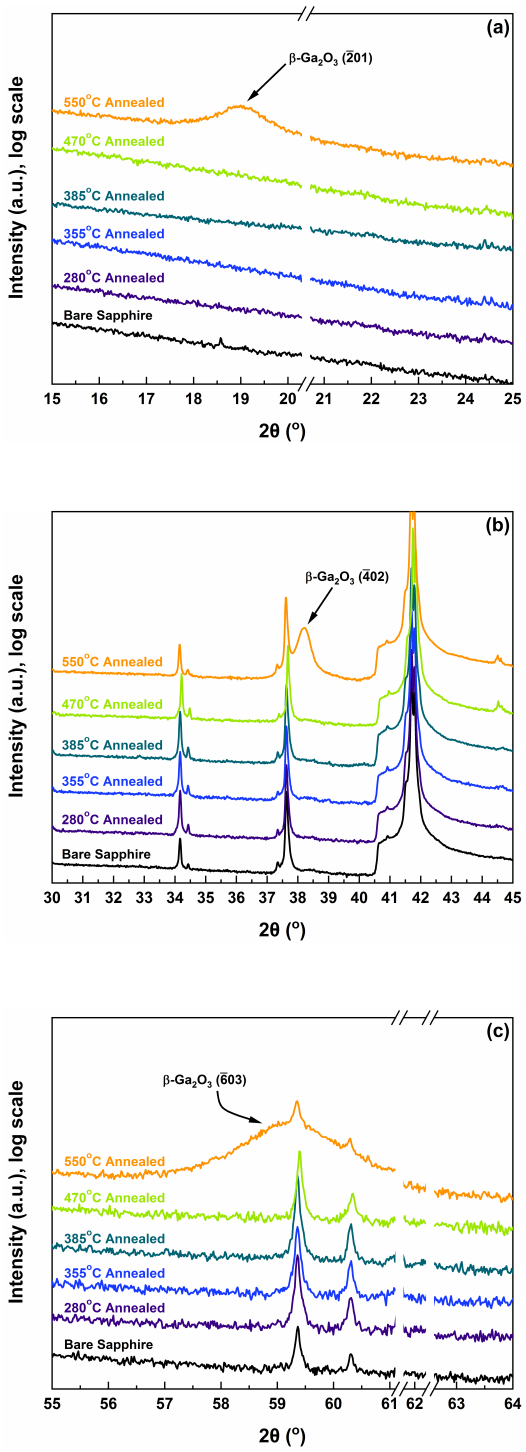

Figure 2.8: 1D XRD patterns for annealed Ga_2O_3 samples on sapphire–annealing was done in air for 1 h starting from samples grown at 190°C. 1D XRD pattern of the bare c-plane sapphire substrate is included as reference to help distinguish thin film peaks in the patterns. Regions of the patterns that include thin film peaks are shown in panels (a), (b), and (c). The data have been collected using cobalt X-ray source. However, the patterns have been converted to Cu wavelength for easier comparison with literature patterns.

resulting in atomic structures in the bulk with short-range order (considering that 190°C is the onset of crystallinity formation) which can rearrange to form highly oriented $(\bar{2}01)$ planes of the thermodynamically stable β-Ga_2O_3 at a low thermal budget in the absence of the competing metastable α-Ga_2O_3 domains in the bulk. This conclusion was supported further by the fact that similarly processed gallium oxide films on glass (i.e., completely amorphous films with the least atomic order in the bulk) did not show any signs of crystallinity upon annealing at any temperatures studied in this work. This method, i.e., ALD growth at the low temperature of 190°C to get a relatively less disordered structure in the bulk followed by only 1 h anneal at the higher temperature of 550°C, is overall more energy-efficient than growth of as-deposited films at high substrate temperatures while resulting in a pure β-Ga_2O_3 epitaxial film with no α-Ga_2O_3 inclusions that can be detected by XRD in the film. Additional XRD measurements (including rocking scans and off-specular φ-scans) were also performed on the 550°C annealed film, and the results are presented in the Appendix. Moreover, optical properties of the annealed film are presented in the Appendix along with those for the film before annealing.

2.4 Summary and Conclusions

Atomic layer deposition was utilized to deposit gallium oxide thin films on commonly used foreign substrates in the low process temperature range aiming at achieving crystalline films. While films deposited on Si(100), Si(110), Si(111), and glass were amorphous at all conditions studied in this work, it was found that Ga_2O_3 starts to crystallize on c-plane sapphire at deposition temperatures as low as 190°C such that α-$Ga_2O_3(006)\|\alpha$-$Al_2O_3(006)$

and β-$Ga_2O_3(\bar{4}02)||\alpha$-$Al_2O_3(006)$. At higher deposition temperatures, as-deposited films contained a mixture of α-Ga_2O_3 and β-Ga_2O_3 epitaxial phases preserving the same preferred orientation as the 190°C films. While all the as-deposited films had large refractive index values (e.g., n > 1.8 at 632.8 nm) along with atomically smooth surfaces and resistivity values close to undoped bulk gallium oxide, the best as-deposited film properties on sapphire were obtained at T_{sub} = 277°C, beyond which the crystal structure slightly degraded and the bandgap decreased. Cross-section TEM analysis of this film revealed that pseudomorphic α-Ga_2O_3 in the as-deposited films originates from the sapphire substrate surface and continues to grow as long as an underlying isostructural template is sustained by the stepwise growth characteristic of the ALD technique. Meanwhile, beyond the few monolayers of pseudomorphic α-Ga_2O_3 formed all along the film-substrate interface, β-Ga_2O_3 also starts to appear and increasingly develop as the deposition continues and the film thickness increases. To suppress the formation of α-Ga_2O_3 inclusions in the bulk of the film while preserving a low thermal budget process, the 190°C as-deposited films, which were at the onset of crystallinity, were annealed in air. Annealing such films at T > 470°C resulted in formation of pure β-Ga_2O_3 phase with the epitaxial relationship of β-$Ga_2O_3(\bar{2}01)||\alpha$-$Al_2O_3(006)$ while suppressing the formation of α-Ga_2O_3 inclusions in the bulk of the film which was attributed to the negligible population of α-Ga_2O_3 in the starting film and the presence of short-range order in the starting film, thereby facilitating the formation of highly oriented β-Ga_2O_3 planes in the absence of the competing layer-by-layer pseudomorphic ALD growth of α-Ga_2O_3 on sapphire. Realization of low thermal budget high quality crystalline Ga_2O_3 films on sapphire as a result of this work enables the development of next-generation solid-state electronic devices that can withstand higher

voltages while meeting stringent requirements of efficiency and form factor faced by the microelectronic industry.

Chapter 3

Bridging the Gap Between Gallium Oxide and Gallium Nitride: Heteroepitaxy via Atomic Level Scaffolding

3.1 Chapter Overview

Gallium oxide (Ga_2O_3) is an emerging wide bandgap material with exceptional properties, which compete with and complement gallium nitride (GaN) properties, for improving the performance and efficiency of power electronic devices and expanding the wavelength span of optoelectronic devices. However, challenges in growing high quality crystalline Ga_2O_3 on non-native substrates hinder the development of Ga_2O_3 semiconductor heterostructures

and integration of Ga_2O_3 with GaN electronics. This work demonstrates a deposition strategy for obtaining crystalline Ga_2O_3 on GaN-compatible non-native substrates as a key enabling technology for implementation of Ga_2O_3 in next-generation electronic devices. Plasma-enhanced atomic layer deposition is used to create a highly symmetric atomic scale scaffold of gallium atoms by taking advantage of a sacrificial GaN monolayer as an intermediate step during Ga_2O_3 growth. Establishing such scaffold together with the use of highly reactive plasma species allow this GaN-mediated Ga_2O_3 deposition approach to be performed at low thermal budget while resulting in a highly oriented α-Ga_2O_3 film with vanishing amounts of nitrogen and carbon impurities as well as a larger bandgap and larger refractive index compared to the conventionally deposited Ga_2O_3. The deposition strategy presented in this work opens new horizons for accelerated development of high performance and energy-efficient Ga_2O_3 electronics.

3.2 Experimental Details

Depositions were done at 277°C on single-side polished (R_a < 0.3 nm) prime quality c-plane sapphire wafers (see reference [8] or the Appendix for detailed specifications of the wafers) by using a Kurt J. Lesker ALD 150-LX system equipped with a remote inductively coupled plasma (ICP) source and a load lock. The error in determining the actual deposition temperatures was ±3°C. The pressure of the reactor was ∼1.1 Torr with ∼1000 sccm continuous flow of argon. In addition, 60 sccm oxygen or forming gas was introduced to the reactor during plasma exposures with ∼600 W forward power. This setup is also explained in detail elsewhere [8, 57]. Triethylgallium, TEG, (Strem Chemicals, Inc.) was electronic

grade (99.9999% Ga) in a stainless steel Swagelok cylinder assembly which was not heated during the depositions; all other gases (argon, oxygen, and N_2/H_2 forming gas) were of ultrahigh purity (99.999%, Praxair Canada, Inc.). Substrates were exposed to 60 s plasma to remove contamination and pretreat the surface prior to deposition. Reference GaN depositions were done by using a recipe consisting of 0.1 s TEG dose, 3 s argon purge, 15 s forming gas plasma dose, and 2 s argon purge. Reference Ga_2O_3 depositions were done by using a recipe consisting of 0.1 s TEG dose, 20 s argon purge, 10 s oxygen plasma dose, and 12 s argon purge (reducing the two purge times down to 3 s and 2 s, respectively, did not change the deposition results for the reference Ga_2O_3). The details of the optimization procedures that were used in this work (similarly performed for both GaN and Ga_2O_3) are explained in references [4] and [5]. GaN-mediated Ga_2O_3 depositions were done by using a recipe consisting of 0.1 s TEG dose, 6 s argon purge, 15 s forming gas plasma dose, 13 s argon purge, 1.5 s oxygen plasma dose, and 10 s argon purge (the forming gas plasma dose time was chosen to ensure completion of GaN formation reactions while the oxygen plasma dose time was chosen to ensure complete conversion of nitride to oxide using GaN and Ga_2O_3 enthalpies of formation [75] as guides).

Ellipsometry measurements were done by using a J.A. Woollam M-2000DI spectroscopic ellipsometer, permanently mounted on the reactor at an incident angle of 70°, in the spectral range of 0.73-6.40 eV (equivalent to 190-1700 nm) at intervals less than 0.05 eV. Ellipsometry data analysis was done by using CompleteEASE software. Thickness and optical constants of the films were obtained based on Tauc–Lorentz modeling of the ellipsometry data (see reference [8] and section 2.3.1 for detailed explanation of the modeling procedure).

Out-of-plane coupled 1D XRD scans were performed by using a Rigaku Ultima-IV diffractometer equipped with a cobalt source, a D/Tex ultrahigh-speed position sensitive detector, and a K-β filter at a scan rate of 2°/min and 0.02° steps (which is equivalent to 0.6 s/step exposure). The patterns were converted to copper wavelength for easier comparison with the literature.

Cross-section TEM lamella was prepared by low-energy ion polishing (to minimize damage) using a ThermoFisher Helios Hydra DualBeam PFIB system. HRTEM images were obtained by using a Titan 80-300 HRTEM instrument. Atomic resolution STEM analyses (including STEM images, EDS maps, and nano-beam diffraction patterns) were performed by using a Thermo Scientific Themis Z S/TEM instrument equipped with 4 windowless EDS detectors arranged symmetrically around the sample to allow EDS mapping of light elements such as C, N, and O.

3.3 Results and Discussion

3.3.1 Revealing the Atomic Level Scaffold

Figure 3.1a and 3.1c show views along the c-axis of the position of atoms in a monolayer of w-GaN [63,76] and a slice of α-Ga_2O_3 [63,65] revealing that the position of Ga atoms in a monolayer of w-GaN coincides with the position of Ga atoms in α-Ga_2O_3 after a 30° in-plane rotation of coordinates. With such an atomic scale scaffold of Ga atoms in place (see yellow dashed lines in Figure 3.1a and 3.1c as guides to the eye), the highly reactive oxygen plasma can readily interact with nitrogen atoms in the w-GaN monolayer and transform it

to α-Ga_2O_3. It is worth noting that formation of no more than one monolayer of w-GaN in each cycle is essential in establishing a scaffold that is compatible with the position of Ga atoms in α-Ga_2O_3; this indicates the crucial role of ALD in the success of this GaN-mediated deposition process.

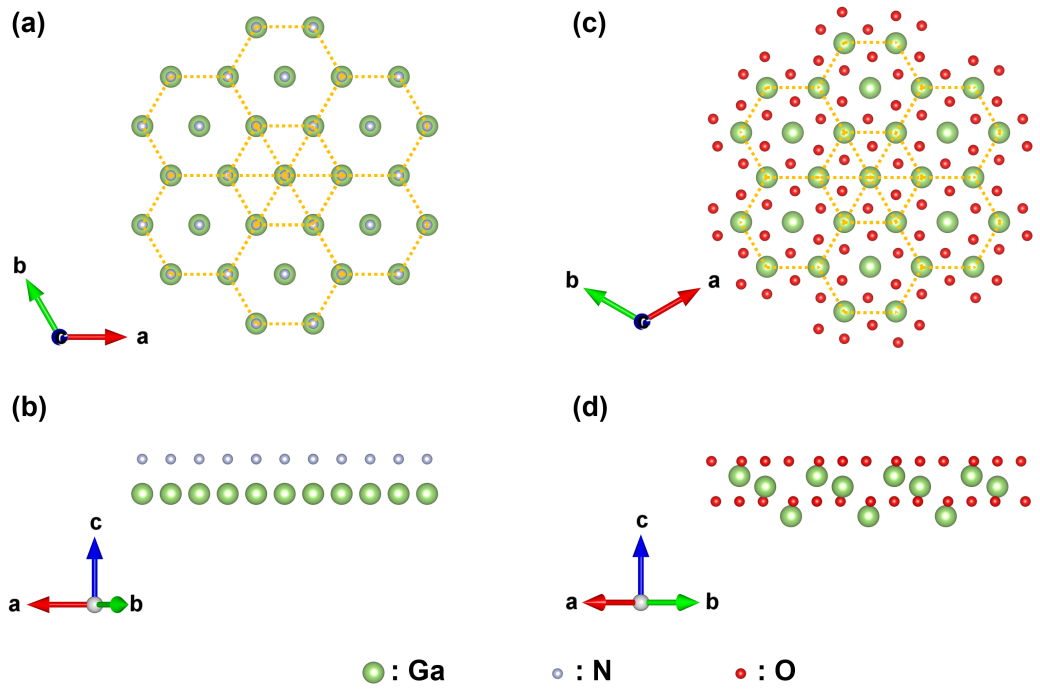

Figure 3.1: Views of a monolayer of w-GaN (a) along and (b) perpendicular to the c-axis, as well as views of a slice of α-Ga_2O_3 (c) along and (d) perpendicular to the c-axis. Yellow dashed lines show the atomic scale scaffold of Ga atoms as guides to the eye.

As can be seen by comparing Figure 3.1b and 3.1d, which show views of the same w-GaN monolayer and α-Ga_2O_3 slice perpendicular to the c-axis, nitrogen atoms are being removed and oxygen atoms placed in the existing hexagonal scaffold in each cycle, while Ga atoms merely need to move a short distance (< 2 Å) along the c-axis (to compare, the Ga–O bond lengths in α-Ga_2O_3 [65] are ∼2 Å) to yield α-Ga_2O_3. As will be confirmed by our results, these transformations and displacements are subtle enough to happen at the low deposition temperature of 277°C using plasma species.

3.3.2 Crystal Structure of Gallium Oxide Grown at 277°C

We chose c-plane sapphire as our non-native substrate due to availability of abundant data for achieving high quality w-GaN on this substrate [67, 77]: As shown in Figure 3.2a, depositing a thick ($\sim$22 nm) layer of GaN by using our optimized ALD process at 277°C on c-plane sapphire results in heteroepitaxial w-GaN such that w-GaN(002)$\|\alpha$-Al_2O_3(006); this is evident because only these peaks are observed parallel to the surface in out-of-plane XRD scans (note that the corresponding scan of the bare sapphire substrate is included as a reference to better distinguish thin film peaks in the pattern). Previous work in our group [77] has confirmed that in addition to this thick GaN layer being a highly oriented heteroepitaxial layer, the first few monolayers of GaN are free from defects which make them an excellent GaN template to start our work with.

Figure 3.2c shows a schematic of the GaN-mediated Ga_2O_3 deposition steps used in this work as well as the out-of-plane XRD results for an $\sim$22 nm film deposited at 277°C using such approach. As shown in Figure 3.2c, an intense peak for α-Ga_2O_3(006) is observed right next to α-Al_2O_3(006) peak. No other peaks from α-Ga_2O_3 are present which indicates that the α-Ga_2O_3 film is a highly oriented film with α-Ga_2O_3(006) planes oriented parallel to the surface. This confirms that α-Ga_2O_3(006) planes have grown parallel to w-GaN(002) planes. Meanwhile, β-Ga_2O_3 peaks are hardly detectable in Figure 3.2c which is indicative of their low population in the film (see the XRD pattern of the bare sapphire substrate to better distinguish thin film peaks in Figure 3.2c).

As a reference, depositing Ga_2O_3 directly on sapphire (i.e., without any GaN layers involved) at the same deposition temperature resulted in a mixture of α-Ga_2O_3 and β-Ga_2O_3

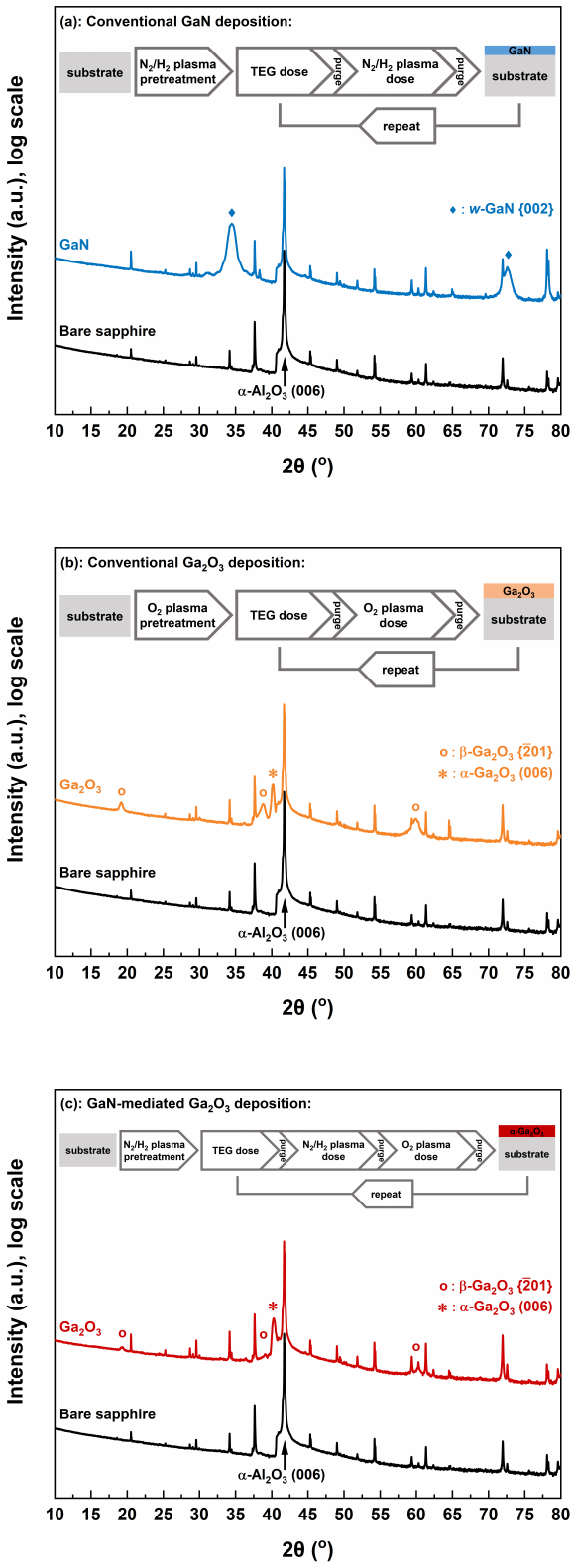

Figure 3.2: Out-of-plane coupled XRD patterns and schematic of the deposition steps for (a) conventional GaN deposition, (b) conventional Ga_2O_3 deposition, and (c) GaN-mediated Ga_2O_3 deposition. In each case, the XRD pattern of the bare sapphire substrate is included as a reference to better distinguish thin film peaks in the patterns.

in the film; this is shown in Figure 3.2b where peaks from α-Ga_2O_3(006) planes as well as β-$Ga_2O_3(\bar{2}01)$ family of planes are observed parallel to the surface (the corresponding scan of the bare sapphire substrate is included as a reference to better distinguish thin film peaks in the pattern). Our previous results on direct deposition of Ga_2O_3 on sapphire [8] (also see Chapter 2) show that even though a few monolayers of pseudomorhic α-Ga_2O_3 exist along the sapphire substrate interface, a mixture of α and β phases form in the bulk of such film by using the conventional deposition process. Comparing the observed intensity ratio of β-Ga_2O_3 and α-Ga_2O_3 peaks in Figure 3.2b and 3.2c, we estimate that the population of β-Ga_2O_3 in the film is $\ll 10\%$ (by ratio of mass of β-Ga_2O_3 to mass of α-Ga_2O_3 and β-Ga_2O_3, collectively) as a result of using the GaN-mediated deposition approach.

These results demonstrate that if the Ga atoms establish a hexagonal arrangement (i.e., an arrangement with a higher degree of symmetry) by using forming gas plasma to form a monolayer of w-GaN, subsequent exposure to oxygen plasma can successfully interchange the anions while preserving the Ga scaffold thereby leading to formation of a high quality α-Ga_2O_3 layer. This self-regulated crystallization process is favored further by considering that the stacking sequence of atoms in both w-GaN and α-Ga_2O_3 is of the hexagonal closest packing (hcp) type with both N anions in w-GaN and O anions in α-Ga_2O_3 being surrounded by 4 Ga atoms (i.e., both anions have a coordination number of 4), while β-Ga_2O_3 has the stacking sequence of a distorted cubic closest packing (ccp) type with coordination number of 6 for two of the O anions and 4 for one of the O anions. Therefore, even though β-Ga_2O_3 domains are demonstrated to form in the absence of structural restrictions to atomic diffusion in the reference Ga_2O_3 film (see Figure 3.2b, reference [8], and chapter 2), presence of a hexagonal framework of Ga atoms by using a GaN-mediated

deposition strategy enables the ability to control the crystallinity of the film in situ and to achieve α-Ga_2O_3 while minimizing β-Ga_2O_3 inclusions.

Using such a hexagonal scaffold at the atomic scale also offers the potential to provide a means by which metal dopant atoms (especially those that are known to be compatible with w-GaN) can be incorporated into the GaN layer in situ (see references [78] and [79] for methods to incorporate dopant atoms into ALD films in situ), subsequently oxidized, and thereby be embedded in the α-Ga_2O_3 structure during the deposition.

3.3.3 Cross-Section TEM Analysis of α-Gallium Oxide Grown at 277°C

To investigate the structure of the α-Ga_2O_3 film deposited by the GaN-mediated approach further, cross-section TEM analysis was performed, and representative results are shown in Figure 3.3. The TEM analyses show that the entire film ($\sim$22 nm) is crystalline (see, for example, the HRTEM image in Figure 3.3a and the STEM images in Figure 3.3c and 3.3d) and confirm the crystal structure to be predominantly α-Ga_2O_3 such that α-Ga_2O_3(006) planes are parallel to the surface (also see the electron diffraction patterns of focused regions of the film and the substrate in Figure 3.3e and 3.3f, respectively). It is worth noting that because α-Ga_2O_3 is isostructural to the sapphire substrate (both having the corundum structure) with $< 5\%$ lattice mismatch [8, 62, 65], the diffraction patterns of these two materials are expected to be very similar if their crystals are oriented the same way. This is consistent with the results presented in Figure 3.3e and Figure 3.3f. In addition to these figures, line profiles of nano-beam electron diffraction patterns (not shown here), which show the diffraction patterns at several locations of the lamella, confirm the predominant

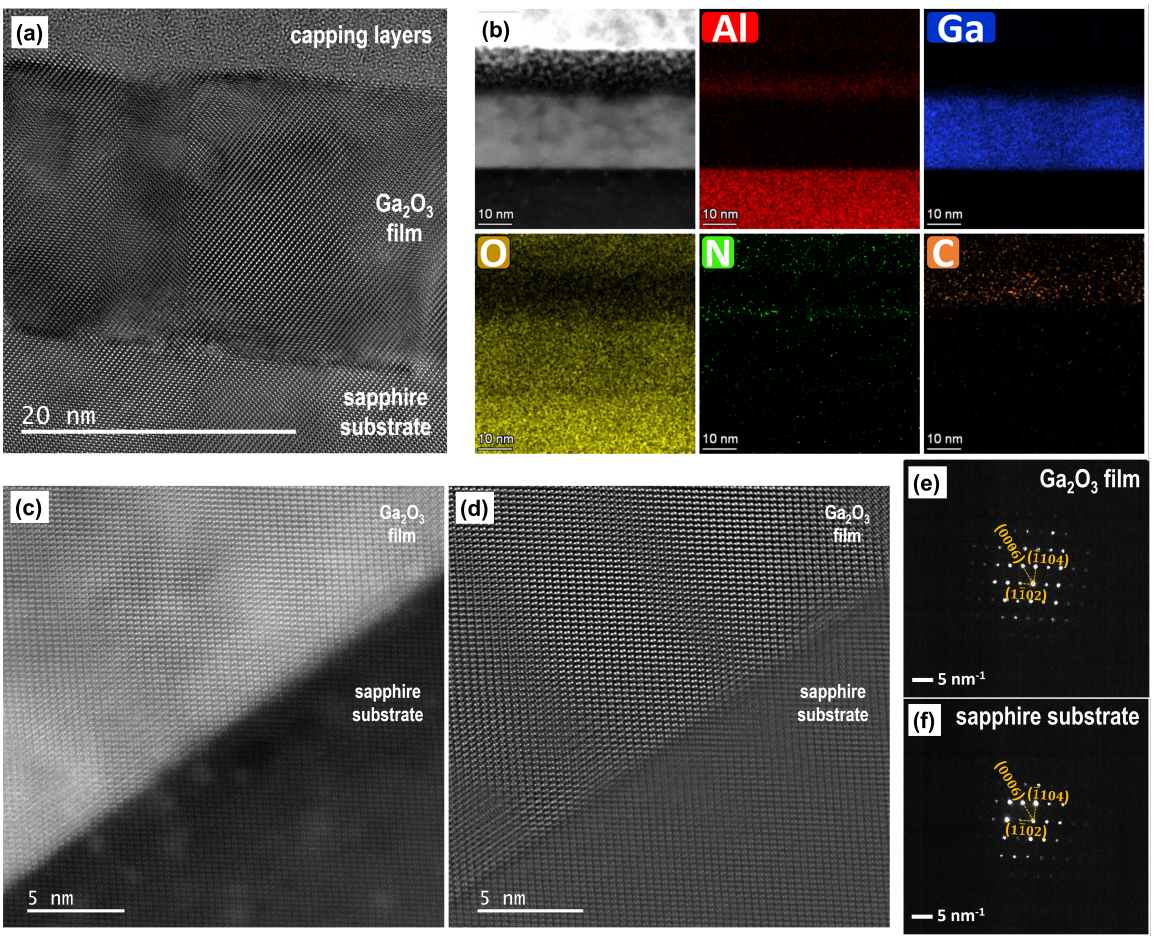

Figure 3.3: TEM analysis results for the GaN-mediated in-situ oxidized Ga_2O_3 film including (a) HRTEM image, (b) background subtracted EDS intensity maps obtained in STEM mode, (c) atomic resolution STEM image obtained with a HAADF detector, (d) the same image shown in (c) after using a combination of high-pass and radial Wiener filters to highlight atomic columns, and (e, f) nano-beam electron diffraction patterns of focused regions of the film (e) and the sapphire substrate (f). Capping layers in frame (a) consist of an 3nm aluminum nitride deposited by ALD followed by carbon and tungsten deposited before TEM lamella preparation.

presence of the α-Ga_2O_3 phase. Energy dispersive X-ray spectroscopy (EDS) analyses, in Figure 3.3b, show the low amount of impurities (both C and N) in the film and further prove the high quality of the α-Ga_2O_3 film.

3.3.4 Optical Properties at 277°C

In addition to crystal structure, investigating optical properties of thin films can provide insights into the quality and performance of the material. To that end, in-situ ellipsometry measurements were performed on the GaN-mediated in-situ oxidized Ga_2O_3 film, as well as a reference Ga_2O_3 film with no GaN layers involved during its deposition, and a reference GaN film. In all cases, the substrate was c-plane sapphire, and the measurements were performed after 450 doses of TEG (which resulted in an $\sim$22 nm α-Ga_2O_3 film deposited by using the GaN-mediated approach, as well as an $\sim$26 nm reference α-Ga_2O_3/β-Ga_2O_3 mixed-phase film, and an $\sim$22 nm reference GaN film, respectively – the difference in thickness of the two Ga_2O_3 films is consistent with the fact that β-Ga_2O_3 has a larger molar volume than α-Ga_2O_3 [22, 23]; thus, inclusion of β-Ga_2O_3 domains in the film results in a thicker film for a constant number of TEG doses).

As shown in Figure 3.4, the values of extinction coefficient (k) for the two Ga_2O_3 films are remarkably similar to each other and different from the GaN film: Both Ga_2O_3 films have larger bandgaps compared to the reference GaN film (see the energy at which k starts to deviate from zero or the listed values included in Figure 3.4); meanwhile, the α-Ga_2O_3 film deposited by using the GaN-mediated approach has a slightly larger bandgap compared to the reference α-Ga_2O_3/β-Ga_2O_3 mixed-phase film. Figure 3.4 also shows that while the

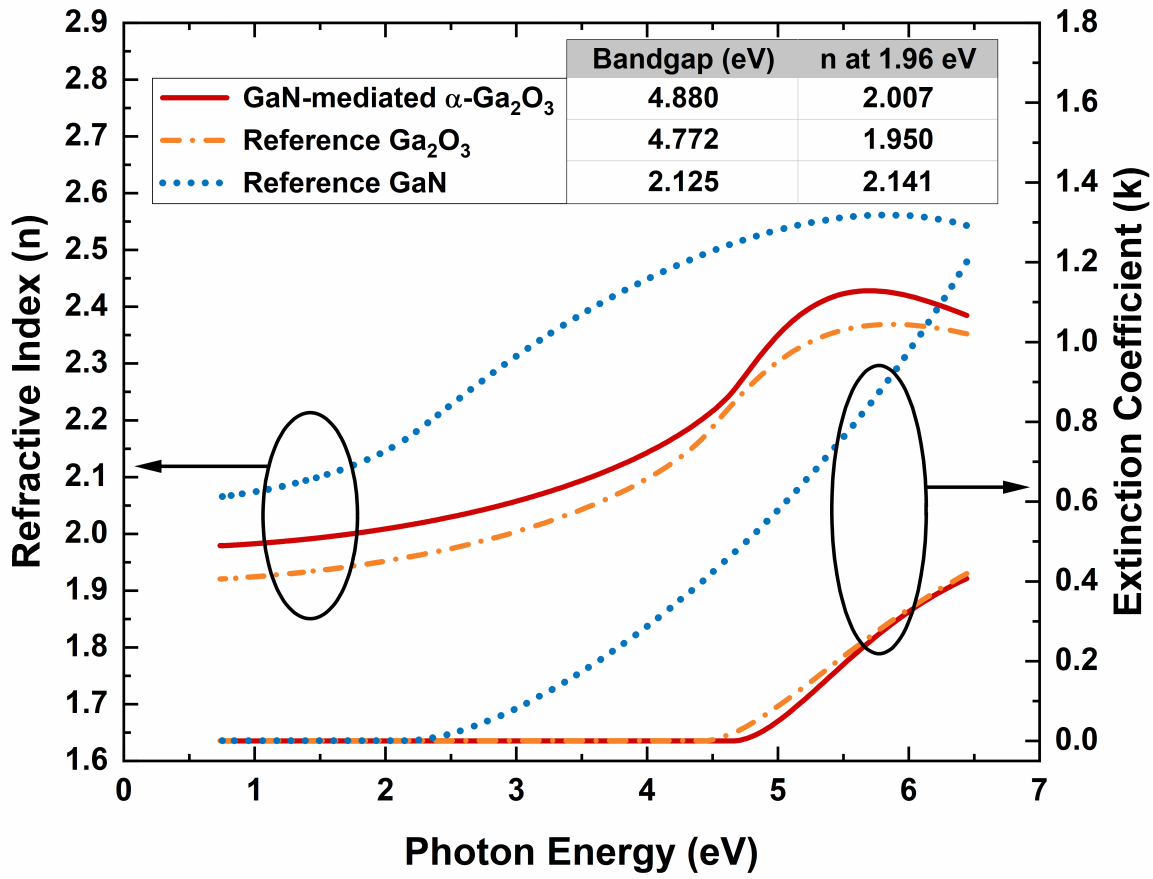

Figure 3.4: Optical constants of the GaN-mediated in-situ oxidized Ga_2O_3 film compared to two reference films after equal number of TEG doses. The values of bandgap and refractive index at the photon energy of 1.96 eV (corresponding to the wavelength of 632.8 nm) are listed for easier comparison.

refractive index (n) for the two oxide films are both smaller than GaN (as expected), using the GaN-mediated deposition strategy results in a Ga_2O_3 film with larger refractive index values over the entire measured spectral range. This observation is consistent with the crystal structure of the films noting that α-Ga_2O_3 has a higher atomic packing density (i.e., smaller molar volume) than β-Ga_2O_3, and thus is expected to have a larger refractive index compared to the β phase [22, 23]. As seen in Figure 3.4, specifically at the photon energy of 1.96 eV (equivalent to 632.8 nm), the GaN-mediated α-Ga_2O_3 film has a high refractive index value of 2.007 ($\pm$0.001), which is higher than the reported value of 1.97 for bulk

β-Ga_2O_3 wafers [60] as well as other literature reports for Ga_2O_3 [23].

3.4 Summary and Conclusions

In summary, this work presented a deposition strategy for obtaining high quality α-Ga_2O_3 on GaN-compatible non-native substrates with atomic level control over the crystal structure. The results confirmed that sustained hexagonal scaffolding at the atomic scale, as a result of using a GaN-mediated Ga_2O_3 deposition approach, enabled by plasma-enhanced ALD, plays a unique role in steering the atoms to form the crystal structure of α-Ga_2O_3 at a low thermal budget. This approach minimizes the formation of β-Ga_2O_3 domains and hinders formation of a mixed-phase material. It also makes integration of GaN and Ga_2O_3 components on a monolithic substrate possible and facilitates fast-track exploitation of GaN technology advancements for development of Ga_2O_3 electronics. Development of a low temperature GaN-compatible deposition technology for Ga_2O_3 as a result of this work is a key enabling technology for wide bandgap semiconductors leading to energy-efficient electronic devices, not only in performance but also an energy-efficient fabrication process.

Chapter 4

Deposition of β-Gallium Oxide Films: Achieving High Quality Films on Non-Native Substrates Using Metastable Buffer Layers

4.1 Chapter Overview

In an attempt to overcome challenges in growing high quality crystalline Ga_2O_3 on non-native substrates and in order to enable the development of Ga_2O_3 semiconductor heterostructures and integration of Ga_2O_3 with GaN electronics, this chapter demonstrates a deposition strategy for obtaining β-Ga_2O_3 films on non-native substrates (including GaN-compatible non-native substrates) as a key enabling technology for implementation of

Ga_2O_3 in next-generation electronic devices. A high quality layer of a metastable Ga_2O_3 phase (i.e., a phase other than the β-Ga_2O_3 phase) is deposited prior to β-Ga_2O_3 growth. This high quality metastable Ga_2O_3 layer serves as an intermediate layer on which highly oriented crystalline β-Ga_2O_3 with minimal inclusion of other Ga_2O_3 polymorphs is grown; this process is independent of the instrument and can achieve β-Ga_2O_3 even on non-native substrates. Establishing such intermediate layer together with the use of highly reactive plasma species (for example, using plasma-enhanced atomic layer deposition) allow this Ga_2O_3 deposition approach to be performed at low thermal budgets while resulting in a highly oriented β-Ga_2O_3 film with vanishing amounts of other Ga_2O_3 polymorphs compared to the conventionally deposited Ga_2O_3. The deposition strategy presented in this chapter opens new horizons for accelerated development of high performance and energy-efficient β-Ga_2O_3 electronics.

4.2 Experimental Details

Depositions were done at 277°C on single-side polished (R_a < 0.3 nm) prime quality c-plane sapphire wafers (see reference [8] or the Appendix for detailed specifications of the wafers) by using a Kurt J. Lesker ALD 150-LX system equipped with a remote inductively coupled plasma (ICP) source and a load lock. The error in determining the actual deposition temperatures was ±3°C. The pressure of the reactor was ∼1.1 Torr with ∼1000 sccm continuous flow of argon. In addition, 60 sccm oxygen or forming gas was introduced to the reactor during plasma exposures with ∼600 W forward power. This setup is also explained in detail elsewhere [8, 57]. Triethylgallium, TEG, (Strem Chemicals, Inc.) was electronic

grade (99.9999% Ga) in a stainless steel Swagelok cylinder assembly which was not heated during the depositions; all other gases (argon, oxygen, and N_2/H_2 forming gas) were of ultrahigh purity (99.999%, Praxair Canada, Inc.). Substrates were exposed to 60 s plasma to remove contamination and pretreat the surface prior to deposition. Conventional Ga_2O_3 depositions (used as one of the reference Ga_2O_3 depositions and as the deposition method for the topmost β-Ga_2O_3 layer in this chapter) were done by using a recipe consisting of 0.1 s TEG dose, 20 s argon purge, 10 s oxygen plasma dose, and 12 s argon purge (reducing the two purge times down to 3 s and 2 s, respectively, did not change the deposition results for the conventional Ga_2O_3 deposition). The details of the optimization procedures that were used in this work are explained in references [4] and [5]. GaN-mediated α-Ga_2O_3 depositions (used as one of the reference Ga_2O_3 depositions) were done by using a recipe consisting of 0.1 s TEG dose, 6 s argon purge, 15 s N_2/H_2 forming gas plasma dose, 13 s argon purge, 1.5 s oxygen plasma dose, and 10 s argon purge (details of this deposition approach are explained in detail in reference [7] and chapter 3.)

Ellipsometry measurements were done by using a J.A. Woollam M-2000DI spectroscopic ellipsometer, permanently mounted on the reactor at an incident angle of 70°, in the spectral range of 0.73-6.40 eV (equivalent to 190-1700 nm) at intervals less than 0.05 eV. Ellipsometry data analysis was done by using CompleteEASE software. Thickness and optical constants of the films were obtained based on Tauc–Lorentz modeling of the ellipsometry data (see reference [8] and chapter 2.3.1 for detailed explanation of the modeling procedure).

Out-of-plane coupled 1D XRD scans were performed by using a Rigaku Ultima-IV diffractometer equipped with a cobalt source, a D/Tex ultrahigh-speed position sensitive

detector, and a K-β filter at a scan rate of 2°/min and 0.02° steps (which is equivalent to 0.6 s/step exposure). The patterns were converted to copper wavelength for easier comparison with the literature.

Cross-section TEM lamella was prepared by low-energy ion polishing (to minimize damage) using a ThermoFisher Helios Hydra DualBeam PFIB system. Atomic resolution STEM analyses (including STEM images and nano-beam diffraction patterns) were performed by using a Thermo Scientific Themis Z S/TEM instrument equipped with a high-angle annular dark-field (HAADF) detector.

4.3 Results and Discussion

4.3.1 Low Thermal Budget Deposition Approach and the Resulting Crystal Structure

In our previous work (see chapter 3 and reference [7]), we demonstrated a GaN-mediated deposition strategy for Ga_2O_3 growth by which we were able to manipulate chemical reactions and phase transformations on the surface and, therefore, navigate the deposition process to obtain high quality α-Ga_2O_3 films on GaN-compatible non-native substrates by going through an intermediate GaN scaffold. Here, we introduce a deposition strategy that achieves high quality β-Ga_2O_3 films by using metastable Ga_2O_3 as an intermediate layer (also referred to as buffer layer and/or seed layer in the following pages) prior to β-Ga_2O_3 deposition. We choose α-Ga_2O_3 metastable polymorph as the seed layer to demonstrate the process due to availability of previous data (in chapter 3 and reference [7]) for achiev-

ing high quality α-Ga_2O_3 on non-native substrates. We show that by depositing the seed layer before β-Ga_2O_3 deposition, a conventional deposition process that used to produce a mixed-phase Ga_2O_3 film successfully achieves high quality epitaxial β-Ga_2O_3 on the underlying metastable layer. To compare, we also show that depositing Ga_2O_3 directly using the conventional deposition process (i.e., without any seed layers being deposited) at the same deposition temperature and conditions results in a multiphase film containing a mixture of α-Ga_2O_3 and β-Ga_2O_3 in the film.

The entire deposition is optimized to achieve crystallinity at the low temperature of 277°C, thereby establishing an energy-efficient fabrication process for growing β-Ga_2O_3 films on non-native substrates on which an intermediate layer of metastable Ga_2O_3 can be initially grown to serve as the template. Once such template is available, the deposition process would proceed in a conventional way to achieve β-Ga_2O_3 at a low thermal budget (i.e., at temperatures that are hundreds of degrees lower than the processes currently in use for β-Ga_2O_3 deposition). Fabrication of Ga_2O_3 devices on non-native substrates using this deposition strategy also allows for the transfer of thermal management technologies that are already established for wide bandgap electronics [56] which will mitigate the low thermal conductivity of β-Ga_2O_3 and make devices available that are able to concurrently handle higher power, higher voltage, and higher operating temperatures.

Figure 4.1 shows a schematic of the deposition steps used to demonstrate our strategy for β-Ga_2O_3 film growth. As seen in Figure 4.1, step (a) consists of depositing a metastable Ga_2O_3 phase on the substrate. In general, step (a) may be performed by any deposition method that can produce metastable Ga_2O_3 on the substrate. As a particular example, we used the GaN-mediated α-Ga_2O_3 deposition method based on our previous work

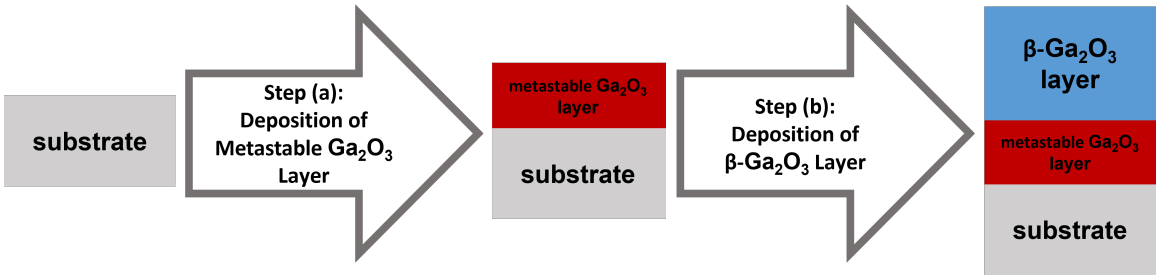

Figure 4.1: Schematic of the deposition steps for the method of the present work for forming a thin film of β-Ga_2O_3 on the substrate.

(see chapter 3 and reference [7]) which was shown to be able to produce very high quality metastable α-Ga_2O_3 and had the added advantage of being able to perform the process on GaN-compatible substrates. We chose sapphire, and more particularly c-plane sapphire, as our substrate due to availability of abundant data for depositing Ga_2O_3 and relevant materials on this substrate [7, 8, 67, 77]. Step (b) shown in Figure 4.1, represents a conventional Ga_2O_3 deposition process, which may be performed by any deposition method, that normally produces a mixture of β-Ga_2O_3 mixed with other Ga_2O_3 polymorphs on the substrate if no buffer layers are involved. A particular example of such processes is the method presented in chapter 2 (also referred to as "conventional Ga_2O_3 deposition" in the following pages) which results in a mixture of α- and β-Ga_2O_3 phases in the film [8].

To demonstrate the quality of the metastable layer, Figure 4.2a and Figure 4.2b to 4.2d show the XRD and the TEM results for an $\sim$22 nm film of metastable α-Ga_2O_3 deposited on c-plane sapphire by using the same method as utilized in this work. As shown in Figure 4.2a, an intense peak for α-Ga_2O_3(006) is observed right next to α-Al_2O_3(006) peak. No other peaks from α-Ga_2O_3 are present in the pattern which indicates that the α-Ga_2O_3 film is a highly oriented film with α-Ga_2O_3(006) planes oriented parallel to the surface. Meanwhile, β-Ga_2O_3 peaks are hardly detectable in Figure 4.2a which is indicative of their

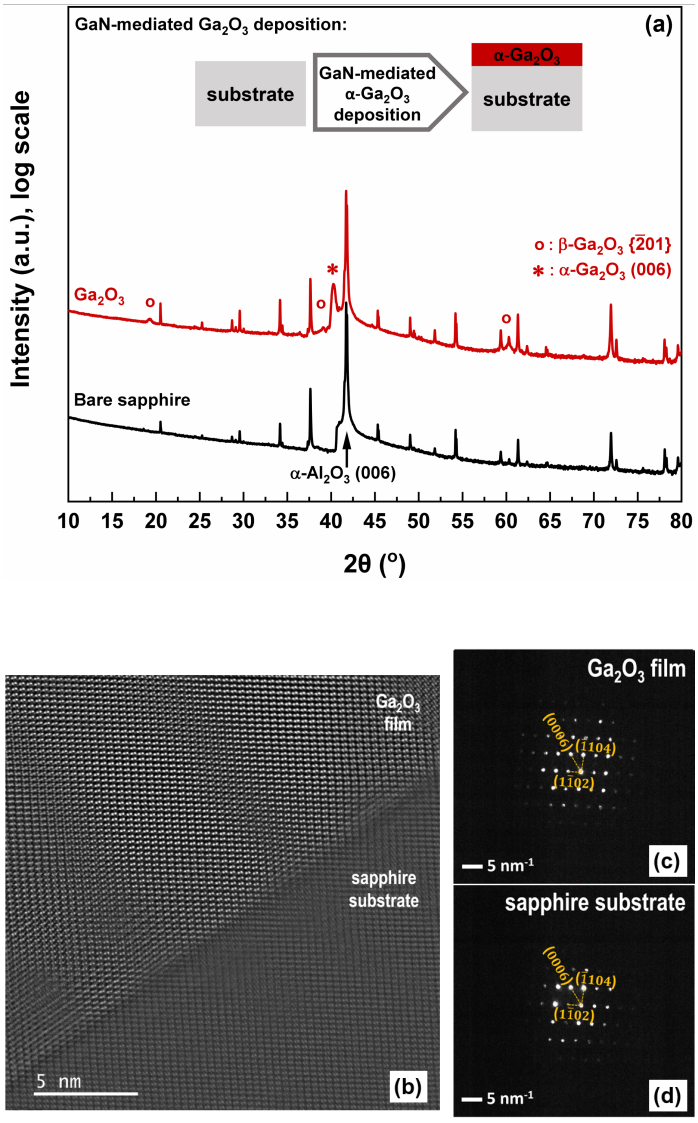

Figure 4.2: (a) Out-of-plane coupled XRD pattern for α-Ga_2O_3 deposited by using the GaN-mediated Ga_2O_3 deposition method (the XRD pattern of the bare sapphire substrate is included as a reference to better distinguish thin film peaks in the pattern), (b) atomic resolution STEM image obtained with a HAADF detector highlighting the atomic columns by using a combination of high-pass and radial Wiener filters, and (c, d) nano-beam electron diffraction patterns of focused regions of the film (c) and the sapphire substrate (d).

low population in the film (note that the XRD pattern of the bare sapphire substrate is also included in Figure 4.2a to better distinguish thin film peaks). Meanwhile, the TEM analyses in Figure 4.2, including the atomic resolution STEM image in Figure 4.2b, as well as similar frames that are not shown here, confirm that the entire film ($\sim$22 nm) is crystalline and that the crystal structure is predominantly α-Ga_2O_3 such that α-Ga_2O_3(006) planes are parallel to the surface. These results are also confirmed from the distinct and intense diffraction spots in the electron diffraction patterns of focused regions of the film and the substrate in Figure 4.2c and 4.2d, respectively.

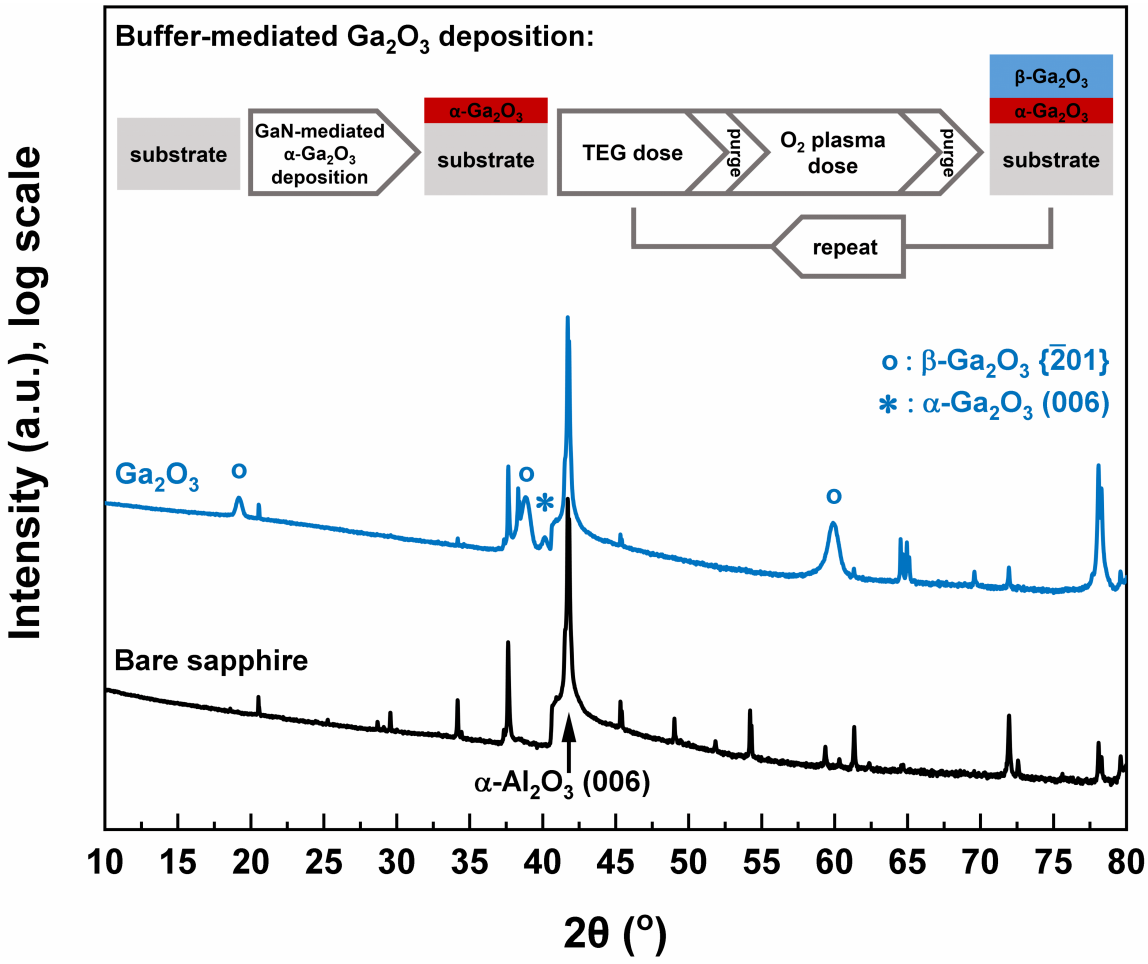

Figure 4.3: Out-of-plane coupled XRD pattern for Ga_2O_3 deposited by using the buffer-mediated epitaxial deposition method. The XRD pattern of the bare sapphire substrate is included as a reference to better distinguish thin film peaks in the pattern.

Figure 4.3 shows a schematic of the deposition steps as well as the out-of-plane XRD scan results for an ~27.5 nm β-Ga_2O_3 film deposited at 277°C by using the buffer-mediated epitaxial deposition approach proposed in this chapter. To explain further, the sample studied in Figure 4.3 consists of ~3 nm α-Ga_2O_3 as the seed/buffer layer deposited by using the GaN-mediated deposition approach of our previous work (see chapter 3 and reference [7]) on which an ~27.5 nm of Ga_2O_3 as the bulk film is deposited by using a conventional deposition approach (see reference [8] as well as chapter 2 for details of the conventional deposition process). As shown in Figure 4.3, three intense peaks from β-$Ga_2O_3(\bar{2}01)$ family of planes are observed parallel to the surface. More specifically, moving from low to high 2θ angles in Figure 4.3, these β-Ga_2O_3 peaks correspond to β-$Ga_2O_3(\bar{2}01)$, β-$Ga_2O_3(\bar{4}02)$, and β-$Ga_2O_3(\bar{6}03)$ planes, respectively. It is worth noting that because the underlying α-Ga_2O_3 seed layer has been shown to be of high phase purity even when deposited as a thick film (see Figure 4.2 and reference [7] for results from an ~22 nm α-Ga_2O_3 film deposited by using the same method as utilized in this work), we attribute the peaks for β-$Ga_2O_3(\bar{2}01)$ family of planes to be coming from the bulk of the overgrown film (i.e., the ~27.5 nm topmost layer) and not from the seed/buffer layer. No other peaks from β-Ga_2O_3 are present which indicates that the overgrown β-Ga_2O_3 film is a highly oriented film with β-$Ga_2O_3(\bar{2}01)$ family of planes oriented parallel to the surface. Meanwhile, the weak α-$Ga_2O_3(006)$ peak observed right next to α-$Al_2O_3(006)$ peak in Figure 4.3, is attributed to the α-$Ga_2O_3(006)$ planes present in the α-Ga_2O_3 seed layer with negligible contributions from α-Ga_2O_3 inclusions in the bulk of the film. The results observed in Figure 4.3 indicate that a single phase β-Ga_2O_3 film has been achieved as a result of using a metastable seed/buffer layer prior to β-Ga_2O_3 deposition in accordance with the buffer-mediated epi-

taxial deposition approach of the present work.

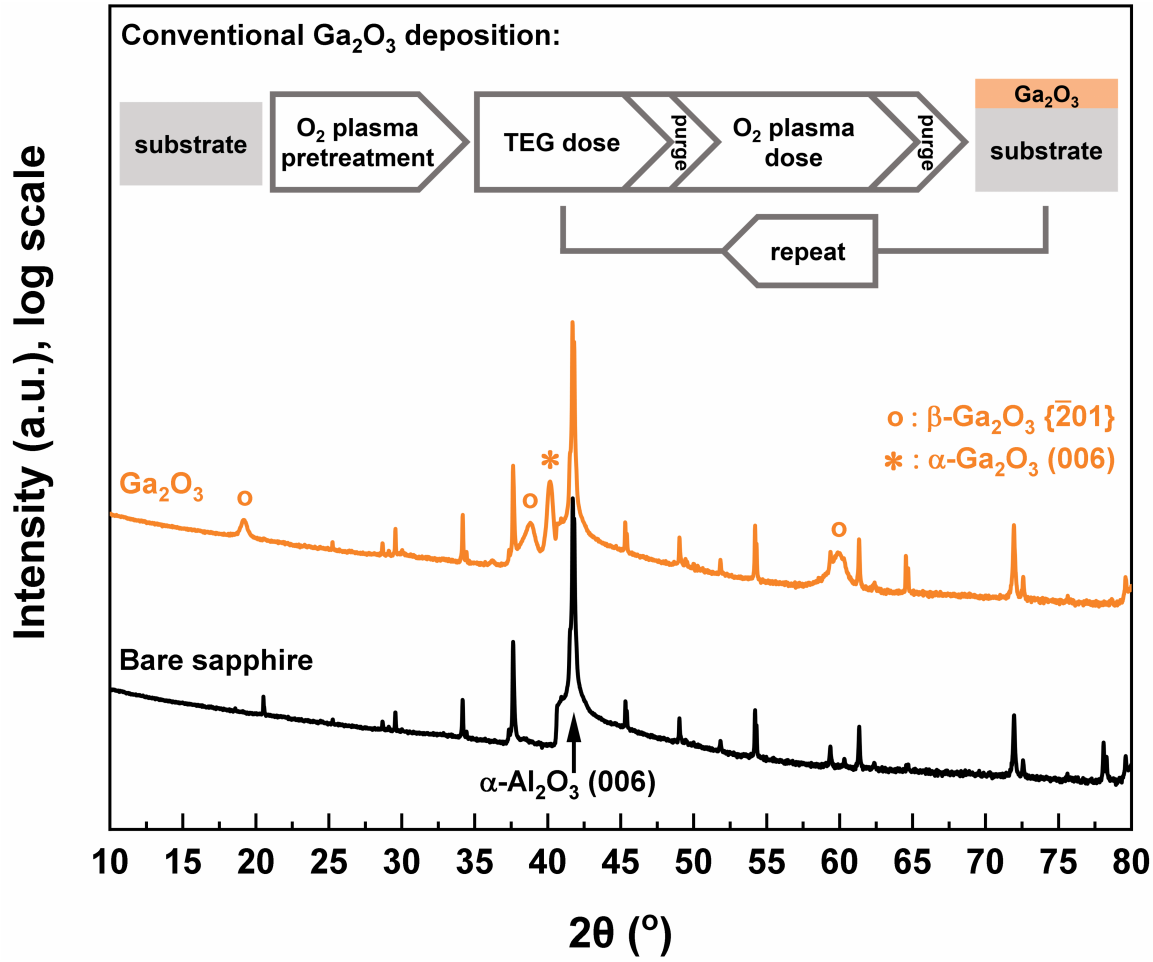

Figure 4.4: Out-of-plane coupled XRD pattern for Ga_2O_3 deposited by using the conventional Ga_2O_3 deposition method. The XRD pattern of the bare sapphire substrate is included as a reference to better distinguish thin film peaks in the pattern.

As a reference, Figure 4.4 shows that depositing Ga_2O_3 directly on the substrate in a conventional way (i.e., without any buffer layers being deposited) at the same deposition temperature and conditions results in a mixture of α-Ga_2O_3 and β-Ga_2O_3 in the film; this is evident from observing intense peaks from α-Ga_2O_3(006) planes as well as β-Ga_2O_3($\bar{2}$01) family of planes parallel to the surface (the corresponding scan of the bare sapphire substrate is included as a reference to better distinguish thin film peaks in the pattern). Our previous results on direct deposition of Ga_2O_3 on sapphire (see chapter 2 and reference [8])

also show that even though a few monolayers of pseudomorhic α-Ga_2O_3 exist along the sapphire substrate interface, a mixture of α and β phases form throughout the bulk of such film by using the conventional deposition process. Comparing the observed intensity of β-Ga_2O_3 and α-Ga_2O_3 peaks in Figure 4.3 and Figure 4.4, a dramatic increase in the population of β-Ga_2O_3 planes in the film is apparent as a result of using the buffer-mediated epitaxial deposition approach of the present invention; it is estimated that the population of β-Ga_2O_3 polymorph in the bulk of the film in Figure 4.3 is increased to $\gg 90\%$ (by ratio of mass of β-Ga_2O_3 to mass of α-Ga_2O_3 and β-Ga_2O_3, collectively) as a result of using the buffer-mediated epitaxial deposition of the present invention (compared to the almost equal proportion of α-Ga_2O_3 and β-Ga_2O_3 polymorphs in the conventional deposition case). This could be attributed to the fact that depositing a dominantly metastable phase as an intermediate layer on the substrate before doing a conventional deposition increases the free energy of the system which makes the formation of β-Ga_2O_3 in the subsequently overgrown film more and more favorable when performing a conventional deposition process on such high energy underlying template. In other words, limiting the formation of β-Ga_2O_3 domains in the seed/buffer layer by employing suitable strategies and/or restrictions (such as using an atomic scale GaN scaffold in our GaN-mediated deposition strategy for growing high quality α-Ga_2O_3), creates a lot of excess free energy in the system; therefore, once restrictions are removed and/or process conditions are changed from metastable growth to mixed-phase or conventional growth, the most stable Ga_2O_3 polymorph (i.e., β-Ga_2O_3) will be much more favorable to form (instead of a mixture of β-Ga_2O_3 with other polymorphs) because maximizing the population of β-Ga_2O_3 polymorph in the bulk of the film will lead the system to reach its lowest energy state.

4.3.2 Optical Properties at 277°C

In addition to crystal structure, we investigated optical properties of the films to gain additional insights into the quality and performance of the material. To that end, in-situ ellipsometry measurements were performed on the Ga_2O_3 film deposited by using the buffer-mediated epitaxial deposition of β-Ga_2O_3 of the present work, as well as a reference Ga_2O_3 film with no seed/buffer layers involved during its deposition (i.e., grown by using the conventional Ga_2O_3 deposition approach), and a reference α-Ga_2O_3 film deposited by using the GaN-mediated Ga_2O_3 deposition approach. In all cases, the substrate was c-plane sapphire, and the measurements were performed after 450 doses of gallium precursor (i.e., triethylgallium or TEG in this instance) for depositing the film under study. This number of TEG doses resulted in an $\sim$27.5 nm β-Ga_2O_3 film deposited on top of the metastable seed layer, as well as an $\sim$26 nm reference α-Ga_2O_3/β-Ga_2O_3 mixed-phase film deposited by using the conventional approach, and an $\sim$22 nm reference α-Ga_2O_3 film deposited by using the GaN-mediated approach, respectively – the difference in thickness of the Ga_2O_3 films while using the same number of TEG doses (i.e., constant Ga content in the films) is consistent with the fact that β-Ga_2O_3 has a larger molar volume than α-Ga_2O_3 [22, 23]; thus, an increase in the amount of β-Ga_2O_3 phase present in the film results in a thicker film for a constant number of TEG doses. Accordingly, with a constant number of TEG doses, the Ga_2O_3 film deposited by using the buffer-mediated epitaxial deposition approach has the largest thickness among all films confirming the largest population of β-Ga_2O_3 in this film.

Figure 4.5 shows the values of extinction coefficient (k), refractive index (n), and

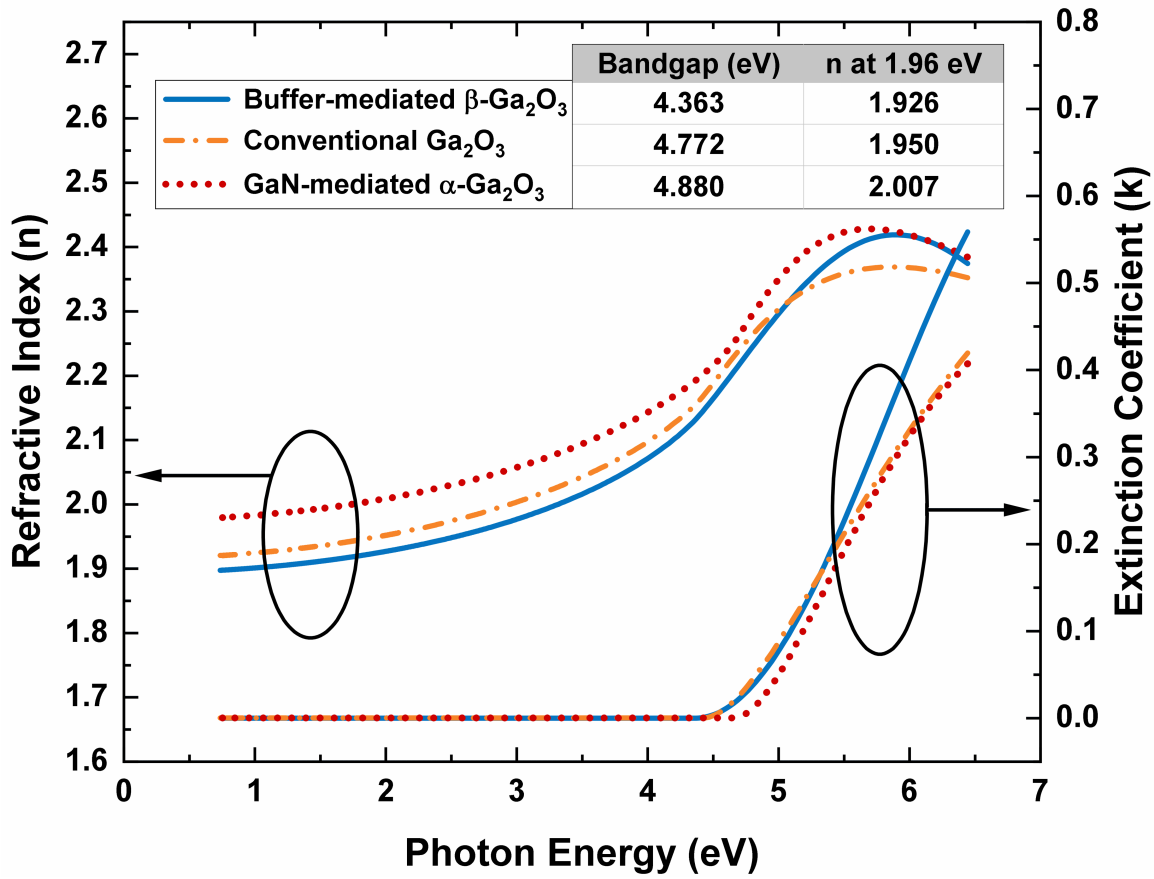

Figure 4.5: Optical constants of the β-Ga_2O_3 film deposited by using the buffer-mediated epitaxial deposition method compared to two reference films after equal number of TEG doses. The values of bandgap and refractive index at the photon energy of 1.96 eV (corresponding to the wavelength of 632.8 nm) are listed for easier comparison.

bandgap for the three Ga_2O_3 films as well. As shown in Figure 4.5, using the GaN-mediated deposition strategy results in a Ga_2O_3 film with largest refractive index values over the entire measured spectral range. This observation is consistent with the crystal structure of the films noting that α-Ga_2O_3 has a higher atomic packing density (i.e., smaller molar volume) than β-Ga_2O_3, and thus is expected to have a larger refractive index compared to the β phase [22, 23]. As seen in Figure 4.5, specifically at the photon energy of 1.96 eV (equivalent to 632.8 nm) at which light absorption does not occur in gallium oxide (i.e., k = 0 at 632.8 nm), the β-Ga_2O_3 film deposited by using the buffer-mediated epitaxial de-

position approach of the present chapter has the lowest refractive index value among the three films while the mixed-phase film deposited by using the conventional deposition approach has a refractive index value between the single phase films; this is consistent with the fact that the conventionally deposited film comprises of α and β-Ga_2O_3 phases. Figure 4.5 also shows that the β-Ga_2O_3 film deposited by using the buffer-mediated epitaxial deposition approach has the lowest bandgap value compared to the other films, and the value of bandgap increases as the α-Ga_2O_3 content increases in the film with the GaN-mediated α-Ga_2O_3 film having the highest bandgap value; these observations are consistent with literature reports for bandgap values of α and β-Ga_2O_3 [11] and further confirm the purity of β-Ga_2O_3 phase in the film deposited by using the buffer-mediated epitaxial deposition approach. Based on Figure 4.5, the values of extinction coefficient (k) for the Ga_2O_3 films are similar to each other; meanwhile, compared to the other films, the β-Ga_2O_3 film deposited by using the buffer-mediated approach has a generally larger extinction coefficient (k) in non-zero regions of the dispersions curve of k, which is indicative of a larger concentration of free carriers in the conduction band of the β-Ga_2O_3 film after the free carriers have been excited to the conduction band by photons having high-enough energy (also see reference [8] for more explanations).

4.4 Summary and Conclusions

This work presented a deposition strategy for obtaining high quality β-Ga_2O_3 films on non-native substrates (including GaN-compatible non-native substrates) at a low thermal budget by taking advantage of an intermediate high quality metastable Ga_2O_3 layer de-

posited prior to β-Ga_2O_3 growth. The results confirmed that using the buffer-mediated epitaxial deposition approach plays a unique role in facilitating the formation of the crystal structure of β-Ga_2O_3 in the overgrown film at a low thermal budget. This approach minimized the formation of non-β-Ga_2O_3 domains and hindered formation of a mixed-phase material. The deposition approach presented in this work makes the development of Ga_2O_3 semiconductor heterostructures and integration of Ga_2O_3 with existing semiconductor device components on a monolithic substrate possible and facilitates fast-track development of Ga_2O_3 electronics. Development of a low temperature technology for β-Ga_2O_3 growth (especially a GaN-compatible one) as a result of this work is a key enabling technology for wide bandgap semiconductors leading to energy-efficient electronic devices that employ advanced materials while being fabricated by using energy-efficient processes.

Chapter 5

Energy-Efficient Heteroepitaxial Gallium Oxynitride Thin Films with Tunable Electrical and Optical Properties

5.1 Chapter Overview

In this chapter, we aim at showcasing a series of depositions that can pave the way for enabling the semiconductor industry to take advantage of the superior properties of both GaN and Ga_2O_3 (i.e., the high electron mobility of GaN for high frequency applications and the high breakdown field of Ga_2O_3 for ultrahigh power applications) by incorporating oxygen in GaN at low thermal budget (< 300°C) while obtaining a series of crystalline

films. We show that our deposition approach, enabled by plasma-enhanced ALD, preserves the GaN crystal structure as the backbone of the films while allowing to incorporate oxygen in that backbone in a controlled manner to increase the bandgap (and therefore move toward increasing the breakdown field, considering that breakdown field $\propto (E_g)^m$ where m is positive).

5.2 Experimental Details

Depositions were done at 277°C on single-side polished (R_a < 0.3 nm) prime quality c-plane sapphire wafers (see reference [8] or the Appendix for detailed specifications of the wafers) by using a Kurt J. Lesker ALD 150-LX system equipped with a remote inductively coupled plasma (ICP) source and a load lock. The error in determining the actual deposition temperatures was ±3°C. The pressure of the reactor was ∼1.1 Torr with ∼1000 sccm continuous flow of argon. In addition, 60 sccm oxygen or forming gas was introduced to the reactor during plasma exposures with ∼600 W forward power. This setup is also explained in detail elsewhere [8, 57]. Triethylgallium, TEG, (Strem Chemicals, Inc.) was electronic grade (99.9999% Ga) in a stainless steel Swagelok cylinder assembly which was not heated during the depositions; all other gases (argon, oxygen, and N_2/H_2 forming gas) were of ultrahigh purity (99.999%, Praxair Canada, Inc.). Substrates were exposed to 60 s forming gas plasma to remove contamination and pretreat the surface prior to deposition. Reference GaN depositions were done by using a recipe consisting of 0.1 s TEG dose, 3 s argon purge, 15 s forming gas plasma dose, and 2 s argon purge. Reference Ga_2O_3 depositions were done by using a recipe consisting of 0.1 s TEG dose, 20 s argon purge, 10 s

oxygen plasma dose, and 12 s argon purge (reducing the two purge times down to 3 s and 2 s, respectively, did not change the deposition results for the reference Ga_2O_3). The details of the optimization procedures that were used in this work (similarly performed for both GaN and Ga_2O_3) are explained in references [4] and [5]. Gallium oxynitride depositions were done by using a recipe consisting of X number of cycles of GaN followed by an oxygen plasma exposure, where the GaN cycles consisted of 0.1 s TEG dose, 6 s argon purge, 15 s forming gas plasma dose, and 13 s argon purge (the forming gas plasma dose time was chosen to ensure completion of GaN formation reactions); after repeating such GaN cycle for X number of times, 1.5 s oxygen plasma dose followed by 10 s argon purge were used to incorporate oxygen in the GaN film (the oxygen plasma dose time was chosen to ensure sufficient reaction of nitride and oxide using GaN and Ga_2O_3 enthalpies of formation [75] as guides and also to keep the experimental parameters consistent with the parameters in chapter 3). The $(GaN)_X$:O_1 reaction sequence was repeated to achieve the desired film thickness (the films are also referred to as X:1 throughout this chapter, and X is referred to as the "cycle ratio").

Ellipsometry measurements were done by using a J.A. Woollam M-2000DI spectroscopic ellipsometer, permanently mounted on the reactor at an incident angle of 70°, in the spectral range of 0.73-6.40 eV (equivalent to 190-1700 nm) at intervals less than 0.05 eV. Ellipsometry data analysis was done by using CompleteEASE software. Thickness and optical constants of the films were obtained based on Tauc–Lorentz modeling of the ellipsometry data (see reference [8] and section 2.3.1 for detailed explanation of the modeling procedure).

Out-of-plane coupled 1D XRD scans were performed by using a Rigaku Ultima-IV

diffractometer equipped with a cobalt source, a D/Tex ultrahigh-speed position sensitive detector, and a K-β filter at a scan rate of 2°/min and 0.02° steps (which is equivalent to 0.6 s/step exposure). The patterns were converted to copper wavelength for easier comparison with the literature.

The surface morphology of the films was examined by using a Bruker Dimension Edge atomic force microscope (AFM) with Si cantilevers (which did not have backside coating) in tapping mode with drive voltages between 2.0 and 2.2 V at a scan rate of 1 Hz. Areas as large as 3 μm by 3 μm were scanned, and the results did not change by analyzing smaller surface areas. NanoScope Analysis software was used to remove tilt by applying a first-order-flattening filter and to analyze the data.

Resistivity was measured by using the van der Pauw method by a Nanometrics HL5500 instrument equipped with a high impedance buffer amplifier/current source (HL5580).

Details of X-ray photoelectron spectroscopy (XPS) analyses along with the corresponding results are included in the Appendix.

5.3 Results and Discussion

5.3.1 Bandgap, Thickness, and Optical Properties at Different Cycle Ratios

The bandgap (E_g), thickness, and optical properties of the films on sapphire obtained from ellipsometry after 450 doses of the gallium precursor (TEG) at different GaN:O cycle ratios (i.e., different values of X) are shown in Table 5.1 as well as Figures 5.1a and 5.1b.

	sample [duration]	thickness (Å)	E_g (eV)	n @ 1.770eV (700nm)	n @ 1.960eV (632.8nm)	n @ 2.480eV (500nm)	MSE
	Pure GaN Reference **[450 cycles]**	220.32 ± 3.74	2.125 ± 0.033	2.122	2.141	2.224	10.318
X = 20	(GaN)x20-Ox1 **[450 TEG doses]**	278.49 ± 1.53	2.638 ± 0.020	2.045	2.057	2.101	5.302
X = 10	(GaN)x10-Ox1 **[450 TEG doses]**	338.69 ± 1.05	3.068 ± 0.017	1.897	1.906	1.938	3.203
X = 5	(GaN)x5-Ox1 **[450 TEG doses]**	285.16 ± 1.07	3.846 ± 0.015	1.867	1.874	1.897	2.514
	Pure Ga_2O_3 Reference **[450 cycles]**	262.10 ± 0.64	4.772 ± 0.020	1.944	1.950	1.973	2.998

Table 5.1: Results of modeling the ellipsometry data for gallium oxynitride films grown on sapphire substrate at different GaN:O cycle ratios (i.e., different values of X) after 450 doses of TEG.

Because sapphire is a dielectric with a very wide bandgap ($\sim$9 eV), the Cauchy model was used to determine optical constants of the sapphire substrate over the entire measured spectral range. A delta offset was also added to the model to correct for strained windows. Because the general structure of the gallium oxynitride films optical constants (n, k) versus wavelength was not known before the measurements, a B-spline model was first used to fit for n, k, and film thickness, and then the model was parametrized to a Tauc–Lorentz model to provide a good starting point for fitting a final Tauc–Lorentz model to the experimental data. This procedure was extremely beneficial in obtaining very low mean-squared error (MSE) values for the final fits and obtaining repeatable fit results (including n, k, E_g, and thickness).

As evident from Table 5.1, bandgap increases with increasing the number of oxygen

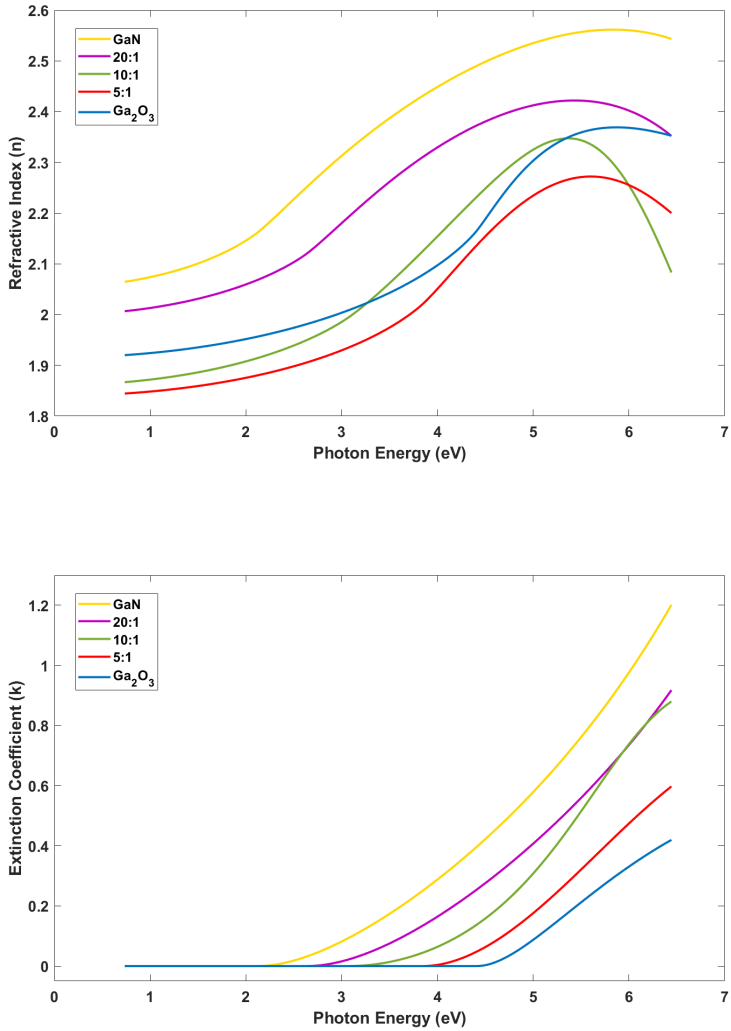

Figure 5.1: Optical constants of gallium oxynitride films grown on sapphire after 450 doses of TEG as a function of photon energy. The error in refractive index and extinction coefficient values is limited to ±0.001 in all cases.

exposures per 450 TEG doses, that is, the films that are grown using a smaller GaN:O cycle ratio (equivalent to a smaller value of X) have a larger bandgap. Comparing the bandgap of gallium oxynitride films with pure GaN and Ga_2O_3 films grown at the same temperature after the same number of TEG doses reveals that the bandgap of the gallium oxynitride films fall between the bandgap of pure GaN and Ga_2O_3 films. A similar trend is observed for the refractive index (n) and the extinction coefficient (k) values in Figure 5.1 as well.

Based on ellipsometry results, gallium oxynitride films are all thicker than the pure GaN film deposited by using the same number of TEG doses. Meanwhile, ellipsometry results show that the X = 10 film appears thicker than the other oxynitride films (see Table 5.1) while also having slightly different dispersion curves for its optical properties (see the dispersion of refractive index (n) and extinction coefficient (k) for this film in Figure 5.1). The reason for these results is not clear, and further analysis (including TEM analysis to confirm the thickness and the internal structure of the films) is required to shed light on these results.

5.3.2 Resistivity as a Function of Cycle Ratio

Figure 5.2 shows the electrical resistivity along with the bandgap of the gallium oxynitride films grown on sapphire. The electrical resistivity and the bandgap of a reference GaN film on sapphire and a reference Ga_2O_3 film on sapphire are also shown in this figure. As shown in Figure 5.2, electrical resistivity of the gallium oxynitride films increases by increasing the number of oxygen exposures per 450 TEG doses, that is, the films that are grown using

a smaller GaN:O cycle ratio (equivalent to a smaller value of X) have a larger resistivity. The resistivity of the gallium oxynitride films falls between the resistivity of pure GaN and Ga_2O_3 films (note that all films were grown using the same number of TEG doses (i.e., 450 doses) except the reference Ga_2O_3 film used for resistivity measurements which was grown using 700 TEG doses to obtain a thicker film ($\sim$38 nm) for resistivity measurements because thinner Ga_2O_3 films would have resistance values outside the instrument measurement capabilities). The same trend is observed for bandgap as well (see section 5.3.1 for more details on variations of bandgap with cycle ratio).

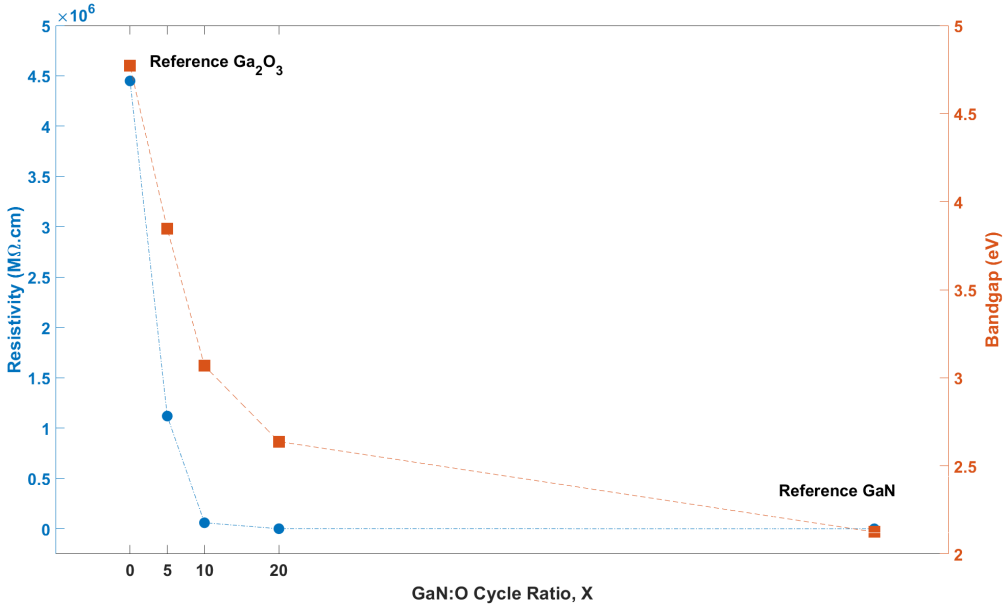

Figure 5.2: Resistivity of the gallium oxynitride films along with a reference GaN film and an $\sim$38 nm Ga_2O_3 film grown on sapphire at the same deposition temperature. All films were grown using the same number of TEG doses (i.e., 450 doses) except the $\sim$38 nm Ga_2O_3 film which was grown using 700 TEG doses to obtain a thicker film for feasible resistivity measurements.

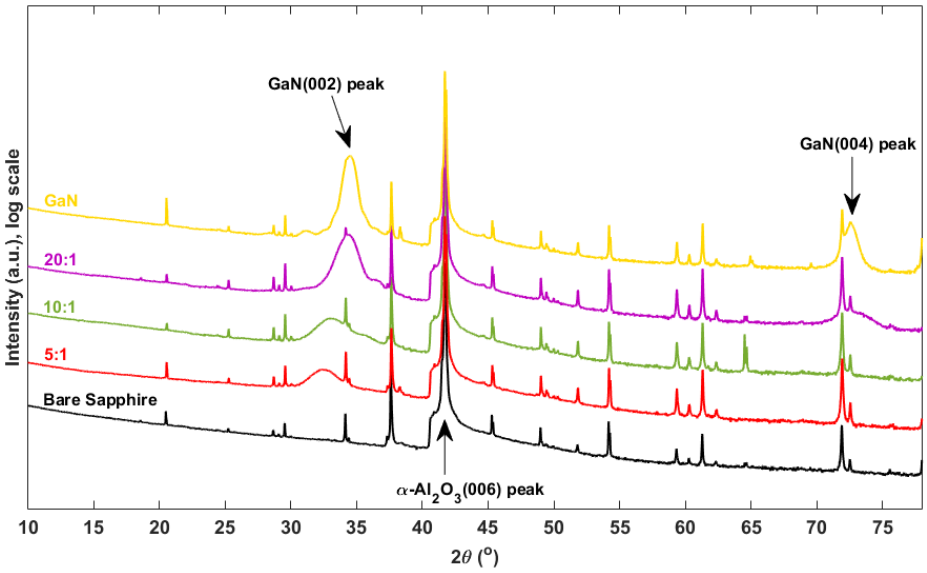

Figure 5.3: Out-of-plane coupled XRD patterns for the gallium oxynitride films along with a reference GaN film grown on sapphire at the same deposition temperature. All films were grown using the same number of TEG doses (i.e., 450 doses). The XRD pattern of the bare sapphire substrate is included as a reference as well to better distinguish thin film peaks in the patterns.

5.3.3 Crystal Structure as a Function of Cycle Ratio

XRD patterns were obtained for gallium oxynitride samples grown at different GaN:O cycle ratios (i.e., different values of X) on c-plane sapphire, Si(100), Si(111), Si(110), and glass. In all cases, the XRD pattern of the corresponding substrate was used as a reference to better distinguish thin film peaks in the patterns. No crystallinity was observed on Si(100), Si(111), Si(110), and glass. Meanwhile, the gallium oxynitride films on c-plane sapphire showed peaks in their XRD patterns at all cycle ratios.

Figure 5.3 shows the results of out-of-plane 1D coupled XRD scans of the gallium oxynitride films along with a reference GaN film deposited on sapphire as well as the corresponding scan of the bare sapphire substrate as reference. The single crystal c-plane sapphire substrate is expected to show a peak at $2\theta = 41.80°$ corresponding to α-Al_2O_3(006)

planes (considering the average of K-α1 and K-α2 peak locations) [62]. The α-Al_2O_3(006) peak is evident in Figure 5.3 as the strongest peak.

Comparing the reference sapphire pattern with patterns of the thin film coated samples in Figure 5.3, a set of major peaks can be distinguished as gallium oxynitride thin film peaks corresponding to regularly arranged planes parallel to the surface. As can be seen in Figure 5.3, these peaks are in close proximity of GaN(002) and GaN(004) peaks of the reference GaN film. Comparing 20:1, 10:1, and 5:1 samples, GaN(002) peak shifts to lower angles (i.e., higher d-spacings) as the oxygen exposure increases (or the cycle ratio, X, decreases). This could be explained by noting that gallium atoms need to be slightly displaced along the c-axis to enable the crystal structure of w-GaN to adjust for oxygen incorporation (see Figure 3.1, considering that α-Ga_2O_3 has the closest structure to w-GaN among Ga_2O_3 polymorphs). Figure 5.3 also shows that the intensity of the GaN(002) peak decreases and its broadness increases by increasing the number of oxygen exposures per 450 TEG doses, that is, the films that are grown using a smaller GaN:O cycle ratio (equivalent to a smaller value of X) have weaker and broader peaks indicative of a possible decrease in their crystalline content. Meanwhile, it is noteworthy that in all cases, the crystalline planes remain highly oriented. Further analysis (including TEM analysis to investigate the internal structure of the films) can be very helpful in clarifying these results.

It was shown in chapter 3 that when oxygen exposure is done after depositing only one cycle of GaN (equivalent to $X = 1$) a hexagonal arrangement of Ga atoms acts as an atomic scale scaffold and navigates the oxygen atoms to convert GaN to α-Ga_2O_3. However, by depositing more than one cycle of GaN (such as depositing 5, 10, or 20 cycles of GaN) prior to oxygen exposure, we no longer have the simple hexagonal scaffold that existed for

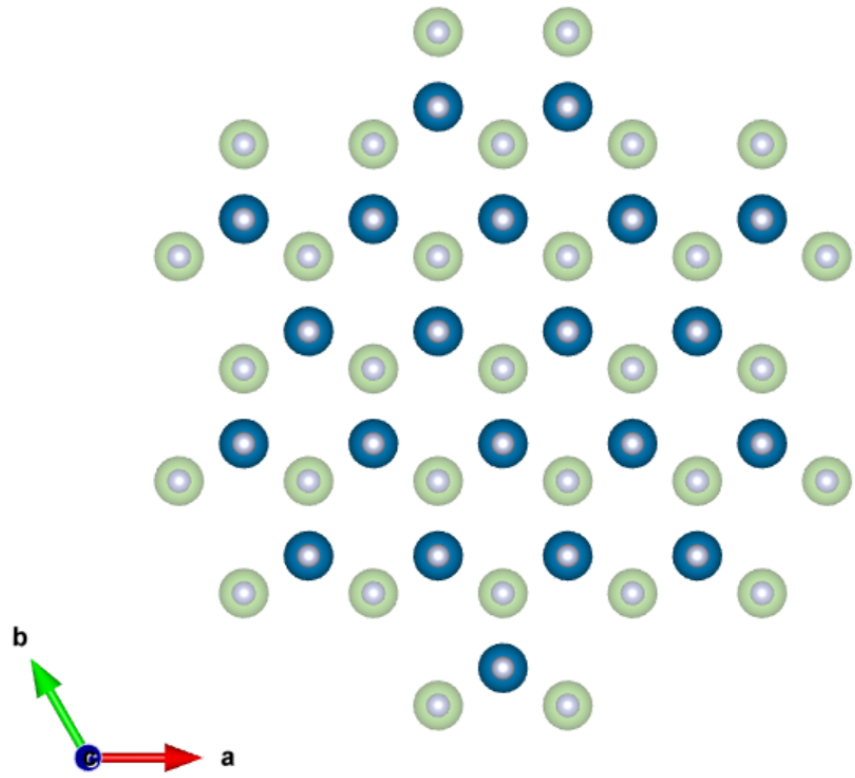

Figure 5.4: View of two monolayers of w-GaN along the c-axis; Ga atoms are green and dark blue circles, and nitrogen atoms are smaller grey circles.

the case of $X = 1$ because each unit cell of w-GaN consists of two layers of such hexagonal scaffolds that are not aligned exactly on top of each other. This has been illustrated in Figure 5.4 where the first hexagonal layer of Ga atoms in a unit cell of w-GaN is shown by using green circles (similar to Figure 3.1 in chapter 3) and the second layer is shown by using dark blue circles. As evident in Figure 5.4, depositing more than one monolayer of w-GaN results in the two hexagonal layers stacking on top of each other in a way that interferes with straightforward formation of α-Ga_2O_3 (compare Figure 5.4 with Figure 3.1c in chapter 3). This crystallographic arrangement of the metal atoms in a w-GaN unit cell along with increased stability of GaN multilayers compared to a monolayer of GaN is consistent with our XRD results showing that gallium nitride retains its stability for thin

	Bare Sapphire Substrate	5:1 (450 TEG doses)	10:1 (450 TEG doses)	20:1 (450 TEG doses)	GaN (450 TEG doses)
R_a	0.058nm	0.942nm	0.656nm	0.694nm	0.251nm
R_q	0.073nm	1.21nm	0.836nm	0.877nm	0.316nm
R_{max} (= Z range)	0.84nm	11.5nm	7.71nm	7.32nm	2.66nm
Skewness [compared to zero]	+0.098	+1.06	+0.551	+0.510	-0.0585
Kurtosis [compared to 3]	3.45 [almost normal]	4.75 [very spiked]	3.72 [spiked]	3.41 [almost normal]	3.12 [almost normal]

Table 5.2: AFM statistics for the gallium oxynitride films along with a reference GaN film grown on sapphire at the same deposition temperature and using the same number of TEG doses (i.e., 450 doses). While the nominal average roughness of the c-plane sapphire substrate is $R_a < 0.3$ nm, an example of actual statistics for a piece of bare sapphire is also included for reference.

film samples deposited using X = 5, 10, and 20; this is evident by the presence of highly oriented GaN(002)-like planes in these samples being merely shifted to higher d-spacings by increasing oxygen exposure. This is not a common observation in the literature for incorporation of oxygen in GaN where amorphous films with varying compositions (either amorphous Ga_2O_3 or amorphous gallium oxynitrides) or β-Ga_2O_3 films are often obtained as a result of attempting to incorporate oxygen in the gallium nitride lattice.

5.3.4 Surface Roughness as a Function of Cycle Ratio

AFM measurements were performed on the gallium oxynitride films deposited on sapphire at several locations on each sample, and the representative statistics are shown in Table 5.2. If one uses the nominal average roughness of the bare sapphire substrate as a reference ($R_a < 0.3$ nm), it is evident that all of the films listed in Table 5.2 are still relatively smooth based on their corresponding values of R_a. In all cases, R_q is slightly larger than R_a, which is expected since R_a is known to represent the mean absolute profile, making no distinction between peaks and valleys, while R_q is more sensitive to peaks and valleys due to squaring

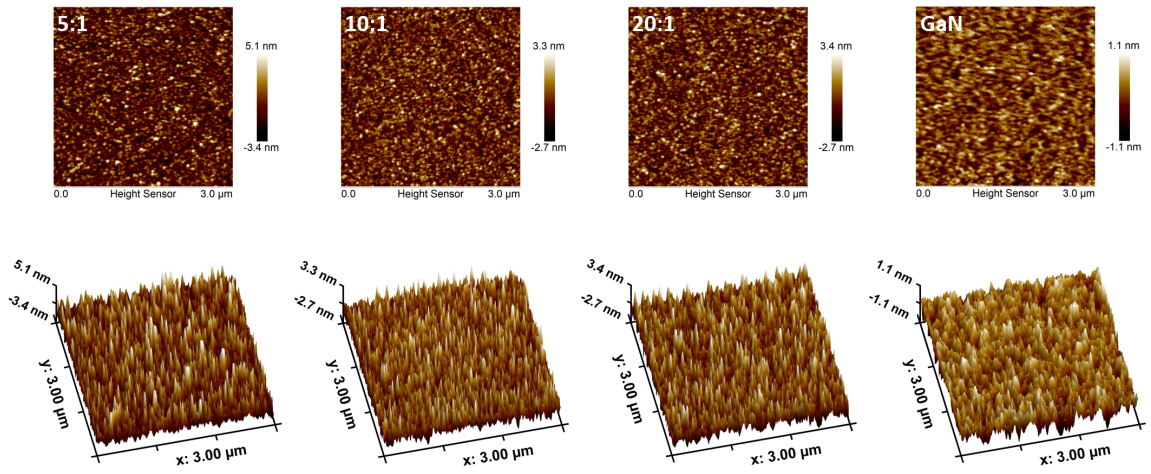

Figure 5.5: 2D and 3D AFM profiles for the gallium oxynitride films along with a reference GaN film grown on sapphire at the same deposition temperature and using the same number of TEG doses (i.e., 450 doses).

of the amplitude in its calculation [74]. As shown in Table 5.2, the 5:1 film is the roughest among all films with the largest R_a, R_q, and R_{max} (even though these values are still small by themselves).

Table 5.2 also lists the skewness parameter as a measure of the degree of bias of the roughness shape. Skewness is not large compared to zero for any of the films, indicating that the height distribution on the surface is almost symmetrical around the mean plane. Another parameter that was extracted from the AFM measurements and is shown in Table 5.2 is the kurtosis value as a measure of the population of sharp features in the surface profile. A value of 3 for the kurtosis parameter indicates that sharp and indented features occur equally frequently in the height distribution, similar to a normal distribution, and that the population of outliers is negligible. As listed in Table 5.2, the 5:1 film has a spiked height distribution compared to the other films, indicated by its larger kurtosis value compared to the other films.

Figure 5.5 provides visual representation of surface profile of the gallium oxynitride

films on sapphire deposited at different cycle ratios along with the reference GaN film. For each sample, the scales of the 2D and 3D profiles are the same and were set in a way that low population tails in the height distribution are excluded. Figure 5.5 confirms the overall smooth surface of the films, consistent with the low roughness values reported in Table 5.2.

5.4 Summary and Conclusions

In this work, we proposed a series of depositions for incorporation of oxygen in the crystal structure of GaN at low temperature and showed that these deposition strategies can be used to tune the structure as well as the properties of the resulting films. We obtained gallium oxynitride films with tunable lattice constant, bandgap, and resistivity that can be used in both electronic and optoelectronic devices either as the active layer of the device or as a passive component used to adjust the properties and the performance of such devices. The results of this work enable growth of gallium oxynitride thin films, with superior material properties offered by ALD, not only with potential applications as high-performance materials in reducing energy consumption but also with an energy-efficient fabrication process.

Chapter 6

Summary and Future Work

6.1 Summary and Contributions to Knowledge

One of the shortcomings in the field of electronics is energy waste that can happen at several stages, including losses that occur because of fundamental material limitations, as well as excessive energy consumption that occurs during the fabrication of the electronic devices. This work demonstrated a number of strategies for energy-efficient fabrication of high quality crystalline films of gallium oxide and oxynitrides as novel wide bandgap semiconductors with potential applications in a broad range of electronic devices. The strategies shown in this work are easy to implement in fabrication process flows, they increase the material selection versatility, and they save energy. Therefore, the strategies presented in this work, can play a positive role in advancing the human society by helping to realize next-generation electronic device components as well as by improving energy accessibility in the world through decreasing energy consumption.

Specifically, in Chapter 2, an optimized atomic layer deposition (ALD) process is used

to deposit gallium oxide (Ga_2O_3) thin films on a variety of common substrates aiming to obtain crystalline gallium oxide at very low temperatures. The onset of crystallinity formation was determined to be as low as 190°C on c-plane sapphire, above which crystalline films consisting of a mixture of α-Ga_2O_3 and β-Ga_2O_3 are obtained. A targeted annealing study was performed to successfully obtain β-Ga_2O_3 on c-plane sapphire at 550°C. Both of these temperatures (190°C and 550°C) are, to the best of our knowledge, the lowest temperatures reported in the literature at which ALD-grown crystalline gallium oxide films are obtained as-deposited and annealed, respectively. These results provide insights into the development of a low-temperature crystalline gallium oxide technology that will lead to energy-efficient electronic devices, not only in performance but also in an energy-efficient fabrication process.

In Chapter 3, a self-regulated process is introduced for controlling Ga_2O_3 crystallinity to achieve α-Ga_2O_3 through a stepwise in-situ plasma-enhanced oxidation of a wurtzite GaN (w-GaN) template. The entire deposition is optimized to achieve crystallinity at the low temperature of 277°C, thereby establishing an energy-efficient fabrication process for growing crystalline Ga_2O_3 films on non-native substrates. This deposition process successfully achieves α-Ga_2O_3 through stepwise construction of an atomic scale hexagonal scaffold of gallium atoms while taking advantage of plasma species to transform nitride to oxide at a low thermal budget. Fabrication of Ga_2O_3 devices on GaN-compatible non-native substrates using this deposition strategy allows for the development of next-generation electronic devices which are able to concurrently handle higher power, higher voltage, and higher operating temperatures. More importantly, the atomic level scaffolding process introduced in Chapter 3 can be used for other materials as well to enable growth of metastable

and stable phases of materials on substrates that are not currently possible.

In Chapter 4, a deposition strategy is presented that achieves high quality β-Ga_2O_3 films by using metastable Ga_2O_3 as an intermediate layer prior to β-Ga_2O_3 deposition. This process enables deposition of high quality β-Ga_2O_3 on substrates that are compatible with different Ga_2O_3 polymorphs (i.e., not just with β-Ga_2O_3 but also with metastable polymorphs) and paves the way for accelerated development of β-Ga_2O_3 devices on non-native substrates.

In Chapter 5, we investigate the possibility of low temperature ALD growth of gallium oxynitride films in an attempt to preserve the crystal structure of w-GaN as the background matrix material while inserting oxygen anions in the GaN lattice to increase the bandgap (and thus the breakdown voltage). Uniform pinhole-free films were obtained for use in electronic device applications or for use as buffer layers in epitaxial growth techniques.

Overall, this thesis provides fundamental understanding of low thermal budget growth of gallium oxide thin films on non-native substrates. Going beyond conventional methods or specific materials, this thesis also demonstrates a unique scaffolding strategy as a means by which desired thin film crystallinity can be achieved even in cases where a suitable substrate is not accessible. Demonstrating the effectiveness of this scaffolding strategy in growing single-phase gallium oxide films on non-native substrates provides the foundation for exploiting the potential of this strategy in growing crystalline phases of other technologically important thin films.

6.2 Future Work

The field of wide bandgap electronics, and especially gallium oxide electronics, is an emerging field with great potential for research and development. An interesting area for future work, using the deposition strategies presented in this work, would be to pursue implementation of the films grown in this study in electronic and optoelectronic devices; this will allow direct measurement of the electronic and optoelectronic properties of these thin films (including their exact breakdown field and electron mobility) and will allow comparison of these properties to the properties of bulk materials. The gallium oxynitride films obtained in this work can be specifically interesting to study in further detail for applications as buffer layers in epitaxial thin film growth.

Bibliography

[1] E. Rafie Borujeny and K. Cadien, "On achieving single-phase crystalline gallium oxide thin films at low thermal budgets," in *The American Vacuum Society 67th International Symposium (AVS 67)*. AVS, Oct. 2021.

[2] ——, "Gallium oxynitride thin films with tunable properties for electronic and photonic applications," in *The American Vacuum Society 67th International Symposium (AVS 67)*. AVS, Oct. 2021.

[3] ——, "Crystallinity control via atomic level scaffolding," in *The International Conference on Atomic Layer Deposition (ALD 2021)*. AVS, Jun. 2021.

[4] ——, "Revisiting process optimization in atomic layer deposition: Going beyond growth rate," in *The International Conference on Atomic Layer Deposition (ALD 2021)*. AVS, Jun. 2021.

[5] ——, "From amorphous to β-gallium oxide: Practical implementation of energetics considerations in process design and optimization," *ECS Meeting Abstracts*, vol. MA2021-01, no. 36, pp. 2104–2104, May 2021.

[6] ——, "Deposition of beta-gallium oxide thin films," United States Patent 63/173,260, Apr. 9, 2021.

[7] ——, "Deposition of alpha-gallium oxide thin films," United States Patent 63/137,874, Jan. 15, 2021.

[8] E. R. Borujeny, O. Sendetskyi, M. D. Fleischauer, and K. C. Cadien, "Low thermal budget heteroepitaxial gallium oxide thin films enabled by atomic layer deposition," *ACS Applied Materials & Interfaces*, vol. 12, no. 39, pp. 44 225–44 237, 2020, doi: 10.1021/acsami.0c08477. [Online]. Available: https://doi.org/10.1021/acsami.0c08477

[9] E. Rafie Borujeny and K. Cadien, "ALD-grown gallium oxide thin films with properties close to bulk wafers," in *The International Conference on Atomic Layer Deposition (ALD 2020)*. AVS, Jun. 2020.

[10] M. A. Mastro, A. Kuramata, J. Calkins, J. Kim, F. Ren, and S. J. Pearton, "Perspective—opportunities and future directions for Ga_2O_3," *ECS Journal of Solid State Science and Technology*, vol. 6, no. 5, pp. P356–P359, 2017. [Online]. Available: http://dx.doi.org/10.1149/2.0031707jss

[11] S. J. Pearton, J. Yang, P. H. Cary, F. Ren, J. Kim, M. J. Tadjer, and M. A. Mastro, "A review of Ga_2O_3 materials, processing, and devices," *Applied Physics Reviews*, vol. 5, no. 1, p. 011301, 2018, doi: 10.1063/1.5006941; 30. [Online]. Available: https://doi.org/10.1063/1.5006941

[12] S. I. Stepanov, V. Nikolaev, V. E. Bougrov, and A. Romanov, "Gallium oxide: Properties and applications - a review," *Reviews on Advanced Materials Science*, vol. 44, pp. 63–86, 2016.

[13] R. K. Ramachandran, J. Dendooven, J. Botterman, S. P. Sree, D. Poelman, J. A. Martens, H. Poelman, and C. Detavernier, "Plasma enhanced atomic layer deposition of Ga_2O_3 thin films," *Journal of Materials Chemistry A*, vol. 2, no. 45, pp. 19 232–19 238, 2014. [Online]. Available: http://dx.doi.org/10.1039/C4TA05007J

[14] F. K. Shan, G. X. Liu, W. J. Lee, G. H. Lee, I. S. Kim, and B. C. Shin, "Structural, electrical, and optical properties of transparent gallium oxide thin films grown by plasma-enhanced atomic layer deposition," *Journal of Applied Physics*, vol. 98, no. 2, p. 023504, 2005, doi: 10.1063/1.1980535; 30. [Online]. Available: https://doi.org/10.1063/1.1980535

[15] D. won Choi, K.-B. Chung, and J.-S. Park, "Low temperature Ga_2O_3 atomic layer deposition using gallium tri-isopropoxide and water," *Thin Solid Films; The proceedings of International Union of the Materials Research Society -International Conference in Asia 2012- IUMRS-ICA 2012*, vol. 546, pp. 31–34, 2013. [Online]. Available: http://www.sciencedirect.com/science/article/pii/S0040609013005130

[16] H.-Y. Shih, F.-C. Chu, A. Das, C.-Y. Lee, M.-J. Chen, and R.-M. Lin, "Atomic layer deposition of gallium oxide films as gate dielectrics in AlGaN/GaN metal-oxide-semiconductor high-electron-mobility transistors," *Nanoscale Research*

Letters, vol. 11, no. 1, p. 235, 2016, iD: Shih2016. [Online]. Available: https://doi.org/10.1186/s11671-016-1448-z

[17] G. X. Liu, F. K. Shan, W. J. Lee, B. C. Shin, S. C. Kim, H. S. Kim, and C. R. Cho, "Growth temperature dependence of Ga_2O_3 thin films deposited by plasma enhanced atomic layer deposition," *Integrated Ferroelectrics*, vol. 94, no. 1, pp. 11–20, 2007, doi: 10.1080/10584580701755716. [Online]. Available: https://doi.org/10.1080/10584580701755716

[18] H. Altuntas, I. Donmez, C. Ozgit-Akgun, and N. Biyikli, "Effect of postdeposition annealing on the electrical properties of β-Ga_2O_3 thin films grown on p-Si by plasma-enhanced atomic layer deposition," *Journal of Vacuum Science & Technology A*, vol. 32, no. 4, p. 041504, 2014, doi: 10.1116/1.4875935; 30. [Online]. Available: https://doi.org/10.1116/1.4875935

[19] ——, "Electrical characteristics of β-Ga_2O_3 thin films grown by PEALD," *Journal of Alloys and Compounds*, vol. 593, pp. 190–195, 2014. [Online]. Available: http://www.sciencedirect.com/science/article/pii/S0925838814000607

[20] A. Mahmoodinezhad, C. Janowitz, F. Naumann, P. Plate, H. Gargouri, K. Henkel, D. Schmeißer, and J. I. Flege, "Low-temperature growth of gallium oxide thin films by plasma-enhanced atomic layer deposition," *Journal of Vacuum Science & Technology A*, vol. 38, no. 2, p. 022404, 2020, doi: 10.1116/1.5134800; 30. [Online]. Available: https://doi.org/10.1116/1.5134800

[21] M. Higashiwaki, K. Sasaki, A. Kuramata, T. Masui, and S. Yamakoshi, "Development of gallium oxide power devices," *physica status solidi (a)*, vol. 211, no. 1, pp. 21–26, 2014, doi: 10.1002/pssa.201330197; 30. [Online]. Available: https://doi.org/10.1002/pssa.201330197

[22] M. Zinkevich and F. Aldinger, "Thermodynamic assessment of the gallium-oxygen system," *Journal of the American Ceramic Society*, vol. 87, no. 4, pp. 683–691, 2004, doi: 10.1111/j.1551-2916.2004.00683.x; 30. [Online]. Available: https://doi.org/10.1111/j.1551-2916.2004.00683.x

[23] H. He, R. Orlando, M. A. Blanco, R. Pandey, E. Amzallag, I. Baraille, and M. Rérat, "First-principles study of the structural, electronic, and optical properties of Ga_2O_3 in its monoclinic and hexagonal phases," *Physical Review B*, vol. 74, no. 19, p. 195123, 2006, iD: 10.1103/PhysRevB.74.195123; J1: PRB. [Online]. Available: https://link.aps.org/doi/10.1103/PhysRevB.74.195123

[24] H. Y. Playford, A. C. Hannon, E. R. Barney, and R. I. Walton, "Structures of uncharacterised polymorphs of gallium oxide from total neutron diffraction," *Chemistry – A European Journal*, vol. 19, no. 8, pp. 2803–2813, 2013, doi: 10.1002/chem.201203359; 30. [Online]. Available: https://doi.org/10.1002/chem.201203359

[25] I. Cora, F. Mezzadri, F. Boschi, M. Bosi, M. Čaplovičová, G. Calestani, I. Dódony, B. Pécz, and R. Fornari, "The real structure of ϵ-Ga_2O_3 and its relation to

κ-phase," *CrystEngComm*, vol. 19, no. 11, pp. 1509–1516, 2017. [Online]. Available: http://dx.doi.org/10.1039/C7CE00123A

[26] R. Roy, V. G. Hill, and E. F. Osborn, "Polymorphs of alumina and gallia," *Industrial & Engineering Chemistry*, vol. 45, no. 4, pp. 819–820, 1953, doi: 10.1021/ie50520a047. [Online]. Available: https://doi.org/10.1021/ie50520a047

[27] S. Yoshioka, H. Hayashi, A. Kuwabara, F. Oba, K. Matsunaga, and I. Tanaka, "Structures and energetics of Ga_2O_3 polymorphs," *Journal of Physics: Condensed Matter*, vol. 19, no. 34, p. 346211, 2007. [Online]. Available: http://dx.doi.org/10.1088/0953-8984/19/34/346211

[28] E. Ahmadi and Y. Oshima, "Materials issues and devices of α-and β-Ga_2O_3," *Journal of Applied Physics*, vol. 126, no. 16, p. 160901, 2019.

[29] E. Ahvenniemi, A. R. Akbashev, S. Ali, M. Bechelany, M. Berdova, S. Boyadjiev, D. C. Cameron, R. Chen, M. Chubarov, V. Cremers, A. Devi, V. Drozd, L. Elnikova, G. Gottardi, K. Grigoras, D. M. Hausmann, C. S. Hwang, S.-H. Jen, T. Kallio, J. Kanervo, I. Khmelnitskiy, D. H. Kim, L. Klibanov, Y. Koshtyal, A. O. I. Krause, J. Kuhs, I. Kärkkänen, M.-L. Kääriäinen, T. Kääriäinen, L. Lamagna, A. A. Łapicki, M. Leskelä, H. Lipsanen, J. Lyytinen, A. Malkov, A. Malygin, A. Mennad, C. Militzer, J. Molarius, M. Norek, Çağla Özgit Akgün, M. Panov, H. Pedersen, F. Piallat, G. Popov, R. L. Puurunen, G. Rampelberg, R. H. A. Ras, E. Rauwel, F. Roozeboom, T. Sajavaara, H. Salami, H. Savin, N. Schneider, T. E. Seidel, J. Sundqvist, D. B. Suyatin, T. Törndahl, J. R. van Ommen, C. Wiemer,

O. M. E. Ylivaara, and O. Yurkevich, "Review article: Recommended reading list of early publications on atomic layer deposition–outcome of the "virtual project on the history of ALD"," *Journal of Vacuum Science & Technology A*, vol. 35, no. 1, p. 010801, 2017, doi: 10.1116/1.4971389; 01. [Online]. Available: https://doi.org/10.1116/1.4971389

[30] S. M. George, "Atomic layer deposition: An overview," *Chemical reviews*, vol. 110, no. 1, pp. 111–131, 2010, doi: 10.1021/cr900056b. [Online]. Available: https://doi.org/10.1021/cr900056b

[31] A. Foroughi-Abari and K. Cadien, *Atomic Layer Deposition for Nanotechnology*, ser. Nanofabrication: Techniques and Principles. Vienna: Springer, 2012, pp. 143–161.

[32] T. Muneshwar, M. Miao, E. R. Borujeny, and K. Cadien, *Atomic Layer Deposition: Fundamentals, Practice, and Challenges*, ser. Handbook of Thin Film Deposition (Fourth Edition). William Andrew Publishing, 2018, pp. 359–377.

[33] S.-J. Ding and X. Wu, "Superior atomic layer deposition technology for amorphous oxide semiconductor thin-film transistor memory devices," *Chemistry of Materials*, vol. 32, no. 4, pp. 1343–1357, 2020, doi: 10.1021/acs.chemmater.9b03237. [Online]. Available: https://doi.org/10.1021/acs.chemmater.9b03237

[34] I. Donmez, C. Ozgit-Akgun, and N. Biyikli, "Low temperature deposition of Ga_2O_3 thin films using trimethylgallium and oxygen plasma," *Journal of Vacuum Science & Technology A*, vol. 31, no. 1, p. 01A110, 2013, doi: 10.1116/1.4758782; 30. [Online]. Available: https://doi.org/10.1116/1.4758782

[35] H. Hao, X. Chen, Z. Li, Y. Shen, H. Wang, Y. Zhao, R. Huang, T. Liu, J. Liang, Y. An, Q. Peng, and S. Ding, "Remote plasma-enhanced atomic layer deposition of gallium oxide thin films with NH_3 plasma pretreatment," *Journal of Semiconductors*, vol. 40, no. 1, p. 012806, 2019. [Online]. Available: http://dx.doi.org/10.1088/1674-4926/40/1/012806

[36] R. O'Donoghue, J. Rechmann, M. Aghaee, D. Rogalla, H.-W. Becker, M. Creatore, A. D. Wieck, and A. Devi, "Low temperature growth of gallium oxide thin films via plasma enhanced atomic layer deposition," *Dalton Transactions*, vol. 46, no. 47, pp. 16 551–16 561, 2017. [Online]. Available: http://dx.doi.org/10.1039/C7DT03427J

[37] T. G. Allen and A. Cuevas, "Electronic passivation of silicon surfaces by thin films of atomic layer deposited gallium oxide," *Applied Physics Letters*, vol. 105, no. 3, p. 031601, 2014, doi: 10.1063/1.4890737; 30. [Online]. Available: https://doi.org/10.1063/1.4890737

[38] A. K. Chandiran, N. Tetreault, R. Humphry-Baker, F. Kessler, E. Baranoff, C. Yi, M. K. Nazeeruddin, and M. Grätzel, "Subnanometer Ga_2O_3 tunnelling layer by atomic layer deposition to achieve 1.1 V open-circuit potential in dye-sensitized solar cells," *Nano Letters*, vol. 12, no. 8, pp. 3941–3947, 2012, doi: 10.1021/nl301023r. [Online]. Available: https://doi.org/10.1021/nl301023r

[39] D. J. Comstock and J. W. Elam, "Atomic layer deposition of Ga_2O_3 films using trimethylgallium and ozone," *Chemistry of Materials*, vol. 24, no. 21,

pp. 4011–4018, 2012, doi: 10.1021/cm300712x. [Online]. Available: https://doi.org/10.1021/cm300712x

[40] T. G. Allen and A. Cuevas, "Plasma enhanced atomic layer deposition of gallium oxide on crystalline silicon: Demonstration of surface passivation and negative interfacial charge," *physica status solidi (RRL) – Rapid Research Letters*, vol. 9, no. 4, pp. 220–224, 2015, doi: 10.1002/pssr.201510056; 30. [Online]. Available: https://doi.org/10.1002/pssr.201510056

[41] P. P. Pansila, K. Kanomata, B. Ahmmad, S. Kubota, and F. Hirose, "Room temperature atomic layer deposition of gallium oxide investigated by IR absorption spectroscopy," *IEICE Transactions on Electronics*, vol. E98.C, no. 5, pp. 382–389, 2015, tI:.

[42] J. W. Roberts, J. C. Jarman, D. N. Johnstone, P. A. Midgley, P. R. Chalker, R. A. Oliver, and F. C.-P. Massabuau, "α-Ga_2O_3 grown by low temperature atomic layer deposition on sapphire," *Journal of Crystal Growth*, vol. 487, pp. 23–27, 2018. [Online]. Available: http://www.sciencedirect.com/science/article/pii/S0022024818300617

[43] J. W. Roberts, P. R. Chalker, B. Ding, R. A. Oliver, J. T. Gibbon, L. A. H. Jones, V. R. Dhanak, L. J. Phillips, J. D. Major, and F. C. P. Massabuau, "Low temperature growth and optical properties of α-Ga_2O_3 deposited on sapphire by plasma enhanced atomic layer deposition," *Journal of Crystal Growth*, vol. 528, p. 125254, 2019. [Online]. Available: http://www.sciencedirect.com/science/article/pii/S0022024819304695

[44] C. L. Dezelah, J. Niinistö, K. Arstila, L. Niinistö, and C. H. Winter, "Atomic layer deposition of Ga_2O_3 films from a dialkylamido-based precursor," *Chemistry of Materials*, vol. 18, no. 2, pp. 471–475, 2006, doi: 10.1021/cm0521424. [Online]. Available: https://doi.org/10.1021/cm0521424

[45] Y. S. Lee, D. Chua, R. E. Brandt, S. C. Siah, J. V. Li, J. P. Mailoa, S. W. Lee, R. G. Gordon, and T. Buonassisi, "Atomic layer deposited gallium oxide buffer layer enables 1.2 V open-circuit voltage in cuprous oxide solar cells," *Advanced Materials*, vol. 26, no. 27, pp. 4704–4710, 2014, doi: 10.1002/adma.201401054; 30. [Online]. Available: https://doi.org/10.1002/adma.201401054

[46] D. R. Boris, V. D. Wheeler, J. R. Avila, S. B. Qadri, C. R. Eddy, and S. G. Walton, "Role of plasma properties in controlling crystallinity and phase in oxide films grown by plasma-enhanced atomic layer epitaxy," *Journal of Vacuum Science & Technology A*, vol. 37, no. 6, p. 060909, 2019, doi: 10.1116/1.5128208; 30. [Online]. Available: https://doi.org/10.1116/1.5128208

[47] V. D. Wheeler, N. Nepal, D. R. Boris, S. B. Qadri, L. O. Nyakiti, A. Lang, A. Koehler, G. Foster, S. G. Walton, C. R. Eddy, and D. J. Meyer, "Phase control of crystalline Ga_2O_3 films by plasma-enhanced atomic layer deposition," *Chemistry of Materials*, vol. 32, no. 3, pp. 1140–1152, 2020, doi: 10.1021/acs.chemmater.9b03926. [Online]. Available: https://doi.org/10.1021/acs.chemmater.9b03926

[48] T. G. Allen, M. Ernst, C. Samundsett, and A. Cuevas, "Demonstration of c-Si solar cells with gallium oxide surface passivation and laser-doped gallium p+ regions,"

IEEE Journal of Photovoltaics, vol. 5, no. 6, pp. 1586–1590, 2015.

[49] F. Boschi, M. Bosi, T. Berzina, E. Buffagni, C. Ferrari, and R. Fornari, "Hetero-epitaxy of ϵ-Ga_2O_3 layers by MOCVD and ALD," *Journal of Crystal Growth*, vol. 443, pp. 25–30, 2016. [Online]. Available: http://www.sciencedirect.com/science/article/pii/S0022024816300859

[50] S. A. Kukushkin, A. V. Osipov, V. N. Bessolov, B. K. Medvedev, V. K. Nevolin, and K. A. Tcarik, "Substrates for epitaxy of gallium nitride: New materials and techniques," *Reviews on Advanced Materials Science*, vol. 17, no. 1, pp. 1–32, 2008.

[51] E. G. Víllora, K. Shimamura, K. Kitamura, K. Aoki, and T. Ujiie, "Epitaxial relationship between wurtzite GaN and β-Ga_2O_3," *Applied Physics Letters*, vol. 90, no. 23, p. 234102, 2007, doi: 10.1063/1.2745645; 08. [Online]. Available: https://doi.org/10.1063/1.2745645

[52] H. Amano, Y. Baines, E. Beam, M. Borga, T. Bouchet, P. R. Chalker, M. Charles, K. J. Chen, N. Chowdhury, R. Chu, C. D. Santi, M. M. D. Souza, S. Decoutere, L. D. Cioccio, B. Eckardt, T. Egawa, P. Fay, J. J. Freedsman, L. Guido, O. Häberlen, G. Haynes, T. Heckel, D. Hemakumara, P. Houston, J. Hu, M. Hua, Q. Huang, A. Huang, S. Jiang, H. Kawai, D. Kinzer, M. Kuball, A. Kumar, K. B. Lee, X. Li, D. Marcon, M. März, R. McCarthy, G. Meneghesso, M. Meneghini, E. Morvan, A. Nakajima, E. M. S. Narayanan, S. Oliver, T. Palacios, D. Piedra, M. Plissonnier, R. Reddy, M. Sun, I. Thayne, A. Torres, N. Trivellin, V. Unni, M. J. Uren, M. V. Hove, D. J. Wallis, J. Wang, J. Xie, S. Yagi, S. Yang, C. Youtsey, R. Yu, E. Zanoni,

S. Zeltner, and Y. Zhang, "The 2018 gan power electronics roadmap," *Journal of Physics D: Applied Physics*, vol. 51, no. 16, p. 163001, 2018. [Online]. Available: http://dx.doi.org/10.1088/1361-6463/aaaf9d

[53] E. READINGER, S. WOLTER, D. WALTEMYER, J. DELUCCA, S. MOHNEY, B. PRENITZER, L. GIANNUZZI, and R. MOLNAR, "Wet thermal oxidation of GaN," *Journal of Electronic Materials*, vol. 28, no. 3, pp. 257–260, 1999.

[54] S. D. Wolter, B. P. Luther, D. L. Waltemyer, C. Önneby, S. E. Mohney, and R. J. Molnar, "X-ray photoelectron spectroscopy and X-ray diffraction study of the thermal oxide on gallium nitride," *Applied Physics Letters*, vol. 70, no. 16, pp. 2156–2158, 1997. [Online]. Available: https://doi.org/10.1063/1.118944

[55] N. H. Tran, R. N. Lamb, L. J. Lai, and Y. W. Yang, "Influence of oxygen on the crystalline-amorphous transition in gallium nitride films," *The Journal of Physical Chemistry B*, vol. 109, no. 39, pp. 18 348–18 351, 2005.

[56] R. Guggenheim and L. Rodes, "Roadmap review for cooling high-power GaN HEMT devices," in *2017 IEEE International Conference on Microwaves, Antennas, Communications and Electronic Systems (COMCAS)*. IEEE, 2017, pp. 1–6.

[57] A. Afshar, "Materials characterization and growth mechanisms of ZnO, ZrO_2, and HfO_2 deposited by atomic layer deposition," Ph.D. dissertation, University of Alberta, 2014, doi: 10.7939/R3542JH2V.

[58] I. Bhaumik, R. Bhatt, S. Ganesamoorthy, A. Saxena, A. K. Karnal, P. K. Gupta, A. K. Sinha, and S. K. Deb, "Temperature-dependent index of refraction of monoclinic

Ga_2O_3 single crystal," *Applied Optics*, vol. 50, no. 31, pp. 6006–6010, 2011, j2: Appl. Opt. [Online]. Available: http://ao.osa.org/abstract.cfm?URI=ao-50-31-6006

[59] H. Fujiwara, *Spectroscopic Ellipsometry: Principles and Applications*. John Wiley & Sons, 2007.

[60] T. Corporation, "β-Ga_2O_3 substrates," iD: doc:5e855a5de4b074c5ec279f40; M1: Web Page. [Online]. Available: https://www.tamuracorp.com/products/gao/index.html

[61] M. Supplies, "Beta gallium oxide wafer and crystal substrates semi-insulating type," iD: doc:5e855c2be4b05aac66dc33de; M1: Web Page. [Online]. Available: https://www.msesupplies.com/products/ga2o3-beta-gallium-oxide-crystal-substrates

[62] L. Pauling and S. B. Hendricks, "The crystal structures of hematite and corundum," *Journal of the American Chemical Society*, vol. 47, no. 3, pp. 781–790, 1925, doi: 10.1021/ja01680a027. [Online]. Available: https://doi.org/10.1021/ja01680a027

[63] K. Momma and F. Izumi, "VESTA 3 for three-dimensional visualization of crystal, volumetric and morphology data," *Journal of Applied Crystallography*, vol. 44, no. 6, pp. 1272–1276, 2011, doi: 10.1107/S0021889811038970; 01. [Online]. Available: https://doi.org/10.1107/S0021889811038970

[64] S. Geller, "Crystal structure of β-Ga_2O_3," *The Journal of chemical physics*, vol. 33, no. 3, pp. 676–684, 1960, doi: 10.1063/1.1731237; 01. [Online]. Available: https://doi.org/10.1063/1.1731237

[65] M. Marezio and J. P. Remeika, "Bond lengths in the α-Ga_2O_3 structure and the high-pressure phase of Ga_2–x$FexO_3$," *The Journal of Chemical Physics*, vol. 46, no. 5, pp. 1862–1865, 1967, doi: 10.1063/1.1840945; 01. [Online]. Available: https://doi.org/10.1063/1.1840945

[66] M. A. Herman, W. Richter, and H. Sitter, *Epitaxy: Physical Principles and Technical Implementation*. Berlin: Springer, 2004, iD: doc:5e855fbde4b080bc95bb239f; ID: 248640036; M1: Book, Whole.

[67] P. Motamedi and K. Cadien, "Structure-property relationship and interfacial phenomena in GaN grown on C-plane sapphire via plasma-enhanced atomic layer deposition," *RSC Advances*, vol. 5, no. 71, pp. 57 865–57 874, 2015. [Online]. Available: http://dx.doi.org/10.1039/C5RA07709E

[68] M. Yoshida, "Mass spectrometric study of $Ga(CH_3)_3$ and $Ga(C_2H_5)_3$ decomposition reaction in H_2 and N_2," *Journal of the Electrochemical Society*, vol. 132, no. 3, p. 677, 1985. [Online]. Available: http://dx.doi.org/10.1149/1.2113929

[69] S. Nakagomi and Y. Kokubun, "Crystal orientation of β-Ga_2O_3 thin films formed on c-plane and a-plane sapphire substrate," *Journal of Crystal Growth*, vol. 349, no. 1, pp. 12–18, 2012. [Online]. Available: http://www.sciencedirect.com/science/article/pii/S0022024812002722

[70] Y. Lv, J. Ma, W. Mi, C. Luan, Z. Zhu, and H. Xiao, "Characterization of β-Ga_2O_3 thin films on sapphire (0001) using metal-organic chemical vapor deposition

technique," *Vacuum*, vol. 86, no. 12, pp. 1850–1854, 2012. [Online]. Available: http://www.sciencedirect.com/science/article/pii/S0042207X12002308

[71] S. Nakagomi and Y. Kokubun, "Crystal orientations of β-Ga_2O_3 thin films formed on c-plane GaN substrate," *physica status solidi (b)*, vol. 253, no. 6, pp. 1217–1221, 2016, doi: 10.1002/pssb.201552794; 30. [Online]. Available: https://doi.org/10.1002/pssb.201552794

[72] X. Yang, X. Du, L. He, D. Wang, C. Zhao, J. Liu, J. Ma, and H. Xiao, "Fabrication and optoelectronic properties of Ga_2O_3/Eu epitaxial films on nanoporous GaN distributed bragg reflectors," *Journal of Materials Science*, pp. 1–10, 2020.

[73] J. W. Elam, Z. A. Sechrist, and S. M. George, "ZnO/Al_2O_3 nanolaminates fabricated by atomic layer deposition: Growth and surface roughness measurements," *Thin Solid Films*, vol. 414, no. 1, pp. 43–55, 2002. [Online]. Available: http://www.sciencedirect.com/science/article/pii/S0040609002004273

[74] R. R. L. Oliveira, D. A. C. Albuquerque, T. Cruz, F. Yamaji, and F. Leite, *Measurement of the Nanoscale Roughness by Atomic Force Microscopy: Basic Principles and Applications*, ser. Atomic Force Microscopy – Imaging, Measuring and Manipulating Surfaces at the Atomic Scale. IntechOpen, 2012, pp. 147–174.

[75] C. L. Yaws, "Yaws' handbook of thermodynamic properties for hydrocarbons and chemicals, chapter 5: Enthalpies of formation of solids – table for elements and inorganic compounds," 2009, tY:

GEN. [Online]. Available: https://app.knovel.com/hotlink/toc/id:kpYHTPHC09/yaws-handbook-thermodynamic/yaws-handbook-thermodynamic

[76] R. Juza and H. Hahn, "über die kristallstrukturen von Cu_3N, GaN und InN metallamide und metallnitride," *Zeitschrift für anorganische und allgemeine Chemie*, vol. 239, no. 3, pp. 282–287, 1938, doi: 10.1002/zaac.19382390307; 05. [Online]. Available: https://doi.org/10.1002/zaac.19382390307

[77] P. Motamedi, N. Dalili, and K. Cadien, "A route to low temperature growth of single crystal GaN on sapphire," *Journal of Materials Chemistry C*, vol. 3, no. 28, pp. 7428–7436, 2015. [Online]. Available: http://dx.doi.org/10.1039/C5TC01556A

[78] Y.-H. Liang and E. Towe, "Progress in efficient doping of high aluminum-containing group III-nitrides," *Applied Physics Reviews*, vol. 5, no. 1, p. 011107, 2018, doi: 10.1063/1.5009349; 09. [Online]. Available: https://doi.org/10.1063/1.5009349

[79] Z. Gao and P. Banerjee, "Review article: Atomic layer deposition of doped ZnO films," *Journal of Vacuum Science & Technology A*, vol. 37, no. 5, p. 050802, 2019, doi: 10.1116/1.5112777; 09. [Online]. Available: https://doi.org/10.1116/1.5112777

Appendix A

Specification of the Substrates

Single-Side Polished Sapphire Wafer	
Grade	Prime
Orientation	C-plane (0001), 0.2 ± 0.1° off M-axis, 0 ± 0.1° off A-axis
Dopant	Undoped
Thickness	430 ± 25 µm
Front Surface	Epi-polished, R_a < 0.3 nm
Back Surface	Fine-ground, R_a = 0.8 – 1.2 µm
Single-Side Polished Si (100) Wafer	
Grade	Prime
Orientation	(100) ± 0.5°
Dopant	Boron (p-type)
Resistivity	1 – 10 Ω.cm
Thickness	500 ± 25 µm
Front Surface	Mirror Polished
Back Surface	Lapped, Etched
Single-Side Polished Si (110) Wafer	
Grade	Prime
Orientation	(110) ± 0.5°
Dopant	Boron (p-type)
Resistivity	5 – 10 Ω.cm
Thickness	525 ± 25 µm
Front Surface	Mirror Polished
Back Surface	Lapped, Etched
Single-Side Polished Si (111) Wafer	
Grade	Prime
Orientation	(111) ± 1°
Dopant	Phosphorus (n-type)
Resistivity	320 – 480 Ω.cm
Thickness	500 – 550 µm
Front Surface	Mirror Polished
Back Surface	Lapped, Etched
Glass Slides	
Grade	Precleaned Plain Pearl Microscope Slides
Thickness	1.0 – 1.2 mm

Table A.1: Specification of the substrates.

Appendix B

Further Analysis of Gallium Oxide Thin Films of Chapter 2

B.1 X-ray diffraction analysis by 2θ-ω (rocking) scans

To examine the broadness of thin film peaks for crystalline films on sapphire and examine possible strain in those films, XRD measurements were performed using rocking scans (aka 2θ-ω scans) by Bruker D8 Discover diffractometers producing K-α radiation of either cobalt or copper, Vantec 500 detectors and a sample-to-detector distance of 20 cm at an exposure of 140 s/step with 0.4° to 0.5° ω scan steps. To perform the measurements, 2θ was kept constant by moving both the detector and the X-ray source altogether while ω was being scanned. The 2θ angle was chosen such that the three peaks corresponding to α-Al_2O_3(006), α-Ga_2O_3(006) and β-Ga_2O_3($\bar{4}$02) can be simultaneously captured in each frame.

The resulting patterns are shown in Figure B.1 (The data for the bare sapphire and the

as-deposited film has been collected using cobalt X-ray source. However, all the patterns have been converted to Cu wavelength for easier comparison with each other and with literature patterns). The small broadness of the thin film peaks in Figure B.1 indicates the high crystalline quality of both α-Ga_2O_3(006) and β-$Ga_2O_3(\bar{4}02)$ in the thin films (film intensity distributions while varying ω in Figure B.1 are as narrow as the single crystal substrate intensity distribution).

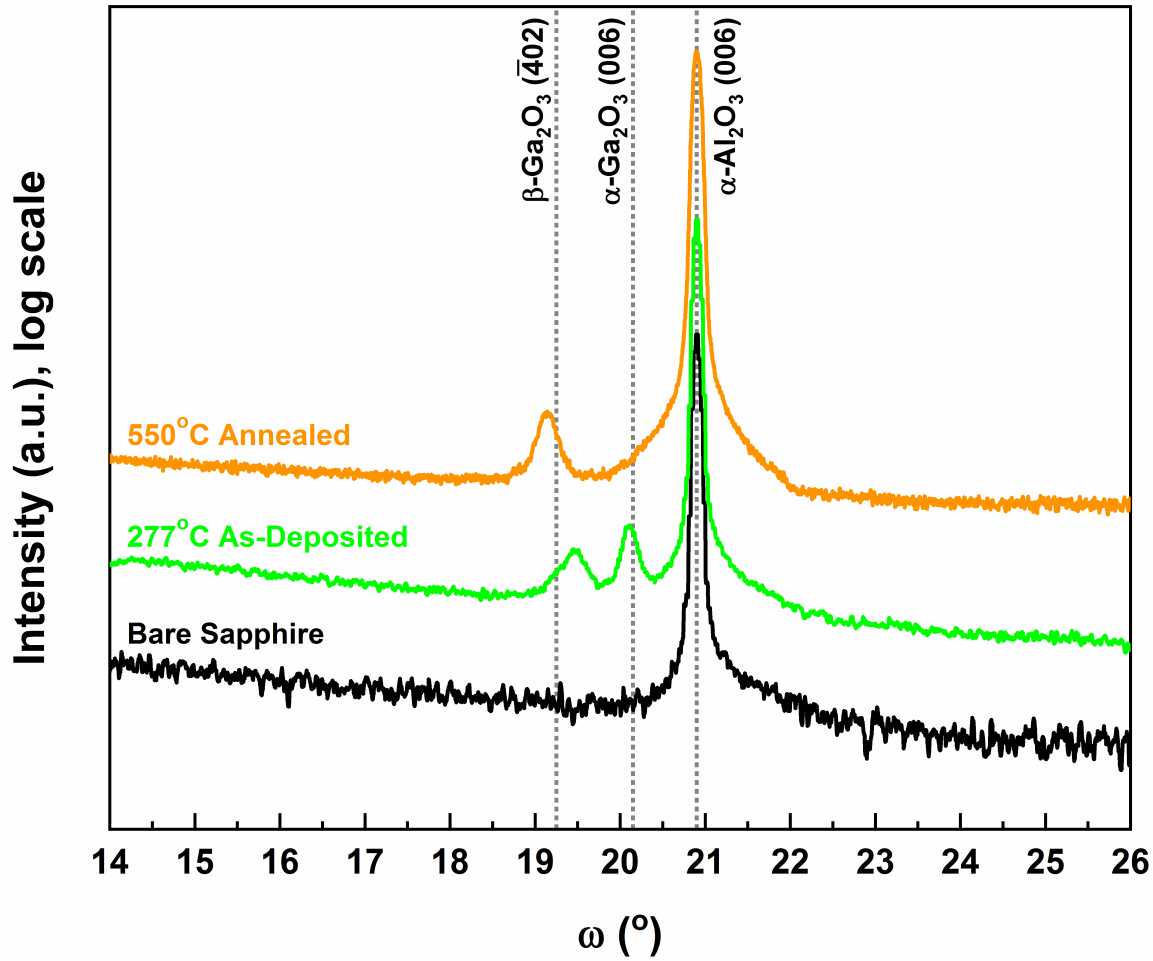

Figure B.1: Results of XRD rocking scans (aka 2θ-ω scans) for Ga_2O_3 samples on sapphire collected at 2θ = 41° (based on Cu wavelength). Dotted lines specify peak positions in relaxed crystals. Rocking curve of the bare c-plane sapphire substrate is also included as reference. The data has been collected using either cobalt or copper X-ray source. However, all the patterns have been converted to Cu wavelength for easier comparison with each other and with literature patterns. The intensities in this figure have been normalized such that the intensity of the α-Al_2O_3(006) peak is the same in all the patterns.

Sample (on c-plane sapphire)	Crystalline phase and plane	Calculated strain
277°C As-Deposited	α-Ga_2O_3 (006)	- 0.19%
	β-Ga_2O_3 ($\bar{4}$02)	+ 1.04%
550°C Annealed	β-Ga_2O_3 ($\bar{4}$02)	- 0.50%

Table B.1: The amount of strain in the 277°C as-deposited film on sapphire as well as the 550°C annealed film on sapphire based on deviation of the film peak positions from expected relaxed peak positions observed in XRD rocking curves.

Moreover, Figure B.1 shows that both the 277°C as-deposited film on sapphire as well as the 550°C annealed film on sapphire are partially strained. The strain in each phase in these epitaxial films was calculated based on the deviation of the film peak positions from expected relaxed peak positions, and the results are listed in Table B.1 indicating that the amount of strain in the films is small.

B.2 In-plane X-ray diffraction analysis by off-specular φ-scans

In order to study in-plane orientation of β-Ga_2O_3 domains on sapphire (i.e. to study planes that are non-parallel to the sample surface), XRD measurements were performed using off-specular φ-scans by a Bruker D8 Discover diffractometer equipped with an IμS copper source along with MONTEL optics producing Cu K-α radiation, a LYNXEYE XE detector at exposures ranging from 35 to 50 s/step with 0.25° φ-scan steps. More specifically, φ-scans were performed at the 2θ angle of each plane of interest while the sample was tilted to an appropriate χ angle so that the normal to the plane of interest bisects the beam path.

Figure B.2 shows the patterns corresponding to α-Al_2O_3(102) and β-Ga_2O_3($\bar{4}$01) planes

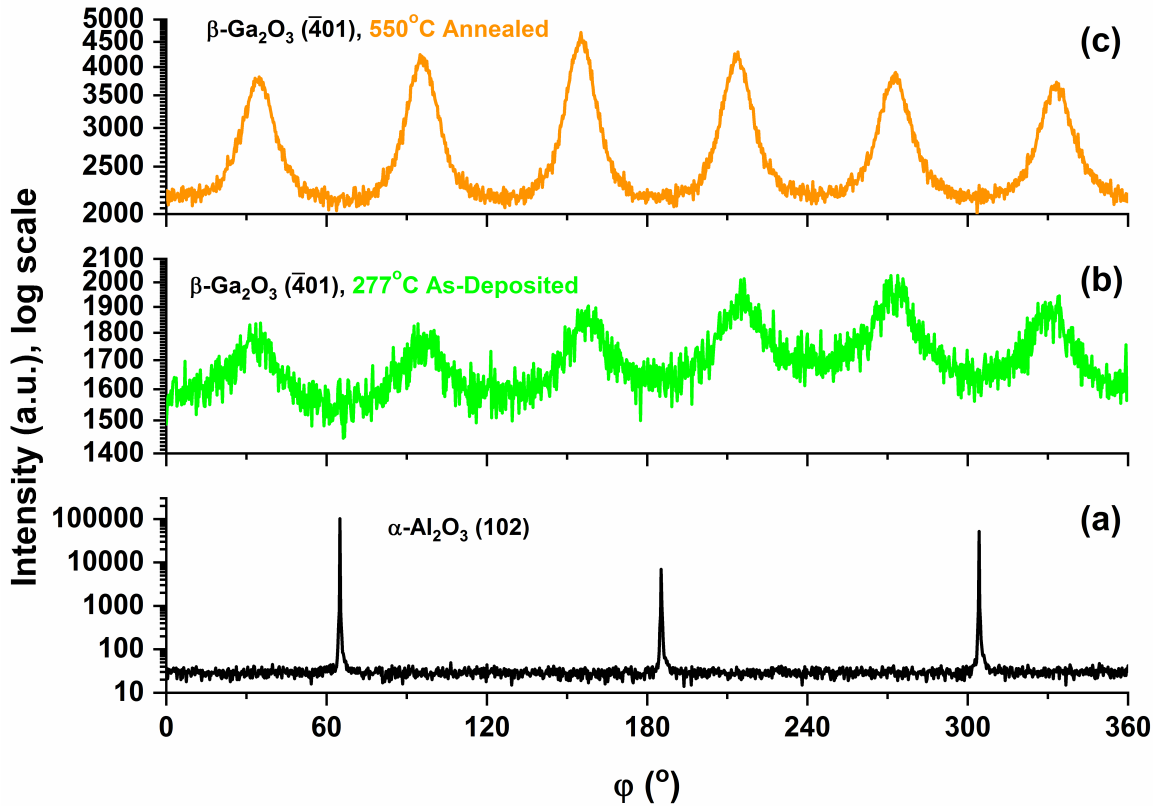

Figure B.2: Results of off-specular φ-scans for (a) sapphire (102), (b) β-$Ga_2O_3(\bar{4}01)$ in the 277°C as-deposited film, and (c) β-$Ga_2O_3(\bar{4}01)$ in the 550°C annealed film.

observed in off-specular φ-scans for the 277°C as-deposited film on sapphire as well as the 550°C annealed film on sapphire. Appearance of three peaks in the α-$Al_2O_3(102)$ φ-scan reveals the three-fold symmetry of the underlying sapphire substrate (belonging to the space group $R\bar{3}c$). Meanwhile, considering the centrosymmetric structure of β-Ga_2O_3 (belonging to the space group C2/m) two peaks are expected to be observed in β-$Ga_2O_3(\bar{4}01)$ φ-scan. Appearance of six peaks in β-$Ga_2O_3(\bar{4}01)$ φ-scan each one having 30° φ-offset from the α-$Al_2O_3(102)$ peaks, reveals that there are three in-plane orientations of β-Ga_2O_3 in the film matching the symmetry of the underlying sapphire substrate, with approximately same population, and all with the same normal orientation of β-$Ga_2O_3(\bar{2}01)\|\alpha$-$Al_2O_3(006)$. Similar observations for epitaxial β-Ga_2O_3 films on sapphire have been investigated in de-

tail in the literature (see, for example, references [69] to [72] for relevant discussions) and have been attributed to the fact that β-Ga_2O_3 has a less symmetric crystal structure than α-Al_2O_3 thereby enabling the formation of more than one in-plane orientation of β-Ga_2O_3 on α-Al_2O_3.

B.3 Optical properties of gallium oxide on sapphire before and after annealing

Figure B.3 shows the dispersion of refractive index (n) and extinction coefficient (k) for gallium oxide films on sapphire before and after annealing over the entire ellipsomerty spectral range based on Tauc–Lorentz modeling of the ellipsometry data. In addition, Table B.2 compares the optical bandgap for those films as well as their refractive index (n) at the selected photon energy of 632.8 nm (equivalent to 1.96 eV, at which light absorption does not occur in gallium oxide) and their maximum value of extinction coefficient (k_{max}).

As evident from both Figure B.3 and Table B.2, the 550°C annealed film on sapphire has a larger bandgap, larger k_{max} and overall larger refractive indices compared to the starting film (i.e. the 190°C as-deposited film). These results are consistent with the fact that annealing the 190°C as-deposited film (which is at the onset of crystallinity) at the temperature of 550°C has transformed the film to a highly oriented β-gallium oxide film.

Furthermore, considering that α-Ga_2O_3 has higher packing density of atoms (therefore larger refractive index) than β-Ga_2O_3 and based on the refractive index values reported in Table B.2 (in this Appendix) and Figure 2.2 (in the main text), it is worth noting that

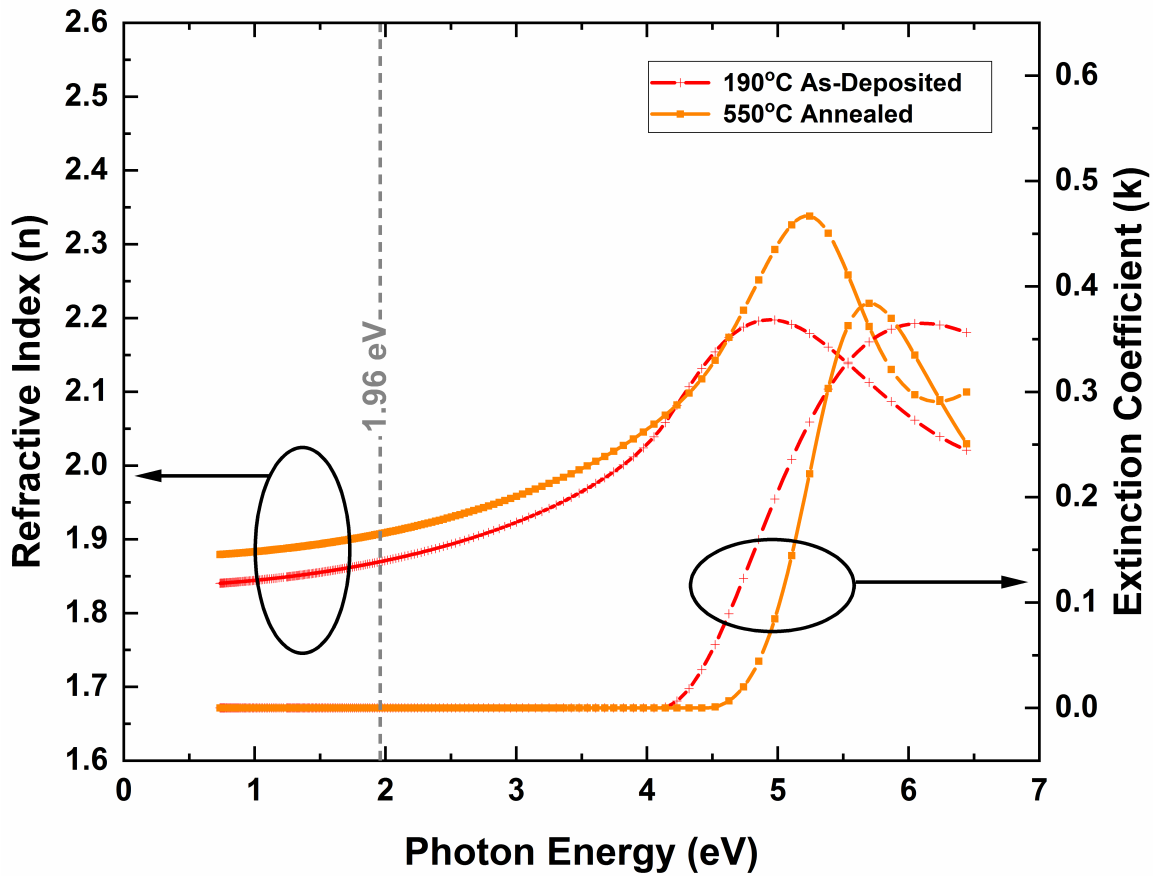

Figure B.3: Optical constants of Ga_2O_3 films on sapphire before and after annealing as a function of photon energy based on Tauc–Lorentz modeling of the ellipsometry data. The photon energy corresponding to 632.8 nm (i.e., 1.96 eV) has been identified by a dashed line for reference.

while the as-deposited films that have high crystalline quality and a higher amount of α-phase mixed with the $beta$-phase (see the film deposited at T_{sub} = 277°C as an example) can have slightly larger refractive index values compared to the 550°C annealed film due to the absence of the α-phase in the 550°C annealed film, the 550°C annealed film still has reasonably large refractive index (n > 1.9 at 632.8 nm) compared to the reported value of 1.97 for bulk β-Ga_2O_3 wafers [60]. Meanwhile, as mentioned in the manuscript, the best as-deposited film properties on sapphire were obtained at T_{sub} = 277°C beyond which the crystal structure slightly degraded and the bandgap decreased; It is worth noting that the

Sample	E_g (eV)	n at 632.8 nm	k_{max}	MSE
190°C As-Deposited	4.094 ± 0.014	1.870	0.365	2.837
550°C Annealed	4.447 ± 0.014	1.908	0.384	1.892

Table B.2: Comparison of optical properties for ∼38 nm Ga_2O_3 films on sapphire before and after annealing based on Tauc–Lorentz modeling of the ellipsometry data. The error in refractive index and extinction coefficient values is limited to ±0.001 in all cases.

550°C annealed film still has a larger bandgap than the films deposited at T_{sub} > 277°C which is an indication of the relatively low defect density in the 550°C annealed film as a pure β-phase epitaxial film with no α-Ga_2O_3 inclusions that could be detected by XRD in the film.

Appendix C

XPS Analysis of Selected Gallium Oxynitride Thin Films of Chapter 5

Chemical composition of the gallium oxynitride films was studied via Angle Dependent X-ray photoelectron spectroscopy (ADXPS) by using a PHI VersaProbe III (VP3) Scanning XPS Microprobe. ADXPS is a non-destructive technique to analyze the thickness and composition of thin-film stacks with ultra thin thickness with a few Å thickness sensitivity to detect chemical elements. All the samples appeared uniform when studied by this technique and no periodicity in the composition was detected.

Chemical composition of a selected gallium oxynitride film (the film with 10:1 cycle ratio, or X = 10) was also studied by using a Kratos AXIS Ultra X-ray photoelectron spectroscopy (XPS) using Al (1486.69 eV) X-ray source at 50° incidence angle. A piece of sample was left exposed to the atmosphere for at least overnight before the XPS analysis while another piece was kept under vacuumat all times before the XPS analysis and only was taken out of vacuum momentarilty to be transferrred to the XPD chamber. Charge

effects were corrected using C 1s peak as follows: Adventitious carbon 1s peak was fitted to determine its constituent sub-peaks and then the aliphatic carbon 1s peak center was shifted to 284.8 eV adjusting the rest of the spectrum. Casa XPS was used for this analysis: Shirley background was applied to subtract the inelastic background; non-linear optimization using the Marquardt Algorithm was used to determine the peak model parameters such as peak positions, widths and intensities; the model peak to describe XPS core level lines for curve fitting was a product of Gaussian and Lorentzian functions.

Figure C.1 shows the aliphatic carbon 1s peak center for all samples (i.e., the film with 10:1 cycle ratio kept under vacuum, the same film freely exposed to atmosphere before the analysis, a reference GaN film, and a reference Ga_2O_3 film) after the adjustment described above at the binding energy (BE) of 284.8 eV.

Survey spectra for the analyzed samples are shown in Figure C.2.

Figure C.3 shows the high resolution scans for the Ga 3d peak indicating that the Ga 3d peak has the lowest binding energy in GaN and the highest binding energy in Ga_2O_3. The Ga 3d peak in the gallium oxynitride films shows a binding energy between the pure films.

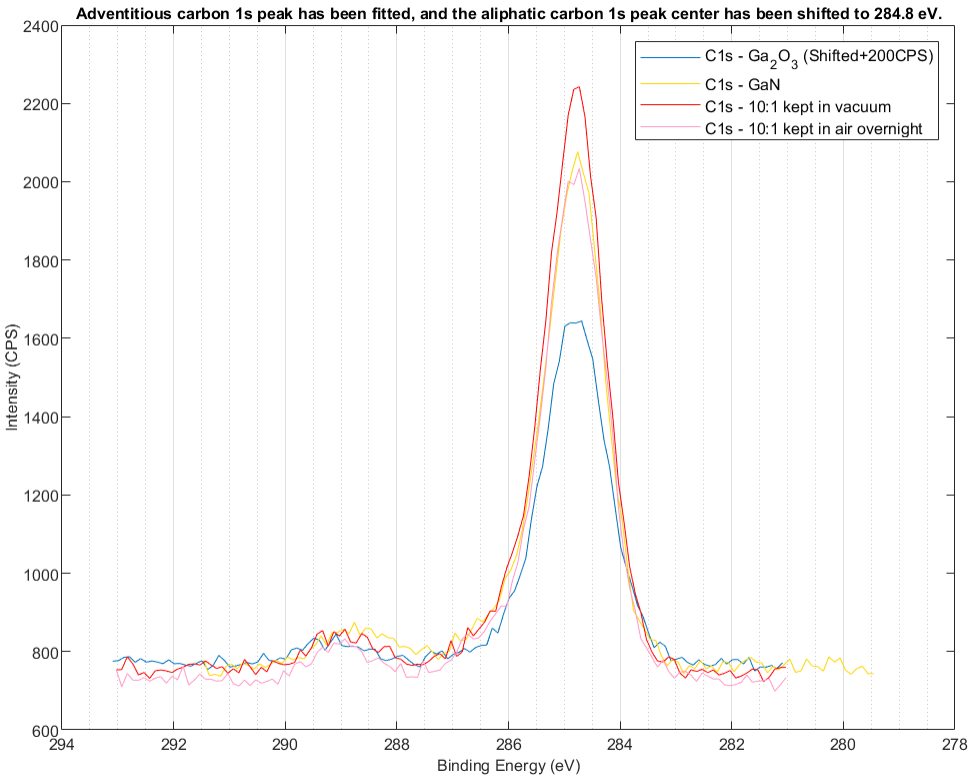

Figure C.1: The aliphatic C 1s peak center for all samples.

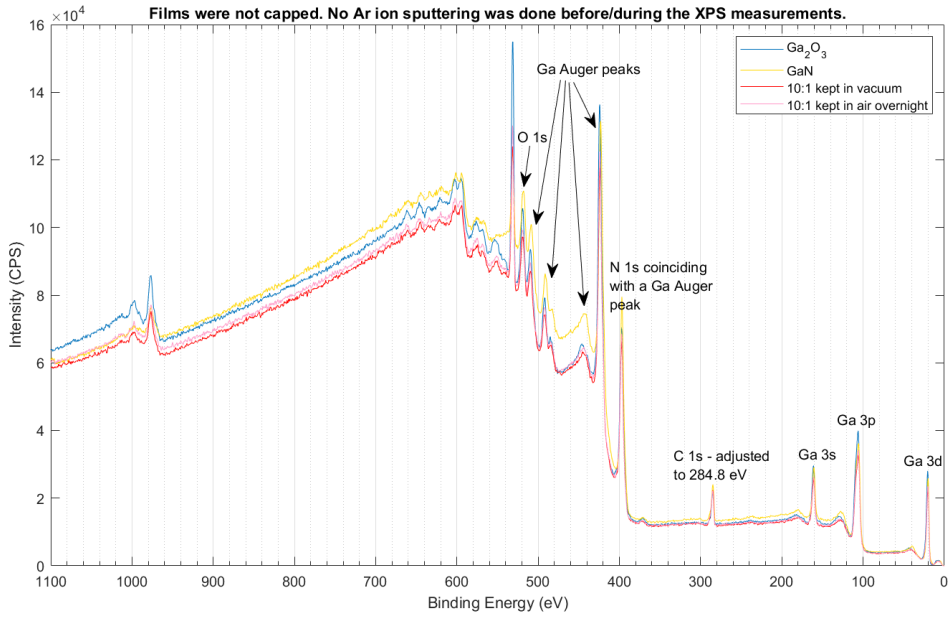

Figure C.2: Survey spectra for the analyzed samples.

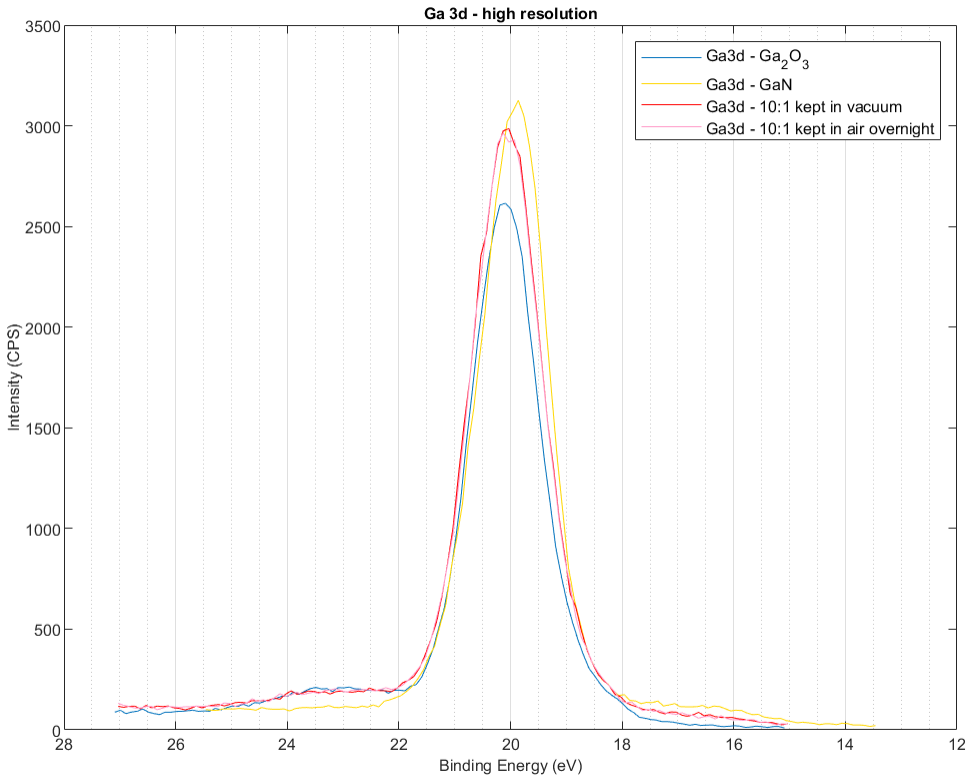

Figure C.3: The high resolution scans for the Ga 3d peak for the analyzed samples.